2010

Active surface topographies in constrained hydrogel films for biomedical applications

Ophir Ortiz
University of South Florida

Active Surface Topographies in Constrained Hydrogel Films for Biomedical Applications

by

Ophir Ortiz

A dissertation submitted in partial fulfillment
of the requirements for the degree of
Doctor of Philosophy
Department of Electrical Engineering
College of Engineering
University of South Florida

Co-Major Professor: Ryan Toomey, Ph.D.
Co-Major Professor: Jing Wang, Ph.D.
Ashok Kumar, Ph.D.
Mark Jaroszeski, Ph.D.
Garrett Matthews, Ph.D.

Date of Approval:
March 30, 2010

Keywords: biomaterials, cells, bioadhesion, thermoresponsive, polymers

This is dedicated to my mother for her

unrelenting support and encouragement throughout my life.

Table of Contents

List of Tables

List of Figures

Active Surface Topographies in Constrained Hydrogel Films for Biomedical Applications

Ophir Ortiz

ABSTRACT

Lung cancer has the highest mortality rate relative to all types of cancers, and unfortunately there still exist numerous challenges towards decreasing this rate. One of these challenges is gaining a clear understanding of why metastatic lung cancer cells attach and detach to colonize other areas of the body. Reports suggest that the attachment of cells to secondary tumor sites does not occur randomly. It is theorized that both the physical and chemical properties of the tissue are able to create a suitable environment for their adhesion. Therefore, the motivation for the work presented herein is to use dynamic thermoresponsive polymer surfaces as a tool towards unraveling this seemingly mysterious behavior of metastatic cancer cells. This type of polymer is able to swell and deswell as a function of temperature. As such, spin-cast thin films of this polymer provide for topographies that have been used to investigate how highly metastatic lung cancer cells are able to rearrange their structure, specifically the cytoskeleton. Changes in cell to surface anchorage as a function of thin film structure can also monitored.

One of the most studied reversibly binding surfaces is poly(N-isopropylacrylamide) (PNIPAAm), which has been considered for the past two decades as a non-destructive method for the harvest of confluent cell sheets. As a result of this property, a series of photocrosslinkable copolymers based on PNIPAAm and methacroyloxybenzophenone (MaBP) have been developed. Coatings are created by spin-casting the polymer followed by ultraviolet (UV) radiation, which triggers the n-π* transition in the benzophenone groups. This leads to the formation of a biradicaloid triplet that abstracts a hydrogen from a neighboring aliphatic C-H group, leading to a stable C-C bond. The characteristics of the polymer film, i.e. thickness, pattern, and topography, can be tuned during the spin casting and subsequent exposure/ developing process. The ease of tunability of this polymer allows for the investigation of the aforementioned parameters and their possible effects on bioadhesion.

Chapter 1

General Overview

Lung cancer is one of the deadliest types of this disease, and as such has been studied extensively for the past 50 years. The adhesiveness of lung cancer cells is one factor that has been the focus of numerous investigations, as this property has a ubiquitous role in metastasis [5]. Reports dating back over 40 years state that malignant cells mutate and express molecules (proteins) which are involved in the adhesion process at different amounts relative to non-cancerous and even malignant but non-motile cells [5]. The methods used for studying the numerous mechanisms involved in this highly complex process vary widely and are implemented from the biology field to almost all fields of engineering. Methods pertaining to biology include immunohistography and assays/ western blots, while methods within the engineering fields (material/biomedical/chemical/mechanical) include atomic force microscopy, scanning electron microscopy, tensile stress tests, and nanoindentation, just to name a few [6-8]. Even with the numerous investigations and data obtained, the two main obstacles to decreasing the death rate of this disease are 1- the lack of tools capable of early diagnosis and 2- inefficient methods of treatment [9].

One possible answer to the lack of diagnostic tools is the use of dynamic and tunable polymer surfaces for the detection of changes in cell adhesiveness.

Dynamic surfaces yield information regarding cytoskeletal rearrangement as a result of strain, while non-dynamic surfaces are able to provide information in only one state. The use of non-dynamic polymer surfaces to probe the adhesion process of both invasive and non-invasive cells has been reported as early as 1912, when spider webs were used to study cell migration, which is a process in which adhesion is involved [10]. In more recent investigations, 1-dimensional polymer surfaces used in cell adhesion studies include polystyrene [11], polydimethylsiloxane (PDMS), poly(DL-lactic-*co*-glycolic acid) (PLA), and polyacrylamide [12]. Although these have yielded further information regarding the effects of a variety of physical and chemical variables, including substrate rigidity and surface charge on this process, these surfaces do not mimic the actual environments to which cells *in vivo* are exposed. 3-dimensional dynamic surfaces allow for the fabrication of surfaces that more closely mimic those of *in vivo* environments, and may provide significant information regarding the effects of strain on adhesiveness. Data obtained with respect to both these factors would be beneficial for early detection of cancerous cells.

1.1 Lung Cancer Overview- Statistics and Milestones

Cancer affects 1 in 4 people in the United States, and is the number one cause of death amongst those under the age of 85 [13]. Unfortunately, historically speaking, this disease has afflicted humankind for centuries. Ancient Egyptians wrote about cancer on papyri circa 3000 BC, even describing

procedures for its diagnosis and treatment. The word cancer was coined by Hippocrates, a Greek physician known as the “father of medicine”. The term is a combination of the words carcinos and carcinoma to describe tumors. Although strides have been made with breakthroughs in the actual causes of this disease, a cure is as of yet unknown [14].

The advent of technologies within the last few decades has yielded favorable results, even helping to decrease the death rates attributed to cancer since 1990 for men and 1991 for women [13]. But upon closer inspection of the data for the most commonly occurring cancer types, some notable differences between cancer types and death rates are apparent. One example is the data pertaining to cancer of the lungs; when the death rates of this cancer are compared to other commonly occurring cancers, which include breast, colon, and prostate, the death rate is almost equal to the incidence rate (Fig. 1.1). This type of cancer is the leading cause of death in the Western hemisphere, with only a 15% survival rate in 5 years [5]. A comparison of this type of cancer to other diseases with high mortality rates also yields alarming results; data from 1950 to 2005 shows a steady decrease in heart and cerebrovascular disease (Fig. 1.2). The mortality rates of lung cancer, on the other hand, are almost stable [13].

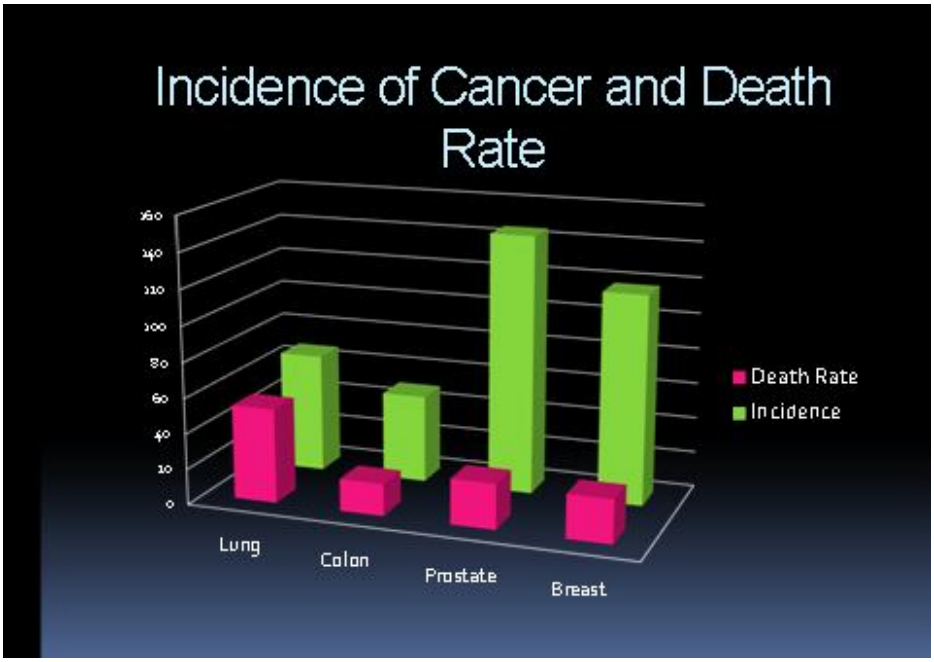

Figure 1.1: Bar graph showing the death rate and incidence of lung cancer versus other commonly occurring types of cancer.

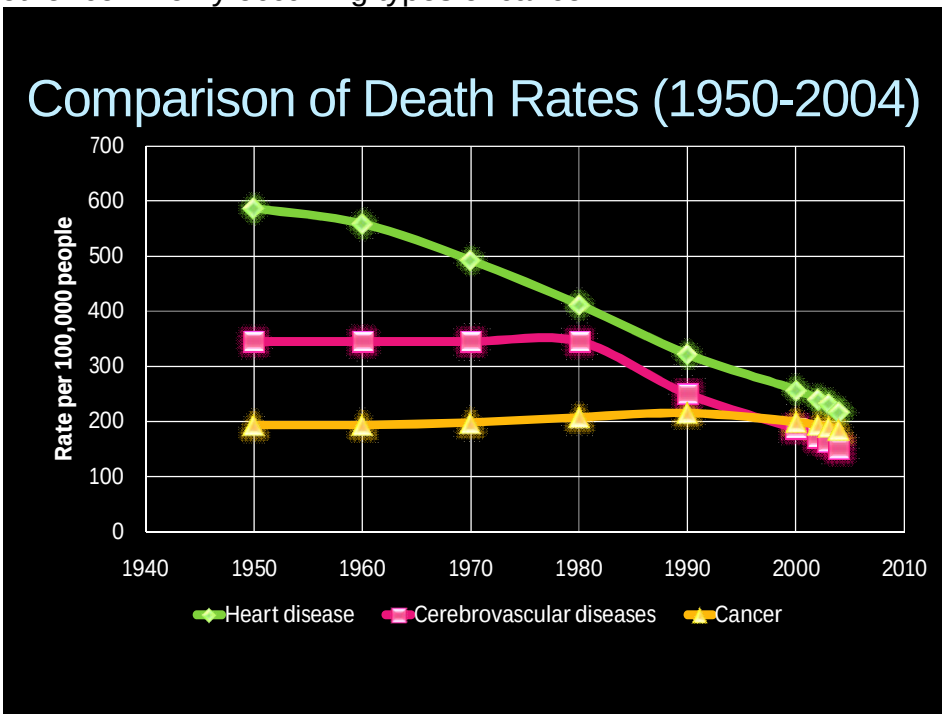

Figure 1.2: Graph comparing the death rates of three prevalent diseases. The decrease in cancer death rates has remained relatively unchanged in the last 50 years.

Even with the aforementioned grim facts concerning cancer and mortality rates, significant progress has been made in the field of oncology; these include the development of what is known as the “seed and soil” hypothesis, the postulation of angiogenesis, the correlation between smoking and lung cancer, and the postulation that tumorigenesis is a multistep process.

One of the first significant milestones in the area of cancer was the theory of preferential growth of cancer cells in certain organs during metastasis. In 1889, an assistant surgeon name Stephen Paget considered the following questions- what is it that decides which organs will become the location of secondary tumors? He went on to analyze the case histories of 735 breast cancer patients and in his seminal publication entitled *The distribution of secondary growths in cancer of the breast* went on to describe the idea that cancer cells spread to organs not by chance, but because certain characteristics of these organs enable the cells to attach and progress in their destructive path. Through these case studies, he observed that the majority of metastasis occurred in the liver, far more than other organs with similar vasculature. The “seed and soil” hypothesis, as it is known, signifies that a seed, in this case cancer cells, will grow only in locations where the soil is fertile, the soil symbolizing organs. This idea was outside of conventional thought of his day, when it was believed that metastatic cancer cells, after traveling through the circulatory or lymphatic system could become lodged almost randomly in any organ, and change the local tissue cells to grow and progress in a similar fashion as the invading cancer cells [15]. This knowledge led to a better understanding of

how cancer spreads through the body, with the importance lying in the fact that metastasis often increases the mortality rate of a patient since it makes the disease that much harder to eradicate.

Another milestone within cancer research is that of angiogenesis and its role in tumor growth. In the late 1930s, an article by Gordon Ide and colleagues with the title *Vascularization of the brown Pearce rabbit epithelioma transplant as seen in the transparent ear chamber* led to the notion that tumors could somehow produce chemicals to induce blood vessel growth [15]. However, it was not until the 1960s that this thought matured into the present-day belief that tumors are indeed capable of transporting molecules to induce angiogenesis. The importance of this finding is the relationship between the process of new blood vessel growth and tumor growth; without blood vessels to transport nutrients and take out waste, the growth is limited. But with proper vasculature, the cancer can become increasingly fatal because it has the proper nutrients necessary for growth to occur.

A third milestone within cancer research was the correlation between smoking and cancer. Although smoking increases the chances of cancerous growths in various parts of the body including the stomach, pancreas, and liver, one of the deadliest forms of cancer is lung cancer, and smoking is now considered to be the most influential factor regarding incidence [16]. With the increase in production and consumption of cigarettes during the first half of the 1900s, lung cancer rates in men sharply increased. This was followed by an increase in lung cancer rates diagnosed in women, a trend which is still being

observed today. The reason for the lag in rate increase for women is a result of a larger percentage of smoking initiation between the years of 1965 and 1975 [16]. Although the relationship between smoking and lung cancer was already suspected by some in the medical field, the paper entitled *Tobacco smoking as a possible etiologic factor in bronchiogenic carcinoma* showed data that helped prove this theory [17]. It is now widely accepted that not only is lung cancer largely attributed to a person's smoking habits, but there also exist detrimental effects to those exposed to second-hand smoke. On a positive note, studies have shown that cessation of this habit will decrease the mortality rate of the smoker [16].

In light of the aforementioned milestones within cancer research, there still exist gaps in knowledge concerning metastatic cancer cells. One gray area is the efficiency of the metastasis process, in the sense that some parts are considered efficient, while others are not. This difference in efficiency is not quite understood. Investigations into haematogenous metastasis using *in vivo* videoscopy along with cell fate analysis have shown that a large percentage of tumorigenic cells are able to travel through a pathway (lymphatic or cardiovascular) in the body and reach a site. A study by Luzzi and colleagues showed that although a large majority (87%) of B16 cancer cells arrested in an organ and extravasated, only .02% formed micrometastasis that could prove fatal [9]. The first steps in this process, which include the travel of the cells through capillaries and arrest in an organ, have therefore been determined to be efficient. The latter steps, which include the "soil" part of Paget's theory, are largely

inefficient. But the exact reasons for this are not completely known. The growth of the tumorigenic cells is closely dependent on the environment, that being the organ that has been invaded.

One promising tool towards cell adhesion research is that of the dynamic polymer surface. Since it is understood that physicochemical properties of surfaces play an essential role in cancer cell adhesion, synthetic polymer surfaces could potentially serve as biomimetic surfaces with which to investigate the affinity of neoplastic cells to varying topographies.

1.2 Introduction to Polymers

The use of synthetic polymers for biomedical applications is a relatively recent and promising tool in the search for understanding the mechanisms of numerous biological events [18]. The benefits of using such a material include the different surfaces that can be generated, which then allow for the investigation of how different chemical and physical surface attributes which mimic *in vivo* environments affect biological processes. Some of the processes that have been explored using polymeric biomaterials include durotaxis and cell adhesion [19, 20].

Before a discussion of the various types of polymers that are currently being pursued can occur, a basic introduction to polymers is necessary. Polymers are found everywhere in nature, from DNA and proteins in the body to rubber and starch. The basic definition of a polymer is a large molecule

composed of *mers*, or repeating units, held together by covalent bonds [21]. Polymers can have different structures which affect their behavior; these include linear, branched, star, comb, network, and semiladder (Fig. 1.3). Additionally, polymers are not necessarily made up of the same repeating unit; they can be made up of more than one. These types of polymers are called *copolymers*. Copolymers can also have various structures, such as linear or branched.

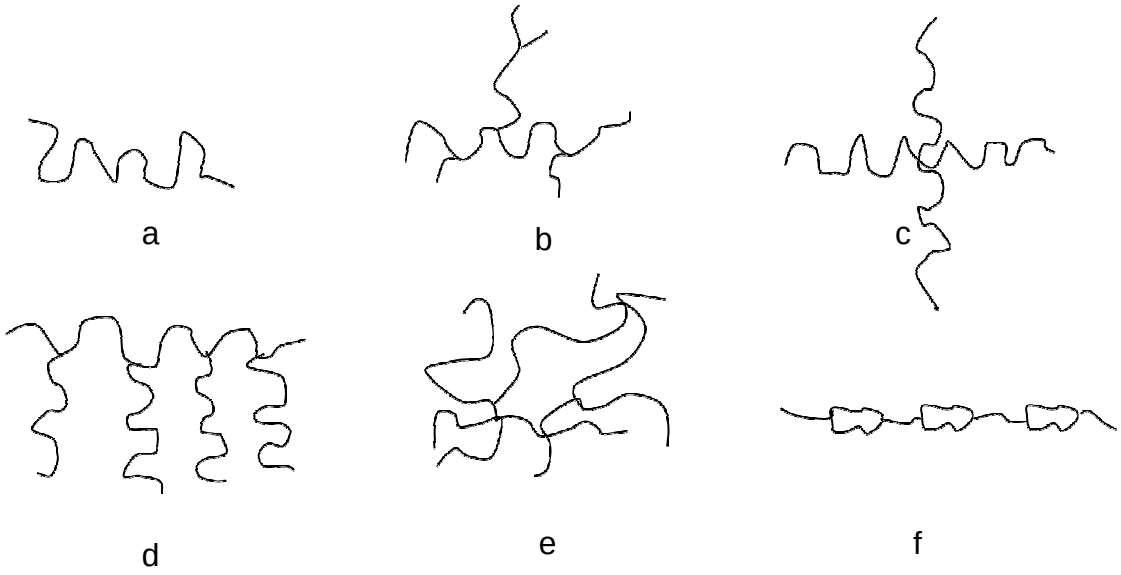

Figure 1.3: Various polymer structures (adapted from [17]): (a) linear, (b) branched, (c) star, (d) comb, (e) network, (f) semiladder.

Various methods for fabricating polymers exist; one widely used method is free-radical chain growth polymerization. This process has three general steps- initiation, propagation, and termination. In the initiation stage, free radicals are generated. Free radicals are atoms with unpaired electrons and can be produced from many sources, including redox reactions. The initiation of these free radicals is the rate-determining step. Propagation is the rapid reaction of the radicalized

molecule with another monomer of the same type, and the subsequent repetition to create the repeating chain. Termination, also known as the death of a reaction, can occur with coupling or disproportionation. The most common method of termination occurs in the case where two radical species react with each other to form a stable single molecule. Another method of terminating a reaction is chain disproportionation. In this method, the reaction is halted when a hydrogen atom is stripped from an active chain. This produces two terminated chains, one saturated and the other with a terminal carbon-carbon double bond [21].

1.2.1 Non-Responsive Polymers for Cell Adhesion

Synthetic polymers exist in a wide range of topographies. The topographies vary as a result of either the synthesis process itself or the processing steps after the polymer surface has been fabricated. Surfaces can be fabricated to have features ranging from a mostly homogenous surface, to one with features in the micro and macro scales. Since the 1960s, conventional cell adhesion or harvesting occurred with the use of homogenous polystyrene surfaces. This polymeric material, without further treatment, is non-fouling [22]. But with surface treatments such as laser, plasma, and chemical, anchorage-dependent cells are able to adhere and proliferate/ differentiate [7, 23, 24]. So, although this surface does not have a similar topographical structure to *in vivo* tissue, surface treatment adds functional groups which then allow for cells to adhere to the polystyrene. Prior to treatment, polystyrene surfaces are regarded

as bacteriological grade since eukaryotic cells are unable to adhere. Post treatment, the number of negative charges increase. These negative charges serve as sites for cell adhesion to occur via interactions with cell membrane proteins. The actual polarity of the charge, according to literature, is not the adhesive factor [25]. The electrical property which influences cell adhesion is the surface charge density. Although the optimum charge value may be cell type dependent as a result of the varying membrane proteins, studies using sulfonated polystyrene for cell adhesion have shown that 2-5 negatively charged groups per square nanometer is appropriate for adequate cell adhesion and spreading [25]. A topic which is related to the surface charge of a surface is wettability. It should be noted that the wettability also changes post chemical or physical treatments of the polystyrene (Fig. 1.4). A more thorough discussion of this topic is included in Chapter 4.

Another commonly used synthetic polymer used for cell adhesion studies is polydimethylsiloxane (PDMS). There are two main reasons why this material is sometimes chosen over polystyrene for cell adhesion studies. The first is that this material is useful in instances where a change in rigidity is to be investigated, as the crosslink density can be easily tuned. The second is that PDMS is widely used for soft lithography purposes to stamp self-assembled monolayers (for instance) for cell adhesion specificity. Cell adhesion experiments have been reported using this polymer, which have concluded that not only do cells anchor and exert traction forces, but also migrate as a result of changes in rigidity (durotaxis) [26].

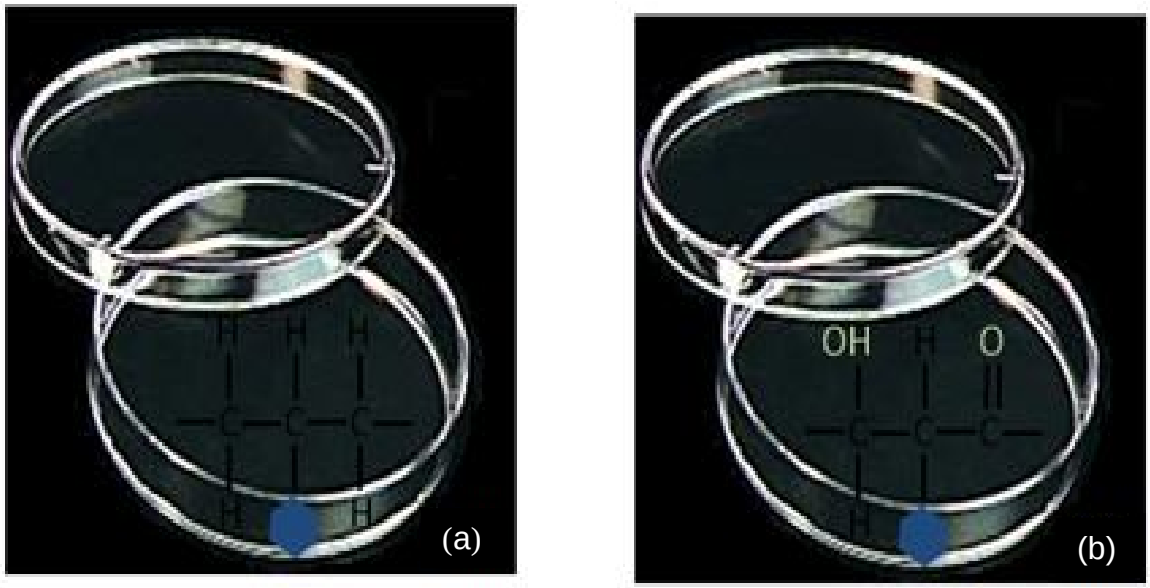

Figure 1.4: Images of (a) untreated and (b) treated polystyrene.

1.2.2 Responsive Polymers for Cell Adhesion

Responsive polymers is a special class of polymers which is widely discussed in literature and has implications within the biomedical field; these are also referred to as “smart”, “intelligent”, and “functional” [27]. This type of polymer reacts to external stimuli by changes in its physical state. The reaction is quick, occurring in a matter of seconds, and reversible [28]. Effects can be in the microscale, with changes in the chain conformation from a collapsed (globule) to a swollen (coil) state. These changes affect the wettability, leading to a hydrophobic or a hydrophilic polymer. Effects can also occur in the macroscale, such as the change in film thickness of a responsive hydrogel due to a change in wettability as a result of the stimuli. The stimuli can be a change in pH, ions,

electricity, or temperature, among others [28]. The two most frequently used are pH and temperature, due to the ease with which these can be applied [28].

Temperature responsive, or thermoresponsive polymers, alter their efficiency of hydrogen bonding with a change in temperature. These polymers are typically uncharged, and are able to interact with water molecules. One type of polymer which has generated considerable interest is poly(*N*-isopropylacrylamide) (PNIPAAm). Hydrogels composed of this polymer are able to swell or deswell when placed in water above and below what is known as the cloud point, or lower critical solution temperature (LCST). The cloud point of PNIPAAm hydrogels is about 32ºC in pure water (Fig. 1.5). The hydrogel is able to swell and deswell as a result of changes in the coil conformations; below the LCST, the polymer chains have an extended coil conformation. Above this temperature, the chains are collapsed, with extremely small amounts of water left in the gel [29]. The ability of this type of polymer to respond to stimuli has been the focus of numerous biomedical engineering reports, as the swelling and deswelling is of great relevance towards numerous efforts within this field, from drug delivery to tissue harvesting. Due to the scope of this work, the focus of the applications discussed in the following sections will be in regard to those that have investigated the effects of physicochemical surface properties on cell adhesion.

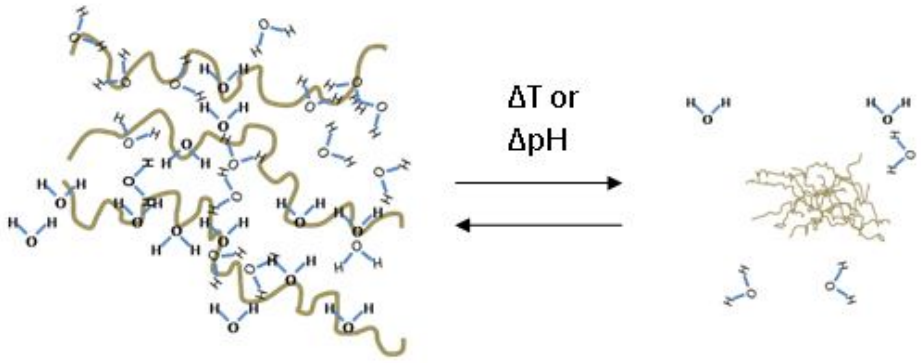

Figure 1.5: Responsive polymers undergo a coil-to-globule phase transition when cued by temperature or pH.

As aforementioned, thermoresponsive polymers have also demonstrated usefulness in the area of tissue engineering [30]. One such example is the fabrication of a 3-D porous hydrogel composed of chitosan-graft-poly(N-isopropylacrylamide). One benefit of using this 3-D hydrogel is that chondrocytes and meniscus cells can be cultivated while maintaining their normal phenotype and morphology [31]. This is in contrast to 1 or 2-D cultivation methods, which change the morphology of the cells to flat and fibroblast-like. This change in morphology also causes the cells to secrete incorrect extracellular matrix components. The implications of this material for the cultivation of these cells are significant due to the problems faced when cartilage cells need to be implanted into a knee following an injury. Conventional methods for implanting cartilage and meniscus cells involve monolayer cultivation, and as such cause incorrect biochemical and mechanical properties to be acquired by the cells, leading to fibrinogenesis at the injury site [31].

The majority of surfaces that have thus far been studied for cell harvesting have been static, and mostly homogenous. One possible method towards an increased level of understanding of how the metastatic process works, which includes adhesion and detachment of cells, is to use 3-dimensional surfaces that can switch states, i.e. are dynamic. Therefore, the focus of this work is to systematically investigate the effects of dynamic 3-dimensional surfaces on highly motile cancer cells. The benefits of using dynamic surfaces, which will be discussed in more detail, include the ability to monitor changes in the cytoskeleton as a function of the degree of polymer swelling. An additional advantage of the polymer discussed within this work is the ability to vary the degree of surface topography swelling by changing the crosslink density of the actual polymer.

1.3 Research Directions and Thesis Summary

As stated in the introduction of this Chapter, one of the deadliest types of cancer is that which occurs in the lungs and proceeds to metastasize. Even though there have been tremendous milestones within cancer research, there still exist numerous questions concerning the process of metastasis and cancer cell adhesion that as of yet remain unanswered. To this end, dynamic thermoresponsive thin films have been investigated as a platform for studying cancer cell adhesion. The focus of the work presented herein is to elucidate some of the mechanisms by which cancer cells preferentially attach or do not

attach with the use of these surfaces. Although numerous reports have been published which involve the use of responsive polymers for cell adhesion purposes, none as of yet have controlled the surfaces to fabricate 3-dimensional topographies of varying scales to study the effects of these on focal adhesions/complexes and morphology, all of which are known to affect phenotype and in turn, cellular signaling pathways.

Chapter 2 discusses the mechanisms involved in bioadhesion, which are of great relevance to the topic of metastatic cancer cell adhesion. This process is highly complex and sensitive, which can be assessed by the effects on cell morphology and the extent to which focal contacts spread. This process is present in metastasis, since one of the requirements for a tumorigenic cell to have the ability to travel through one of the two main “highways” of the body, i.e. the circulatory and lymphatic systems, is to first detach from a primary tumor site. Without this first step, the spreading of malignant cancer cannot occur.

Chapter 3 provides details of the surface topography of PNIPAAm-co-MABP thin films via surface topography characterization. As a result of a difference in thermal coefficient of expansion between the polymer thin film and the rigid substrate, which in this case is silicon, surface instabilities in various forms appear. The form of the instability depends on the processing conditions. Specifically, it was observed that a change in solvent produced a change in the topography, from cusps to blisters. Additionally, quantitative and qualitative data was obtained regarding the surface instabilities, namely the effects of film thickness on the cusp wavelength, amplitude, and width. This information is

necessary due to the application of these films in the biomedical film. Because these films are used for bioadhesion purposes, then surface information is essential, since it is known that both physical and chemical characteristics of a surface will affect whether biological specimens will adhere to the surface.

In Chapter 4, data will be presented concerning the adhesion of cells to dynamic surfaces. Polymer surfaces were fabricated and used as a tool to study the cytoskeletal rearrangement of metastatic cancer cells on these surfaces. The actin cytoskeleton was labeled and imaged using fluorescent microscopy to understand any change in the morphology of the cells when exposed to temperatures above and below the LCST.

Chapter 5 will serve as a summary of the work presented within this dissertation. Future works will also be discussed.

Chapter 2

Fundamentals of Bioadhesion

2.1 Introduction

Under certain conditions, cells may attach to synthetic surfaces. This phenomenon, called bioadhesion, is mediated by the interactions between the surface properties of the substrate and the proteins that surround and penetrate the cell membrane [2]. Although the mechanisms of attachment are as of yet elusive, further investigations are necessary, since it is known that adhesion plays a predominant role in cellular processes, including migration and differentiation [32].

The cell membrane of eukaryotes is a thin sheet (7-10nm) composed of lipids with protein molecules dispersed within [33]. This membrane serves various functions, which include protecting the contents from mixing with the extracellular space, facilitating the exchange of nutrients and waste, and mediating cell-cell and cell-substratum adhesion via cell adhesion molecules (Fig. 2.1, Table 2.1). Cell-cell adhesion occurs when intracellular attachment proteins bind to transmembrane linker proteins [33]. The transmembrane linker protein then binds to either the same protein on the adjacent cell or to the

extracellular matrix. Cell-substratum adhesion is dependent not only on the integral and surface proteins of the cell itself, but also on the physicochemical characteristics of the surface with which it is interacting. The surface can be fouling or non-fouling as a result of the topography, wettability, and surface charge [10].

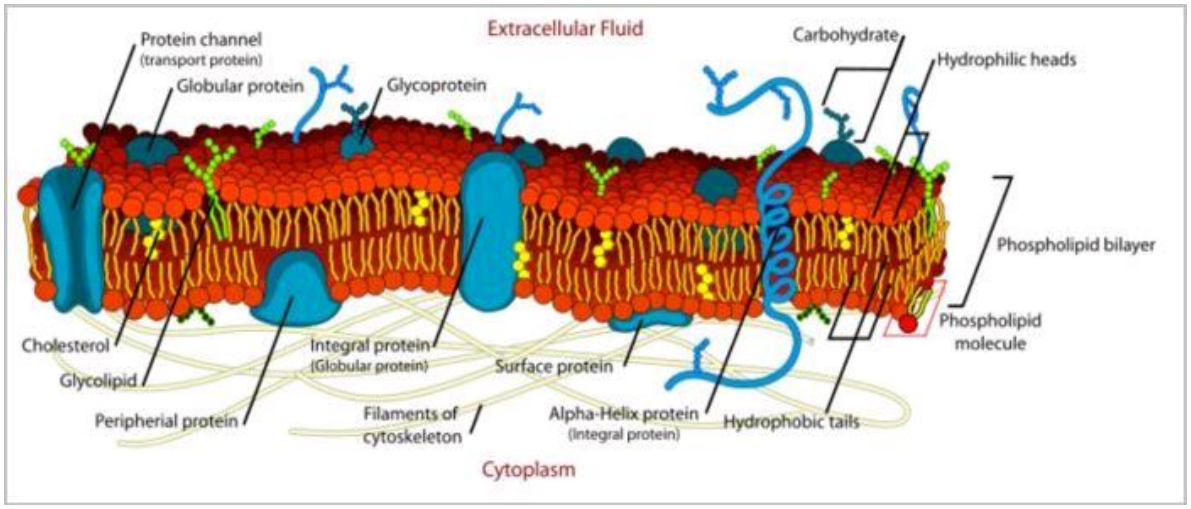

Figure 2.1: Schematic of the cell membrane [31].

Table 2.1: Cell adhesion molecules and their respective functions.

Cell adhesion molecule	Function
Integrin	Glycoproteins that facilitate communication between the cytoskeleton and extracellular matrix
Cadherin	Cause adhesion via hemophilic binding to other cadherins in a calcium-dependent manner
Selectin	Bind to carbohydrate ligands on cells
Ig superfamily	Mediate hemophilic interactions in which an adhesion molecule on the surface of one cell binds to the same molecule on the surface of another cell

2.2 Cellular Adhesion- A Part of the Migration Process

Cellular adhesion is part of a multiple-step migration process for mobile cells which involves a number of cascading events and is directly related to various pathological processes, including cancer [34-36]. During the first step, lamellipodia or filopodia extend from the cell membrane towards the direction of migration. Lamellipodia is a type of microfilament present beneath the cell membrane which aids in maintaining cell shape as well as resisting tension. Filopodia are spike-like protrusions that, along with lamellipodia, help anchor a cell to ECM or to neighboring cells [35]. The cell moves over these anchor sites, and with the retraction of these protrusions at the rear, it is able to move forward.

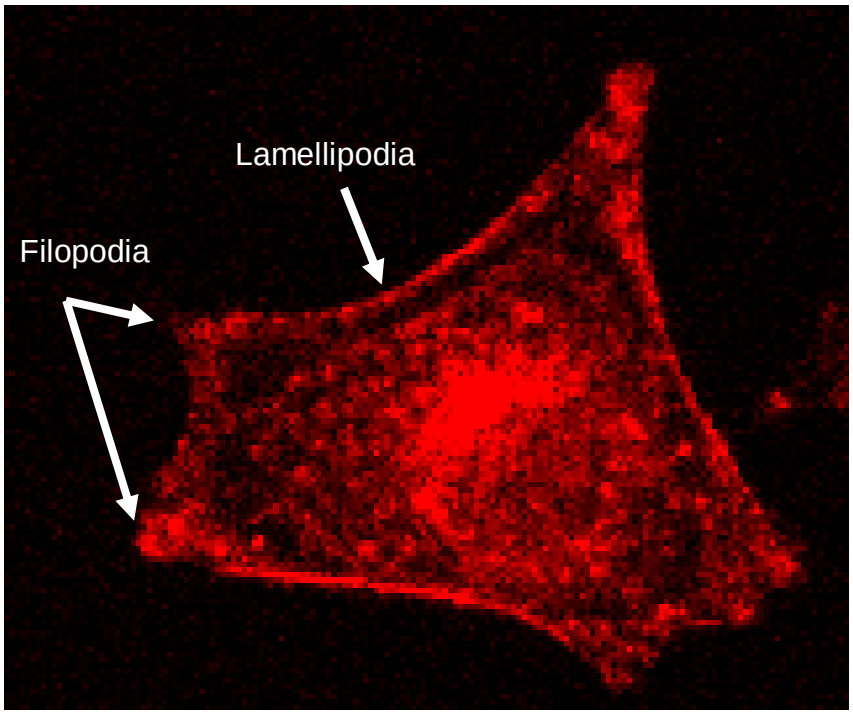

Figure 2.2: Fluorescent microscope image of B16-F10 cell with labeled actin.

2.3 Effects of Surface Topography on Bioadhesion

In vivo, cells come into contact with surfaces which have nano- or micron-scale roughness [1, 37-40]. These different topopgraphies are mainly due to the extracellular matrix (ECM). Although the exact components of the ECM vary with cell type, the general components are proteins and proteoglycans (protein polysaccharide molecules). Except for elastin, the majority of these proteins are glycoproteins (proteins with attached carbohydrate residues); these include fibronectin, laminin, and collagen.

Different parts of the body contain varying amounts of ECM components, and thus have different topographies [1, 40]. For example, the basement membrane, which underlies the epithelium, has a three-dimensional topography in the nanoscale range. An example of this topography is depicted in Figure 2.3, which shows a variation of up to 350 nm. This topography is a result of its composition of pores and fibers with dimensions in the range of 30 to 400 nm. Specifically, the basement membrane is composed of two basal laminae. The first is the basal lamina, which is an adhesive sheet composed of glycoproteins secreted by epithelial cells [33]. Below this layer is the reticular lamina, a sheet comprised of extracellular matrix material. One of its main constituents is collagen, which forms a fine network of fibers. A primary function of this basement membrane is to serve as mechanical reinforcement, which includes protection from invasive cancer cells [41]. Knowledge of this topography has

direct implications within the field of oncology since the epithelium lines the "highway" utilized by metastatic cancer cells- the cardiovascular system [41].

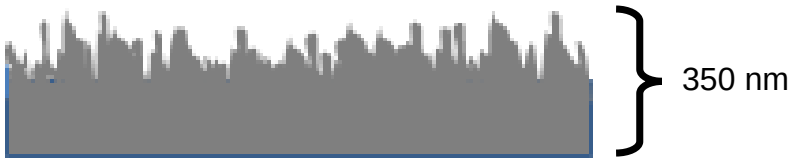

Figure 2.3: Schematic of cross section of corneal epithelial basement membrane, adapted from [1].

In vitro studies suggest there is a direct correlation between the strength of adhesion and the topography [34, 37]. Karuri *et al.* investigated the effects of grooves or ridges on the adhesion strength of human corneal endothelial cells. The ridges, fabricated via photolithography on silicon, ranged in pitch from 400 to 4000 nm. The cells were tested for adhesion strength by subjecting them to shear flow of 40 and 80 Pa. Results indicated that a large majority of the cells were able to withstand the 40 Pa flow (> 80%), but most were not able to stay attached after the 80 Pa flow. The topographies with the highest strength after the higher flow rate were those having a pitch of 400 and 800 nm. It should be noted that although these ridges had the highest strength, this does not necessarily correlate to the affinity of these surfaces for cell adhesion. These findings only indicate that once attached, the cells could withstand (or not) certain shear flows. Their findings did indicate differences in cell binding percentage depending on topography; cells preferentially attached to the 400 and 1200 nm

ridges relative to all other pitches, and in the case of all pitches the morphology was found to align parallel to these patterns.

Other reported investigations into cell adhesion and topography have found a relationship between strength of adhesion and migration, which also has direct implications in tumor cell metastasis. In the case of a highly adhesive substrate, a cell may be anchored to the point that it is immobilized [42]. If cell adhesion is very weak, a cell is unable to anchor to the surface. But if a substrate is adhesive enough for anchor sites to hold it in place and not to the point of being immobilized, a cell is able to perform its physiological functions of migration and differentiation. The adhesiveness of a surface may be mediated through changes in topography, and has been found to affect tumor cell adhesiveness [42]. Cancer cell adhesion will be further discussed below.

2.4 Effects of Wettability on Bioadhesion

Another factor which has been vastly discussed in literature regarding cellular adhesion is wettability [43-45]. Wettability, as the name states, is the ability of a liquid to wet a surface and is commonly explained as the contact angle of a droplet of a liquid (e.g. water) on a surface. When the contact angle is 90º or higher, the material is deemed as being hydrophobic. When the contact angle of the liquid on the surface is below 90º, the material is deemed as hydrophilic. This material property can be tuned using chemical modification of the surface or by changing the roughness. As mentioned in Chapter 1, one

example of the effects of wettability on cellular adhesion is that of polystyrene. This material is non-fouling without surface modification and has been reported to have a contact angle of 90º [46]. Following plasma treatment, this material becomes increasingly hydrophilic with a contact angle of ~75º and is consequently fouling [22]. Besides polystyrene, a number of other surfaces used for bioadhesion have been studied, as the exact relationship between wettability and cellular/protein adhesion is still uncertain. Lampin and colleagues studied the adhesion of corneal and vascular endothelial embryo cells on surfaces with varying hydrophocity. The surfaces were Poly(methyl methacrylate) (PMMA) and were sandblasted to vary the surface roughness. The surface roughness was varied since this is one method of changing the wettability of a surface (besides chemical or UV modification methods). With an increase in roughness, an increase in hydrophobicity (decrease in wettability) was reported. Cell adhesion was more prevalent on the surfaces with the highest degree of surface roughness, indicating that the more hydrophobic surfaces were more biocompatible [43]. It is interesting to note that although the wettability was stated as being a factor in the difference in cells adhesion, the difference in wettability between the sample with the lowest and highest roughness levels was only 3º.

Another method which is used to modify surfaces and hence change the wettability is by exposing them to self assembled monolayers (SAMs). Arima and colleagues mixed two types of alkanethiols for the surface modification experiments. Two representative endothelial cell lines were used, human umbilical vein endothelial cells (HUVECs) and HeLa. It was concluded that the

maximum number of HUVECs adhered to CH3/OH- modified surfaces with a contact angle of ~40º, while the HeLa cells grown on CH3/COOH-modified surfaces had the maximum number of adhered cells with a contact angle of ~50º [44].

As exemplified above, a conclusive answer regarding the exact range of wettability that a surface should possess for maximum adhesion is presently not possible. A number of variables affect this process, including the cell line, roughness, and functional groups (just to name a few). In Chapter 3, the effects of wettability will also be discussed, but in the context of thermoresponsive polymers, where this characteristic is still widely discussed.

2.5 Effects of Strain on Bioadhesion

Another surface characteristic which has been reported to affect cell adhesion is the mechanical properties of the surface, specifically the elasticity (or Young's modulus) [42]. Young's modulus is obtained from various methods, from hanging a weight with a known value from a material, or using micro- or nano indentation. In the case of the weight, the change in strain is measured and used to calculate the modulus. Micro- or nano indentation, on the other hand, is the indentation of a material using a tip with a known area. The force applied to the tip is known, and the area of the indentation is measured. The modulus can then be calculated. There are other methods used, but each has its own advantages and disadvantages. Therefore, data pertaining to values of rigidity to which cells

will attach (with both *in vivo* and *in vitro*) have been reported to occur in a large range.

Most eukaryotic cells are anchorage dependent, that is, they will not actively divide/ differentiate in suspension. Once cells are able to anchor to a substrate, normal physiological processes occur. Evidence has shown that the rigidity of the surface not only affects the strength of adhesion between the cell (focal contacts/complexes) and the ECM/substrate, but that because cell signaling occurs as a result of this process, the phenotype can be drastically affected [26, 42].

The dependence of cell adhesion to the surface rigidity has been studied in a number of cell lines [42]. Anchorage dependent cells are unable to attach to fluids because these are unable to withstand forces that are exerted by the cell. The process by which cells exert mechanical forces to a substrate can be thought of as a feedback mechanism; the surface of a solid is able to exert an opposing force to that generated by the cell, which triggers cell signaling [42]. This feedback mechanism has been reported to affect the process of angiogenesis, in which endothelial cells align and form new blood vessels. Angiogenesis is of great relevance to oncology, as this process is what develops circulatory pathways for metastatic tumors. Without this, tumors are unable to obtain nutrients. Nevertheless, studies have found that tubulogenesis, one of the last steps in angiogenesis, is affected by the surface rigidity [47]. In a study by Deroanne *et al*., endothelial and fibroblast cells were grown on matrigel and polyacrylamide surfaces, each with extracellular matrix proteins. Endothelial cells

were cued to form tube-like structures, which is part of the tubulogenesis process, by using matrigel or matrigel coated with a layer of type 1 collagen as the substrate. The matrigel surfaces are regarded as “soft,” even though no mechanical measurements or data concerning the rigidity were discussed in the report. Western blot analysis revealed a change in protein expression, specifically in the alpha subunit of integrins, and in the expression of vinculin and talin. These proteins are involved in the mechanochemical signal transduction of the cytoskeleton to the substrate, and also from the substrate to the cytoskeleton (Fig. 2.4).

The rigidity to which cells will adhere varies *in vivo*, as tissue is composed of varying amounts of proteins (or sublayer of cells) depending on their location and function. Cells *in vivo* normally attach to other similar cells, or to the protein meshwork that is the extracellular matrix. The elastic moduli of these surfaces range from .01 kPa to 10 kPa [26]. Adhesion as a function of surface rigidity is cell type dependent, as cells have different roles pertaining to the organ function and hence face surfaces with distinct mechanical properties. In a study by Yeung *et al*., the adhesion as a function of increasing substrate stiffness was investigated. The effects on morphology and flatness were measured. The cell lines used in this study were NIH 3T3 fibroblasts, bovine aorta endothelial cells, and human neutrophils. It should be noted that neutrophils are not anchorage dependent, these cells are able to function in their normal physiological state in fluids.

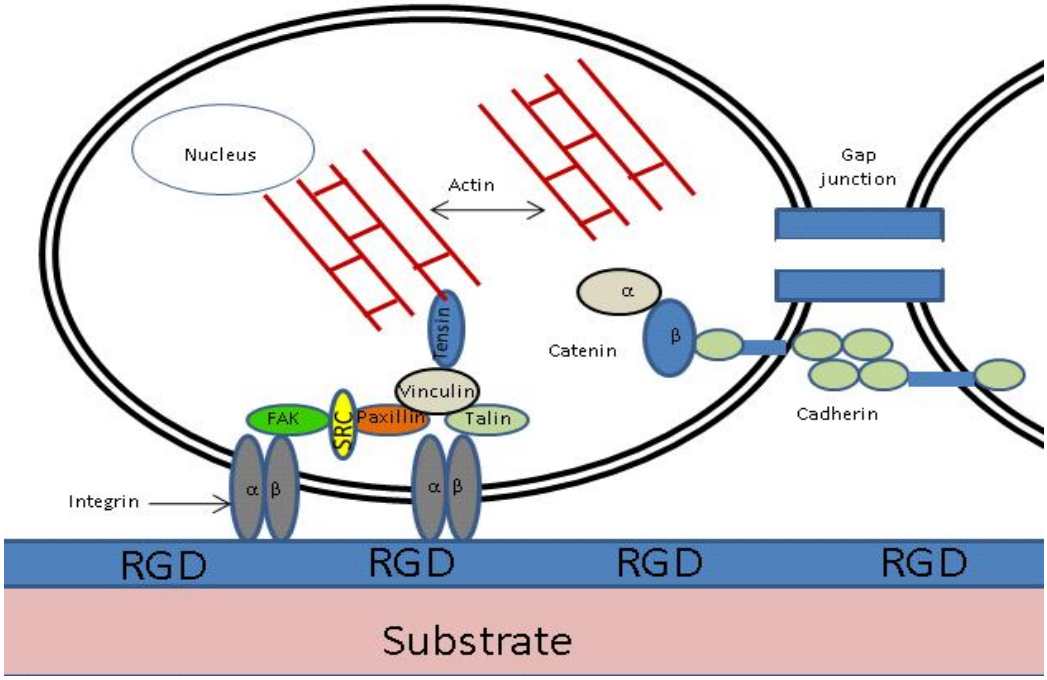

Figure 2.4: Cell adhesion to a biomaterial (adapted from [2]).

Table 2.2: The Young's modulus of various types of tissue.

Tissue	Young's modulus (Pa)
Trabecular bone	14.8 G [48]
Cortical bone	20.7 G [48]
Adipose tissue	20 k [49]

2.6 Neoplastic Cell Adhesion

Although cancer and non-cancerous cells share some of the basic cellular functions (such as they divide, proliferate, differentiate, etc.), there are a number

of differences in these functions, as in most instances cancer cells have different rates at which these occur. Additionally, there are also physical differences, as cancer cells express different proteins (since their goal is to invade and proliferate much faster than non-malignant cells). One basic requirement shared by both cancerous and non-cancerous cells is the importance of cell adhesion molecules for adhering to surfaces. But of course, cancer cells need to grow, detach, then attach again at a secondary site (if motile). So in essence, cell adhesion molecules are essential in the spreading of cancer throughout the body (metastasis). Cancer cells, which are genetically unstable and have a higher mutation rate, are known to invade other tissues. In the case of metastasis, primary cancer cells establish new tumor colonies in select secondary sites [50]. Tumor cells travel through the vascular or lymphatic system, and then attach to cell adhesion molecules at the secondary site. The detachment of malignant tumor cells from neighboring cells is partly due to the lack of specific cell adhesion molecules, such as cadherins, that hold normal cells in place [51]. Changes in the expression of integrins have also been reported in the case of malignant cells [52]. Integrins mediate cation dependent adhesion to extracellular matrix molecules and to cell surface ligands.

2.7 Neoplastic Adhesion and Surface Charge

One factor that has been found to affect cancer cell adhesion, which has also been investigated for non-malignant cells (and discussed in an earlier

section) is the surface charge. An invasive human osteorsarcoma cell line, Saos-2, was used to study how positive and negative surface charges alter the adhesion of bone cancer cells [53]. The surface charge was modified by using silane with different functional groups, specifically methyl (-CH3), hydroxyl (-OH), carboxyl (-COOH), and amino (-NH2) groups. The relevance of choosing these functional groups is that cells frequently encounter them *in vivo*. As was mentioned in Chapter 1 of this dissertation, the surface charge is a parameter which is frequently mentioned in literature as affecting cell adhesion. Although certain reports state that the polarity is what affects the adhesion process, other reports, such as the one presently discussed, state that polarity alone cannot explain this, since cells have been reported to adhere and proliferate on both positive and negatively charged surfaces. This is also the case for the Saos-2 cancer line. The fact that the polarity cannot explain cell adhesion is indicative of many factors that affect this process, including proteins present in the serum and the topography of the surface being used for the culturing.

2.8 Neoplastic Adhesion and Topography

One aspect of metastasis that is as of yet not fully understood is the effect of surface topography on metastatic cell adhesion. The general process, which was discussed earlier within this chapter, is the following:

1. Detachment from a primary tumor
2. Travel through one of the two “highways”, i.e. the circulatory or lymphatic system
3. Attachment to a secondary site
4. Proliferation of malignant cells and degradation of normal cells at secondary site

Although these steps are known to occur, the reason why cells attach at the secondary site is as of yet illusive. It is known that in some instances the secondary site is an organ that is in the path of the circulatory or lymphatic system. That is, after the motile cells are travelling, the next organ they come across (which is of course affected by the direction of blood or lymphatic fluid) becomes the invaded tissue. But this behavior has not been observed for all cell types; some cells, such as those occurring from lung cancer, actually travel further and bypass other organs. A majority of reports show that lung cancer cells travel and invade bone and brain tissue [9].

As in the case of non-malignant cells, motile cancer cells are faced with various types of topographies. Cells either attach to other cells or to ECM matrix. In the case of ECM, these topographies vary as well as a result of the components that are present. Elastin may be present at higher quantities in areas of the body that require more flexibility, such as blood vessels. Collagen on the other hand may be present in areas where structure or tensile strength are necessary, such as cartilage. Although both types of proteins are fibers with dimensions in the nanometers, they assemble differently and hence will affect the

topography of a surface. This is of great relevance to malignant cell adhesion, as previous reports have shown that cancer cells change their morphology and how to adhere to surfaces as a result of the topography [7, 36].

In a study by Lehnert and colleagues, microcontact printing was employed to produce surface patterns. Microcontact printing, a type of soft lithography, is a method in which PDMS stamps are used to stamp a pattern of choice onto a substrate. The actual process steps for making PDMS stamps is reserved for discussion in Chapter 3. Patterns of ECM dots and squares on silicon were produced with varying sizes as well as distances between them. The motivation was to understand how ECM arrangement affects cell anchoring, since it is known that *in vivo* cells adhere to ECM, basal lamina, or to other cells. It was concluded that depending on the dimension of the ECM pattern, the focal adhesion sites terminated at the dots or squares, as visualized by labeling the actin cytoskeleton. In the case of the dots, cells had focal adhesions terminating at the ECM patterned sites when there was a spacing of 5 μm center-to-center, with a size ranging from 1 μm^2 to .25 μm^2. When the dots were .1 μm^2, cells no longer were affected by the pattern, and the cells did not show lateral spreading [39].

2.9 Summary

Bioadhesion is a complex process in which a vast number and variety of molecules and pathways are in concert. The surface characteristics also affect

whether a surface is fouling or non-fouling; these include roughness, mechanical properties, and wettability. Another additional factor is the cell line; as different cells express varying amounts of surface proteins involved in the adhesion process, the actual line used will also affect whether adhesion occurs. A distinction between malignant and non-malignant cell adhesion has also been discussed. As elucidated in this chapter, studies have shown that combinations of these variables can be used to control bioadhesion. But to generalize and conclude that certain conditions apply to all bioadhesion processes is impossible.

Chapter 3

Surface Instabilities in Dynamic Hydrogel Films

3.1 Introduction

Wrinkles are a form of surface instability that exist everywhere in nature, from human skin to fruits, and even crumpled paper produces a similar effect [4, 54]. There are a number of reasons why and how these are formed. For instance, human skin, which is the largest organ in the human body, consists of three layers: the epidermis, the dermis, and the hypodermis. The epidermis is ~50 to 100 μm thick depending on location. It is composed of a layer of dead cells (stratum corneum) and a layer of living keratinizing epithelial cells. The structural components of the dermis are elastin, collagen, and extracellular matrix (Fig. 3.1). Due to their differences in composition, there is a mismatch in elastic modulus. The epidermis is much stiffer than the underlying dermis. Cerda and coworkers have found that the wavelength of the wrinkles is proportional to the skin thickness, which explains why wrinkles in the eyelids, for example, are quite small compared to areas of the body that have thicker thin [54].

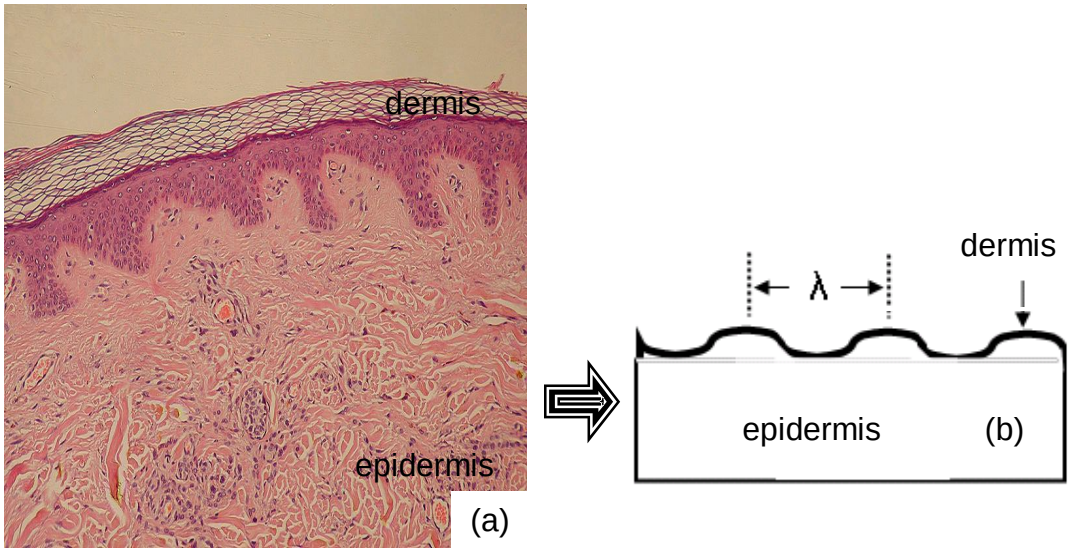

Figure 3.1: (a) Stained slide of epidermis and dermis, 10x [3] and (b) schematic showing the dermis and epidermis [4].

Fruits are another instance in which compressive forces change the topography of the surface. In the case of a plum, for example, the evaporation of water from the fruit causes a change in the foundation, causing it to shrink. The more rigid skin, as a result of the shrinking foundation, also changes, and hence the topography becomes one with wrinkles. However, it should be noted that the compressive forces are different, as the ones in this case are a result of evaporation, whereas in the case of skin the compressive forces are due to a combination of location of the skin vs. muscle contraction, as well as the components of the skin (the amounts of extracellular matrix components elastin, collagen, etc.) present [54].

The study of surface instabilities is currently being investigated, since an understanding of why and how these are formed is necessary in order to apply these materials for devices. Depending on the application, these instabilities may

or may not be desirable. Therefore, understanding their formation as well as their characteristics under and as a result of various conditions is necessary.

3.2 Overview of Surface Tuning Methods

The ability to tune surfaces, especially those involving polymers, has enormous implications in numerous areas, including biomedical and optics [55, 56]. Surfaces can be fabricated using a variety of methods, which include photolithography, electron beam lithography, grafting, focused ion beam, and soft lithography. The end-result of these processes is wide ranging, from sponge-like topographies with 3-dimensional characteristics in the micron range, to basement membrane-like surfaces in the nano-range [1, 57]. Knowledge of how fabrication processes affect surface structure is imperative since these factors affect their efficiency.

Photolithography has been widely used used since the 1970s for the fabrication of electronic devices [58]. This same technology has been employed to fabricate non-electronic devices and surfaces, including microfluidic devices as well as biomimetic surfaces. The general process is to spin-cast a UV-light-sensitive polymer (i.e., photoresist), onto a substrate. The substrate is then placed in a mask aligner with the mask of choice containing the pattern to be produced. The mask, normally glass/chrome, is placed either in close proximity or in contact with the substrate. The sample is then exposed to UV, and subsequently developed using chemicals specific to the type of photoresist used.

The developing step serves the purpose of ridding the surface of uncrosslinked photoresist. This process is also used during soft lithography processing for making SU-8 molds. SU-8 is a highly viscous polymer that produces thick (>2.5μm) films. After patterning, these are used as a mold into which a polymer, polydimethylsiloxane (PDMS), is poured. After a curing step, it is detached from the mold. This PDMS, also referred to as a “stamp”, can then be used to pattern surfaces with, for example, proteins or silanes [59].

3.3 Mechanical Instabilities on Polymer Surfaces

Periodic surface features emerge on surfaces on confined hydrogel films when strain along the confined axis exceeds some critical value. This value is directly related to the anchoring of the film, and how much swelling the free side of the film is able to achieve before reaching this critical value. In the case of a surface having excess strain energy that is unable to be released through swelling, corrugations appear. The surface structure then changes from having virtually no features to one with wrinkle-like patterns. The patterns are related to a number of variables, which include film thickness and solvent exposure. By choosing a specific combination of these variables, the pattern can be controlled from one with bi-cusps to a honeycomb-like surface.

Control of surface topography has direct implications in numerous areas. By having the ability to control the strain of a surface, cell adhesion may be

mediated [47]. This leads to numerous experimental possibilities. For example, metastatic cancer cells could then be tested against different amounts of strain to understand the mechanism in which they readily attach and detach during primary and secondary tumor growth. A second area in which control of strain on a surface could prove beneficial is in tissue engineering; cell sheets could be harvested and cued to detach upon a change in strain. This method would circumvent conventional methods of using proteolytic enzymes to digest and in turn damage extracellular matrix components for detachment purposes.

The appearance of patterns on polymers as a result of mechanical instability has been studied extensively [60-62]. In the case of the polymer presented within this work, the thin films are bound to a silicon surface. When the polymer material comes into contact with a solvent, swelling occurs, as predicted by the Flory-Huggins theory [63]. Another important effect of water adsorption/desorption by the polymer is elastic instability, which is described by the Flory-Rehner theory. Because the film is attached to the silicon, it is unable to swell in the directions parallel to the substrate [63]. This limits the expansion to only one dimension, which causes the film to be in a state of biaxial strain as a result of the solvent exposure and osmotic pressure. To alleviate this excess strain energy, the film buckles, or forms surface corrugations. This change in topography is directly related to the swelling of the polymer, and therefore we predict a change in these surface corrugations, or wrinkles, with a change in film thickness. A variation of the solvent also causes a change in the surface

topography, since it is known that the solubility parameter of a solvent affects the degree of swelling of a polymer, and hence the surface topography [64].

The Tanaka group was at the forefront of describing the morphological and kinetic changes that occur as a result of a free side of a copolymer of acrylamide with sodium acrylate gel swelling while the opposite side is anchored to a substrate [60]. The gel was allowed to swell for increasing amounts of time, from 1,800 to 63,000 seconds. Optical images showed the evolution of the pattern with time; the surface began showing cusps, or folds, at t= 1800 s. The width of the cusps increased until the surface reached a quasiequilibrium, at which point the surface resembled a honeycomb structure. The initial thickness of the polymer film was also varied, and they showed that the thickest gel (2.65 mm) had the highest change in structure relative to the thinner films (1.00 and 2.15 mm). Overall, the wavelength of the cusps increased linearly with an increase in thickness [60].

Recently, other groups have reported numerous methods for producing surface variations in the forms of wrinkles and/ or buckles on polymer surfaces; these include varying the fluence of an ion beam on the surface or depositing a thin metal film above the polymer film [55, 62]. Moon *et al*. used a focused ion beam (Ga^{+}) to produce crosslinks in 3 mm-thick PDMS (elastomer to crosslink ratio of 15:1) polymer films. The mechanism for wrinkle formation in their procedure was described as follows. The crosslinking of the PDMS film, since it mainly occurred at the surface, caused a thermal mismatch between this layer (called the stiff skin) and the bulk polymer, giving rise to the stiff skin buckling

and forming wrinkle patterns. The characteristics of the wrinkle patterns were controlled by varying the ion fluence; wrinkle patterns created using this method include straight, 1-dimensional lines, herringbone, and “nested” [55].

Another method for creating surface patterns involves the coupling of photolithography and depositing metal on PDMS. Huck *et al*. first selectively exposed the polymer to UV irradiation, which made a “stiff skin” on the upper-most layer, as was done in the previous case [62]. The polymer was then heated to 100ºC, and while at this temperature a 50 nm thick film of gold (and a 5 nm titanium adhesive film) was deposited above the polymer. Upon cooling, the compressive stress between the gold film and the polymer was relieved by forming wrinkles and buckles. Although similar in principle to the work performed by the Moon group, as both cases of mechanical instability give rise to instability patterns on the polymer, there are some obvious differences in the procedures utilized. The cause of the thermal mismatch in both cases can be attributed to different methods, and additionally the Huck group had an additional step of pre-treating the PDMS- the polymer was soaked in a solution of benzophenone and dichloromethane, which was followed by photolithography as described above. This step had an additional effect not only in the swelling of the polymer, but in the crosslink density due to the production of free radicals of the benzophenone during UV exposure. The combination of these various steps produced wavy structures with a repetitive pattern described as sinusoidal. Analysis of the buckles showed an inverse relationship between the wavelength and the amplitude with increasing UV exposure time. The wavelength varied from ~22 to

40 μm, while the amplitude varied from ~2.2 to 3.8 μm [62]. Another interesting finding from these experiments was the alignment of the buckles; in locations close to the boundary of the treated PDMS areas, the buckles were perpendicular to the “direction of maximum compressive strain” [63].

Yet another method for varying the surface topography was developed by Sharp *et al*., and involves immersing an aliphatic polyester in water [65]. This method, unlike the two aforementioned, yielded blisters and wells (craters). Polyester (poly-d,l-lactide) (PLA) in chloroform was spin-cast onto silicon. After an annealing step, the samples were placed in heated water. The time that the samples were placed in the water, the temperature of the water, and film thickness were varied. The general process produced blisters ranging from ~0.2 to 1.4 μm in diameter with increasing polyester thickness from ~25 to 200 nm. The blisters collapsed and became craters covered with the polymer once the samples were removed from the water treatment. The mechanism was attributed to buckling instability as a result of osmotically driven swelling between the polyester and water as the poor solvent [65].

The Sharp group was not the first to produce blisters on polymer surfaces; another group that reported this effect is the Li group (circa 1994) [66]. In their work, acrylamide/sodium acrylate (PAAM/SA) in water was cast between a GelBond film and a glass slide. The bottom of the gels were covalently bonded to the GelBond film during this process. After casting, each sample was dipped in water for 24 hours. Swelling of the polymer films in water produced hexagonal pattern formation (cusps). Following the water treatment, samples were exposed

to concentrations of water/acetone ranging from ~30 to 70%, for increasing amounts of time. After approximately 6 hours, formation of bubbles was apparent. The hexagonal patterns had evolved into bubbles as a result of the cusps, or folds, shrinking [66].

A logical question arising from comparing Li's and Sharp's work to the aforementioned instances of mechanical instability is the following- what is the different mechanism driving some procedures to produce wrinkles and/or buckles, while others produce blisters/ craters? To begin dissecting this issue, one obvious difference is the material. In the wrinkle/ buckle examples, PDMS is the polymer in use. In the blister formation investigation, an aliphatic or PAAM/SA polymer is used. The procedures are also different, with the former using the "skin effect" of crosslinked PDMS to produce a thermal mismatch between this and the bulk material. Sharp used a combination of annealing the polymer followed by immersing the sample in heated water, while Li used acetone and water mixtures to evolve cusps from hexagonal shapes to bubbles. The mechanism for bubble formation given by Li was as follows. A cusp, or fold, was initially formed by the swelling of the film in water. The introduction of acetone caused a shrinking of the polymer, at which point the areas between cusps began experiencing compression. After some time, these areas continued this process until the cusps became the boundaries for the bubbles that formed between cusps. A possible explanation, and one which will be further discussed in the results section of this chapter, is the solvating parameter. This parameter is significant within works in which materials, specifically polymers, were exposed

to solvents, since different solvents swell polymers to varying extents and hence affect the amount of residual stress produced. These methods for producing patterns are based on a mechanical instability of some form, and each has produced a change in surface topography as a result of this. Our report, although also based on mechanical instability to control the surface topography, differs in the method and resulting topographies.

The surface corrugations reported in this dissertation have been systematically investigated. The effects of film thickness, geometry of the patterned polymer, and solvent combination were examined. The resulting surface structures were imaged with both AFM and optical microscopy. We observed that the wavelength and width of wrinkles were dictated by the thickness of the polymer. Specifically, an increase in thickness led to an increase in both of these parameters. The geometry of the pattern, on the other hand, did not show a significant change in wrinkle dimensions, as all of the patterns fabricated were of rectangles with varying dimensions. The developing solvent did prove to be a crucial factor in the resulting topography, as a change in topography between wrinkles and bubbles occurred when the solvents were varied from water or combinations of water/ acetone versus only acetone.

3.4 Experimental Section

3.4.1 Preparation of Polymer Coatings

A series of photocrosslinkable copolymers based on PNIPAAm and methacroyloxybenzophenone (MaBP) were developed for these experiments. Coatings are created by spin-casting the polymer followed by ultraviolet (UV) radiation, which triggers the n-π* transition in the benzophenone groups leading to the formation of a biradicaloid triplet that abstracts a hydrogen from a neighboring aliphatic C-H group leading to a stable C-C bond. The transition characteristics of the layer can be tuned by altering the crosslink density.

3.4.2 Preparation of Patterned Thin Films on Silicon

Silicon substrates were plasma treated to create -OH functionality on the native oxide. The substrates were then treated with a fresh solution of 3-Aminopropyltriethoxylilane (1% in acetone) for 10 minutes to create a layer of NH2 groups that bind to the polymer. Following the silane treatment, the substrates were rinsed with fresh acetone and dried with nitrogen. The polymer was then spin-cast onto the wafer at 500 rpm for 3 seconds, followed by 1800 rpm for 20 seconds. Next, a solvent bake was performed, at 100°C for 5 minutes. The sample was allowed to cool down for 10 minutes, after which the mask of choice was placed directly on top of the sample. The mask was varied between one which produced lines 500 μm x 1 cm (with 1 cm being the length of the

sample), and 170 μm x 200 μm lines. Hereafter, the first geometry will be regarded as pattern 1, while the second will be regarded as pattern 2. A UV lamp (λ=350) was placed directly above the mask which was in contact with the sample. The sample was exposed for 5 minutes. The solvent of choice (acetone and/ or water) was then used as the developer.

3.4.3 Atomic Force Microscopy

A Digital Instruments Dimension 3100 Atomic Force Microscope with NanoScope Software was used to obtain non-contact atomic force microscopy images. A silicon tip with a length of 10 μm and a curvature of ~15 nm was used for all measurements. Atomic force microscopy, or AFM, is a technique similar to that of the profilometer, except that the resolution is much smaller (down to nanometers) (Fig. 3.2). A very sharp tip in the shape of a pyramid, known as a cantilever, was dragged across a surface; the change in vertical position due to van der Waals forces reflects the surface topography [28, 29]. AFM was used to obtain the surface roughness of a surface. The software utilizes quadratic averaging for this purpose.

The Root Mean Square (RMS) Roughness is the standard deviation of the Z values within a given area. Z ave is the average Z value within the given area, Zi is the current Z value, and N is the number of points within a given area.

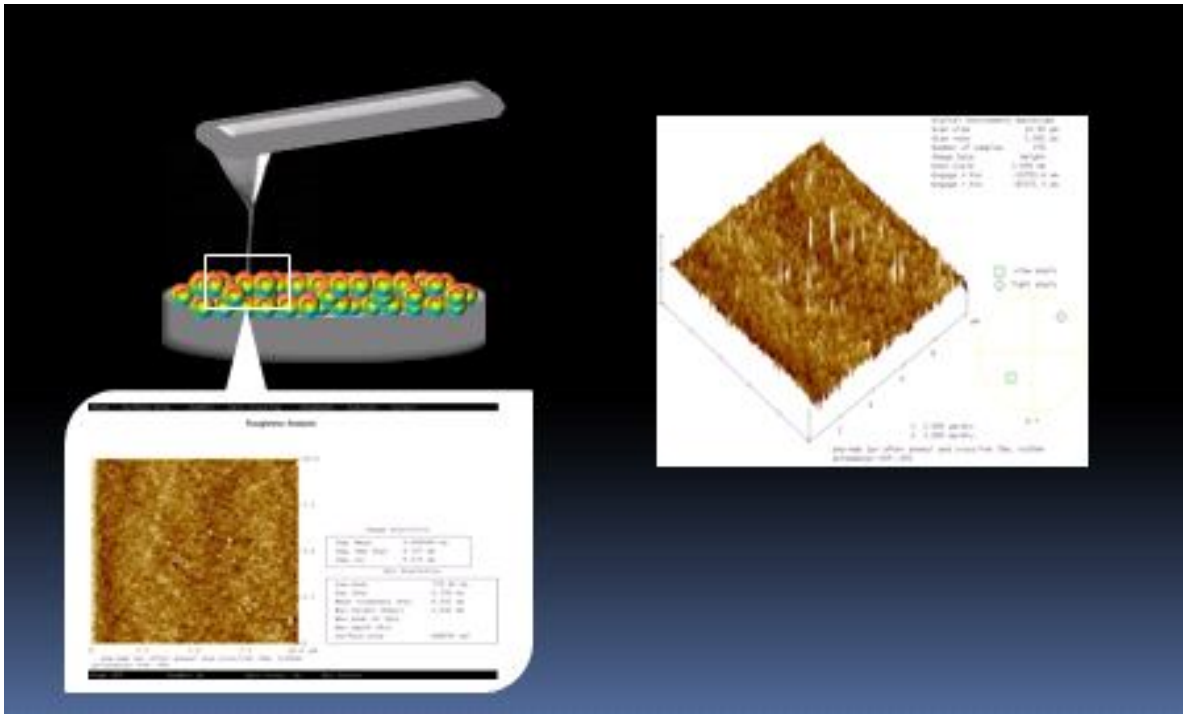

Figure 3.2: Schematic of an atomic force microscope tip and examples of topography images.

3.4.4 Ellipsometry

The polymer film thickness produced after spin casting and crosslinking were assessed with a Rudolph ellipsometer (HeNe laser). Three points were taken for each sample and averaged. This metrology step is a non-destructive method which measures the change in state of polarized light upon reflection from a surface [67]. White light is polarized during the measurement process; this polarized light can be decomposed into two orthogonal vectors, p (parallel to the plane of incidence) and s (perpendicular to the plane of incidence). Circularly polarized light reflects off the sample, which causes the p and s components to experience different amplitude and phase changes (Fig. 3.3) [67].

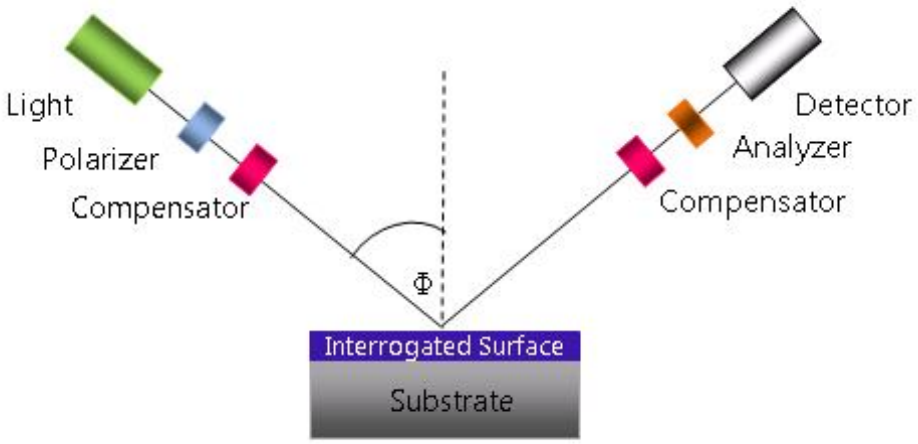

Figure 3.3: Schematic of a constant angle ellipsometer.

3.5 Results and Discussion

3.5.1 Wrinkle Formation

Surface instabilities in the forms of wrinkles were observed after the fabrication process was completed (Fig. 3.4). In an attempt to pinpoint the fabrication step that was causing these wrinkles to occur, a short set of experiments was performed. From these experiments it was determined that the developing step produced wrinkles on the samples. Samples were made using the following conditions:

1. Dip10 minutes in APTES (1% in acetone)
2. Rinse with acetone
3. Solvent bake, 40ºC for 1 min.

4. Spin polymer; 3 s. at 500 rpm, then 20 s. at 1800 rpm
5. Solvent bake, 90 ºC for 2 min.
6. Cool down: 5 min.
7. Expose using photolithography: 5 min. UV exposure
8. Develop: 10 s. acetone rinse, 10 s. DI water rinse (note: this was the developing step for most, but not all samples)
9. Nitrogen dry

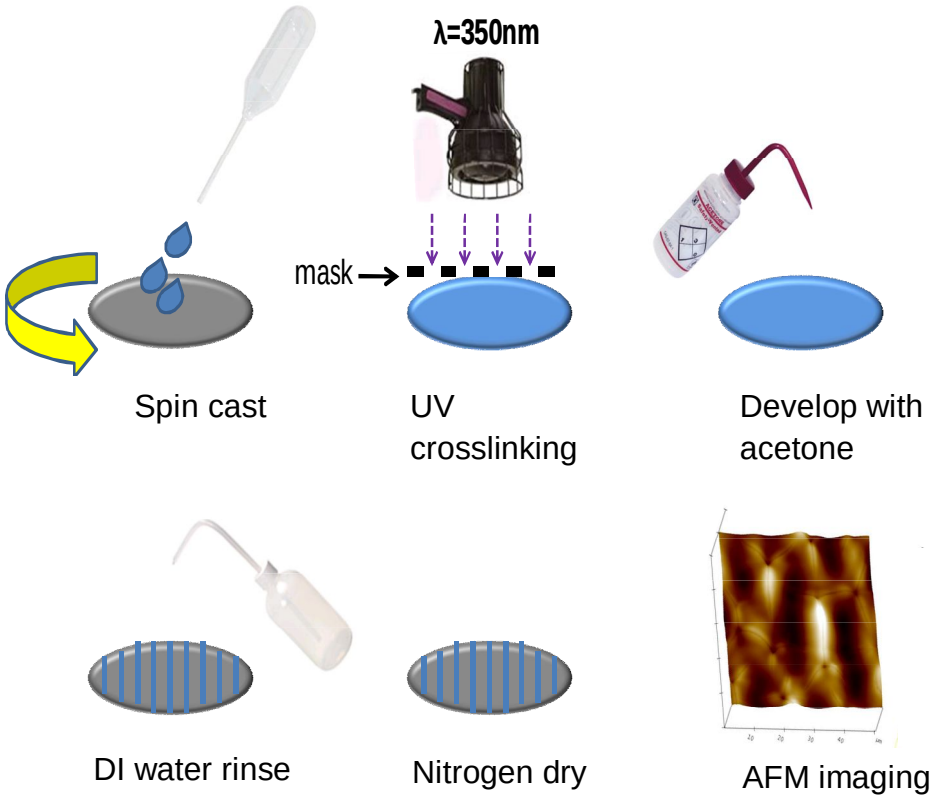

Figure 3.4: Schematic of processing steps; the end result is a patterned polymer surface with surface instabilities.

Half of the samples were developed using acetone and water, and the other half were not developed. After AFM imaging, it was apparent that the samples that had been developed using acetone and water did have wrinkles, while those in which the developing step was omitted did not. Figures 3.5 and 3.6 are samples from this experiment; Figure 3.5 is the height image of a 400 nm thick surface in which the developing step was omitted. This image, scaled at 10 nm, shows that no wrinkles were produced. There were slight variations in film uniformity, but no actual cusps were present. Figure 3.6 is also a height image of a 400 nm film, but in this case there was a developing step of 10s acetone rinse followed by 10s DI water rinse. At a scale of 100 nm, wrinkle formation was apparent.

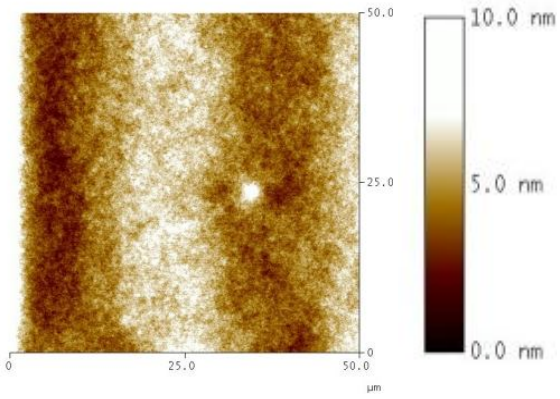

Figure 3.5: AFM image of a 400 nm film without a developing step.

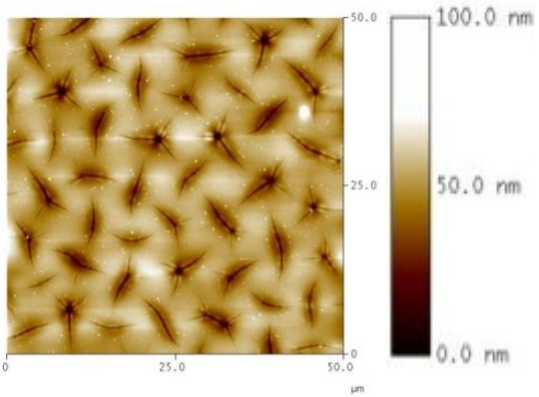

Figure 3.6: AFM image of a 400 nm film with the developing step.

3.5.2 Wrinkle Characterization

Surface corrugations on the polymer were imaged via AFM as previously discussed. The wavelength, width, and amplitude were quantified as the thickness was increased. For each thickness, the edge and middle of the pattern were imaged. The purpose of this step was to ascertain whether there was a difference in topography between the two locations, as it has been previously reported that the topography can depend on the location from the strain [63]. The geometry of the patterned polymer was also varied to examine whether the number of free edges would change the strain, and in turn, the slippage of the polymer film. Figures 3.7 and 3.8 are optical images of the patterns that were used in these experiments.

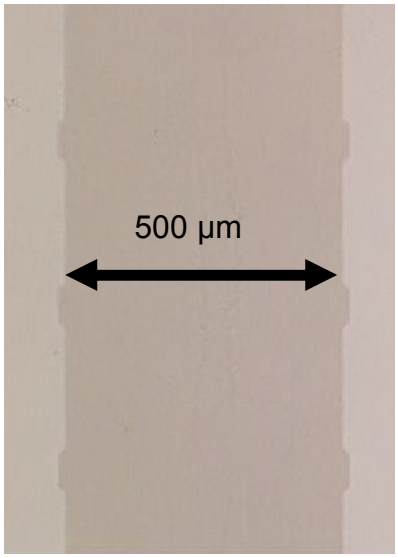

Figure 3.7: Optical image of polymer pattern 1.

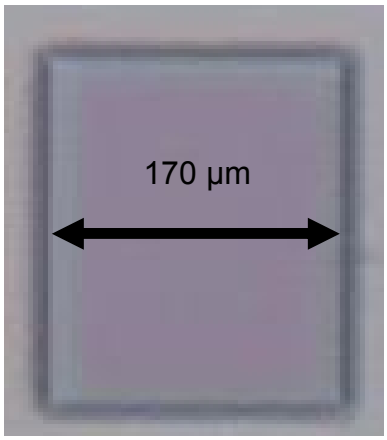

Figure 3.8: Optical image of polymer pattern 2.

The wavelength of the wrinkles was quantified for each thickness using AFM images. Either a section analysis using Nanoscope software of the image was performed to obtain the wavelength (Fig. 3.9), or ImageJ was used to measure the peak-to-peak distance from the section image. The wavelength (λ) increased with an increase in thickness for both pattern 1 and 2, with the

exception of the two thinnest films (30nm and 180 nm). In the case of pattern 1, the wavelength increased from .5 to 23 µm at the edge of the pattern, and from .5 to 30 µm at the middle (Fig. 3.12). Pattern 2 had a similar relationship with the wavelength versus an increase in thickness. At the edge of the sample, λ varied from .3 to 30 µm, while in the middle of the sample the range was from .3 to 32 µm (Fig. 3.13).

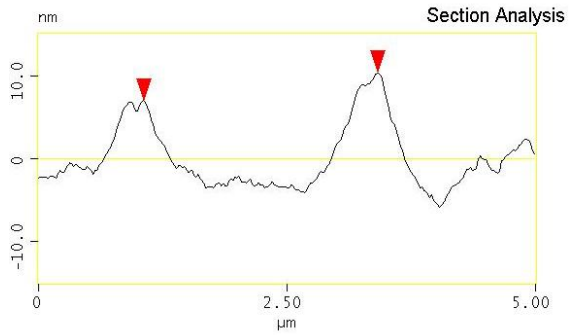

Figure 3.9: Example of wavelength measurement using AFM Nanoscope software section analysis.

The negligible increase in λ when the thickness was varied from 30 to 180 nm may be due to the difference in the actual topography produced and how this parameter was measured; the two thinnest films had a complex topography in which there were wrinkles that crossed under and over each other. This intricate topography might have led to a discrepancy in the measurement, as it is nearly impossible to decipher from the images where one wrinkle ends and another begins.

The wavelengths reported within this work, although they follow a general linear increase with an increase in thickness, differ in that the relationship in other reported cases depend on the wavelength, film thickness, Poisson's ratio (for a skin or foundation), and the strain [68]. This relationship states that the critical thickness for instabilities to occur is 3 times the wavelength. Within this work, the wavelengths are approximately 30 times the thickness.

The width of the wrinkles was also measured as the thickness of the film was increased. As exemplified in Figure 3.10, the width was measured from one area which had a baseline of the topography, to another area after the wrinkle, which also had a baseline. This was done using two methods. One was the section analysis option in the Nanoscope software, and the second was from the actual AFM images. The latter was accomplished in conjunction with ImageJ to measure the distance.

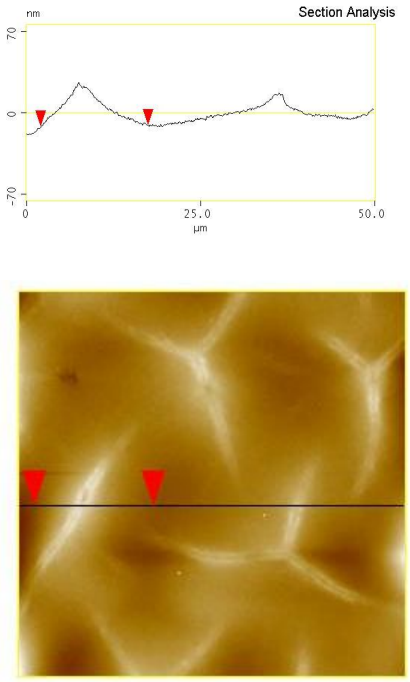

Figure 3.10: AFM image and width measurement of 800 nm thick film with pattern 1. The section analysis of a width measurement of a wrinkle is above.

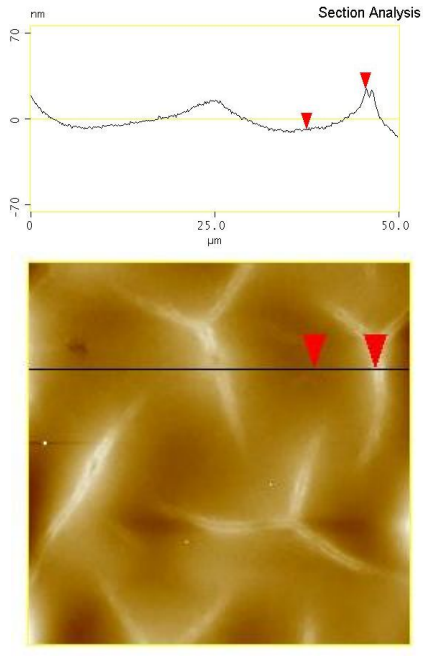

Figure 3.11: AFM image and amplitude measurement of 800 nm thick film with pattern 1. The section analysis of an amplitude measurement of a wrinkle is above.

The width of the wrinkles formed on the samples with pattern 1 ranged from .3 to 15 μm at the edge of the pattern, and from .3 to 17 μm at the middle. Pattern 2 wrinkles ranged from .25 to 7 μm at the edge, and .25 to 11 μm at the middle. The pattern 2 wrinkles yielded the highest width for the 800 nm samples at both locations, while for pattern 1 the highest widths were measured on pattern 1.

The amplitude of the surface corrugations was examined for all thicknesses (Fig. 3.11). As in the case of the wavelength and width, for pattern 1 a significant difference between the edge of the pattern and the middle was not observed. At the edge, the amplitude ranged from .35 to 14 nm, and at the middle ranged from .35 to 17 nm. There was, however, an approximately linear increase in amplitude with an increase in thickness.

It should be noted that these results differ from the case in which wrinkles have been fabricated by evaporating a thin rigid film above a compliant substrate-anchored PDMS layer [69, 70]. In Huang *et al.*'s investigation, nonlinear analysis of PDMS bonded to a rigid substrate was performed. Wrinkles were observed due to the compressive force of the stiff metal film upon the soft polymer, which itself was bonded to another rigid support. From their analysis, it was concluded that wrinkle wavelength remained almost constant as the amplitude increased. This finding elucidates the dependence of surface mechanical instability of a film to the substrate to which it is attached. A relatively elastic support is able to alleviate some of the residual mechanical stress, leading to constant amplitude [70]. A more rigid support, on the other hand,

because it does not yield to the stress, produces an increase in amplitude since the film cannot transfer any of the residual energy to the substrate. The wrinkles formed in Huang's work, although based upon the principles of mechanical stress, are due to a completely different mechanism. The wrinkles presented within this work have another variable not present in their work, and that is the responsive polymer. The polymer is rinsed with two different solvents (each having their respective solubility parameters), and as such it undergoes swelling and shrinking which is a factor in cusp formation, as well as the change in cusp dimension with changes in film thickness and solvent combination. This was shown in Figures 3.5 and 3.6 in which two samples were imaged and compared. The sample without the developing step did not have surface corrugations.

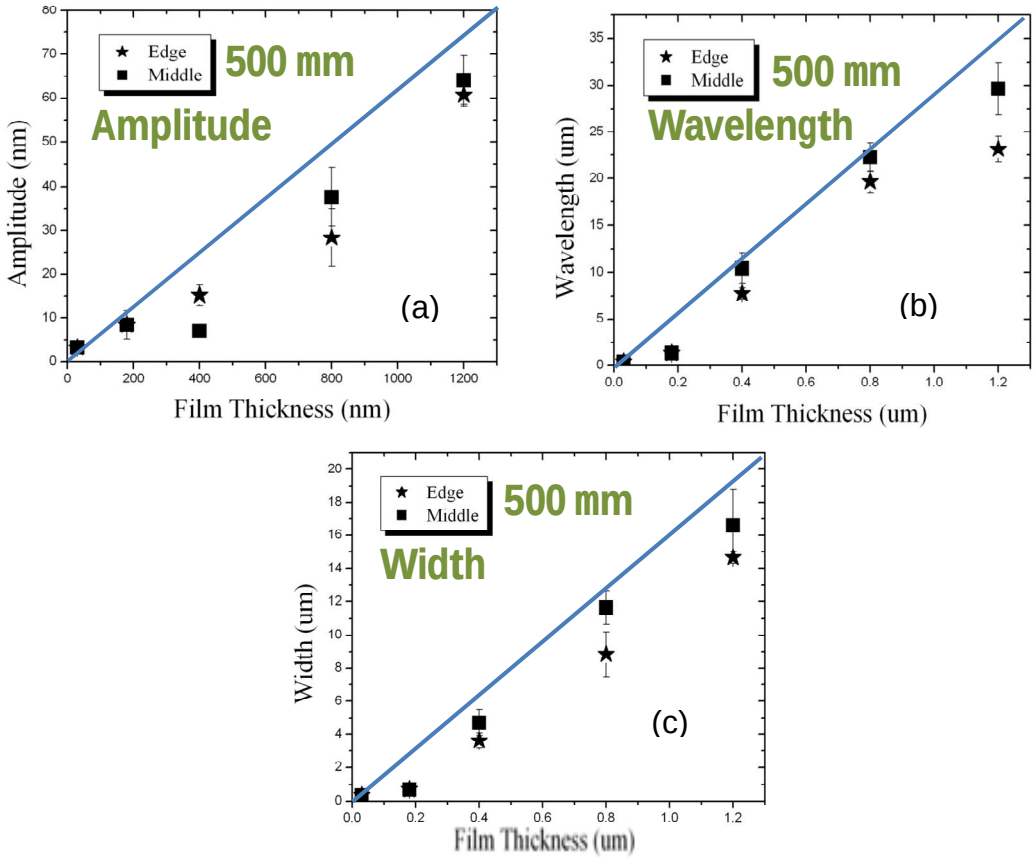

Figure 3.12: (a) Wrinkle amplitude, (b) wavelength, and (c) width versus film thickness for the 500 µm wide polymer lines.

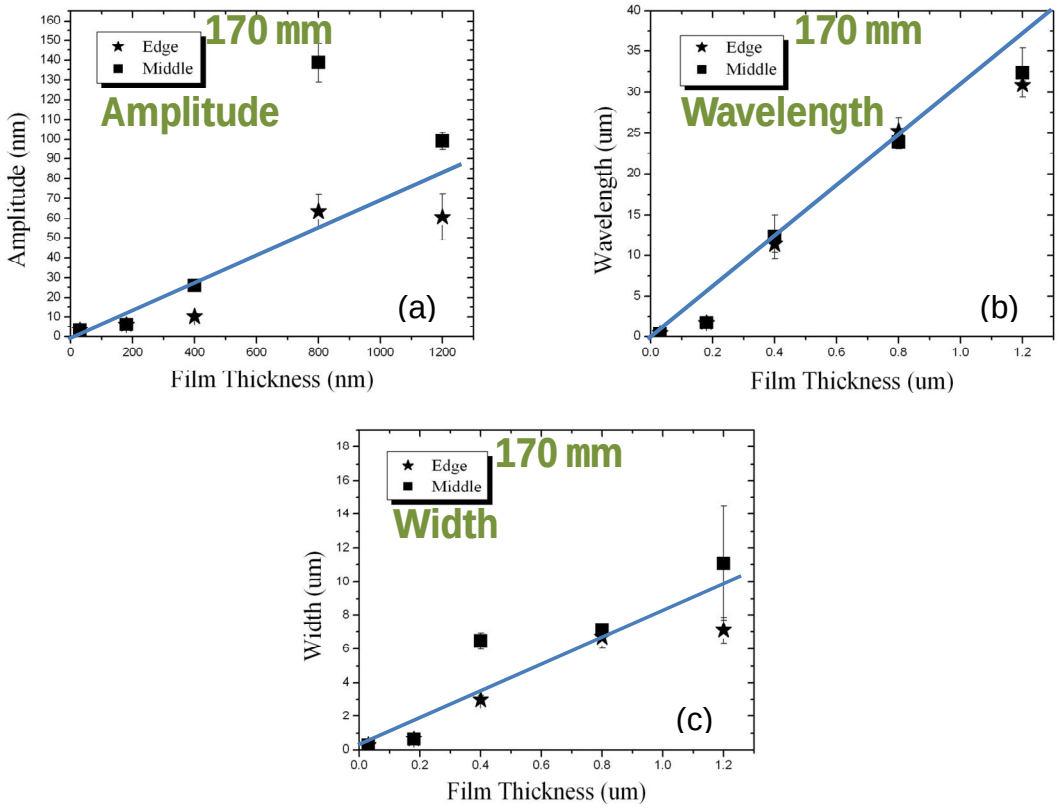

Figure 3.13: (a) Wrinkle amplitude, (b) wavelength, and (c) width versus film thickness for the 170 µm wide polymer lines.

The wrinkle dimensions, as shown in the above data, varied with increasing thickness. This is shown in Figure 3.14 (a) through (c); AFM images of the middle location of three different thicknesses were obtained. Image (a) and (b) are both 5 micron scans; a comparison of these images shows a significant increase in wrinkle dimensions with a film increase of 150 nm. Image (c) is a 50 um scan; it is worth noting that this increase in scan size by a factor of 10 shows both image (b) and (c) with wrinkles that are approximately the same size (as in the length of the branches). The wavelength did not change considerably

between the two film thicknesses, although the amplitude did increase by a factor of ~5.

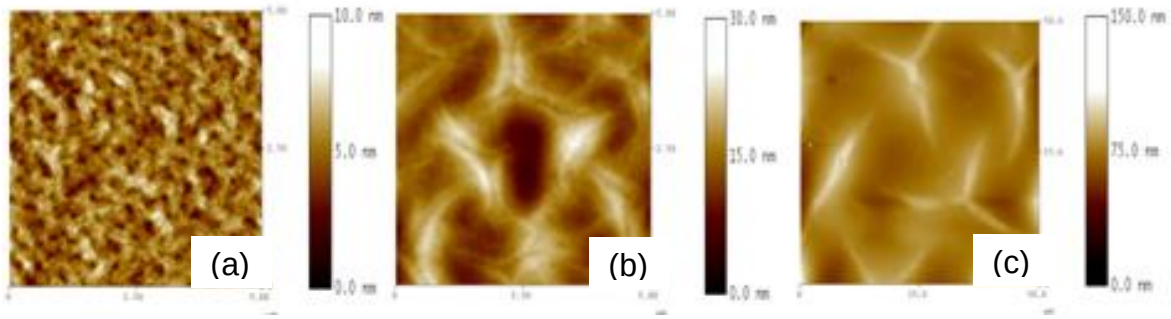

Figure 3.14: AFM images of the middle of (a) 30 nm, (b) 180 nm, and (c) 800 nm films.

Although the data in Figures 3.12 and 3.13 show a similar relationship of wrinkle morphology with increasing thickness, the data from pattern 2 (Fig. 3.13) shows a decrease in wrinkle width by a factor of ~2. This indicates a dependence of this parameter to the pattern geometry. The reason for this is the amount of free edges available in the case of pattern 2, which are four since it is a rectangle. In the case of pattern 1, although these are also rectangles, these patterns span the length of the sample (1 cm). Therefore, the two edges which affect the swelling and contraction of the film the most are the lateral edges. This, in the case of a vast majority of the polymer line, allows for only two free edges to be available for this change in swelling, thus causing an increase in residual stress in the middle of the polymer line. The residual stress in the middle is shown in Figure 3.15; the amplitude of the wrinkles increased as the section analysis was measured from the edge towards the middle of the sample.

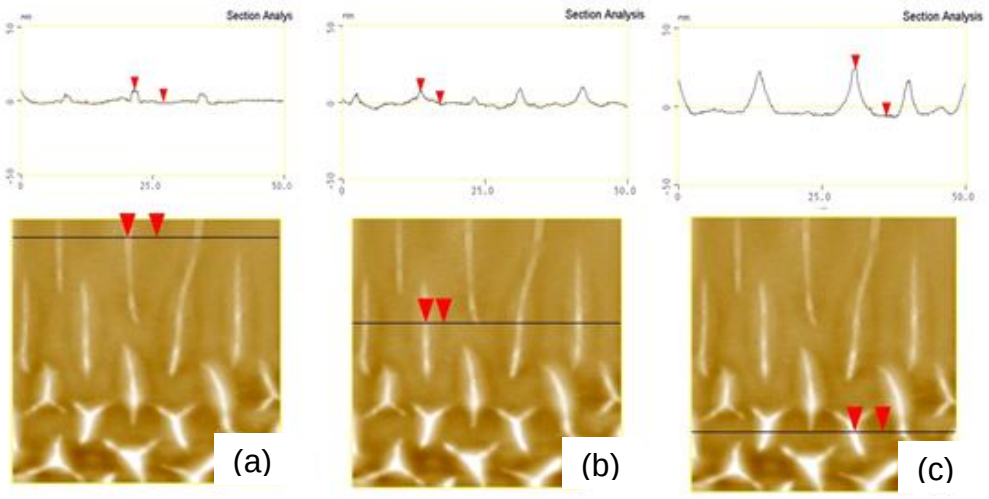

Figure 3.15: AFM images of the same 400nm thick film sample with (a) 10 nm, (b) 10 nm, and (c) 40 nm amplitudes. The images show the change in amplitude as the section analysis is varied from the edge to the center of the sample.

Another interesting effect of strain on wrinkle characteristic is that of wrinkle orientation. Depending on the location of where the sample was imaged, the wrinkles were either a single “line” (having no branches) emanating perpendicular to the edge of the polymer pattern towards the middle of the same pattern, or were unaffected by the edge and had a seemingly random orientation. This effect occurred in film thicknesses between 400 to 1200 nm. This location-dependent orientation of the wrinkles is due to the direction of compressive strain at the edges [62, 70]. The patterned polymer in Figure 3.16 was able to swell horizontally as well as vertically. Following swelling with the solvent, the sample was dried, causing the polymer to compress in the direction opposite to that of swelling. The wrinkles then aligned themselves perpendicular to the edges. But as aforementioned, in the middle of the pattern this relationship does not hold.

This orientation-dependent observation has been previously observed by other groups in the case of mechanically stretching PDMS films [54].

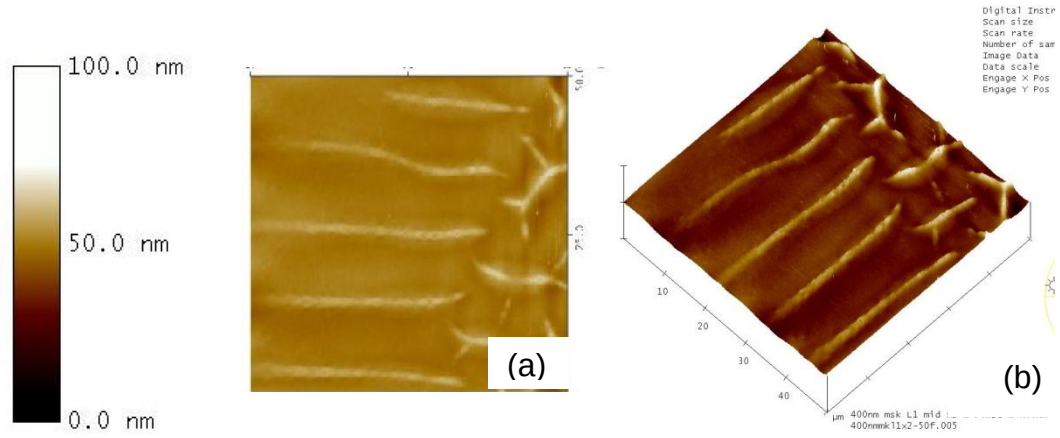

Figure 3.16: AFM image of the edge of a 400nm thick film with pattern 2. The height image (a) and surface view (b) have amplitude scales of 100 nm.

Below 400 nm, specifically with the 30 and 180 nm films, this location-dependent orientation was not observed when the samples were imaged at the edge of the pattern. Because these films were thinner, the compressive forces along the edges were no longer higher than those of the middle. Therefore, there was no perpendicular orientation along the edge. This was observed when comparing, for example, Figure 3.17 of a 30 nm sample, and Figure 3.18, of a 180 nm sample. The scan sizes were changed to accommodate for the difference in wrinkle size. The 30 nm sample does not show any preferential orientation to the edge of the pattern, which was located on the left side of the image. The 180 nm samples also did not show a relationship between wrinkle orientation and the edge of the pattern.

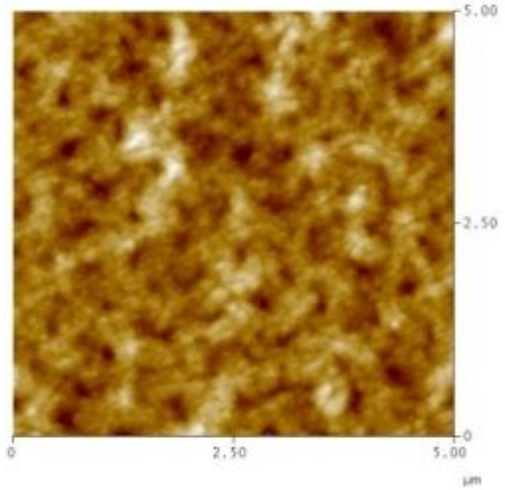

Figure 3.17: 5 µm AFM image of a 30 nm sample with pattern 1.

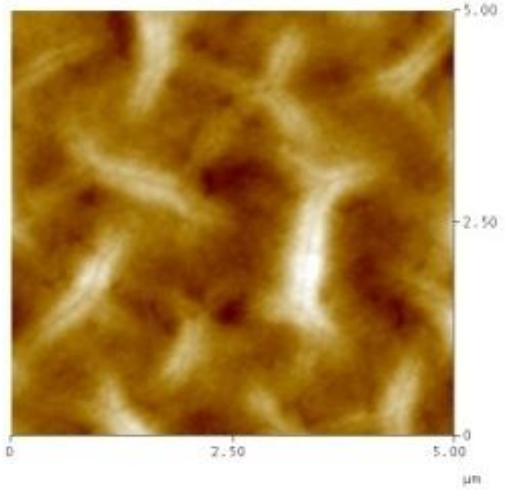

Figure 3.18: 5 µm AFM image of a 180 nm sample with pattern 1.

Another parameter related to the location-dependent orientation of the wrinkles is the number of branches radiating from a primary wrinkle. At the edges of the patterned polymer, the wrinkles do not have branches. Although the exact distance in which the wrinkles began having an increased number of branches is

also related to the thickness, the wrinkles ended up with a maximum of either three or four branches in the middle of the patterned polymer in the 400, 800, and 1200nm samples (Figs. 3.19 and 3.20). This was true for both patterns fabricated. As aforementioned, because the 30 and 180nm thick samples did not show a relationship between the location of the edge and wrinkle orientation, these thinner films had the same number of branches regardless of where the sample was imaged.

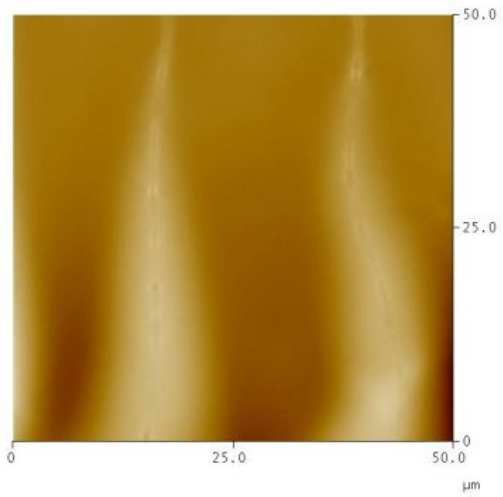

Figure 3.19: 50 µm AFM image of a 1200 nm thick film imaged close to the edge.

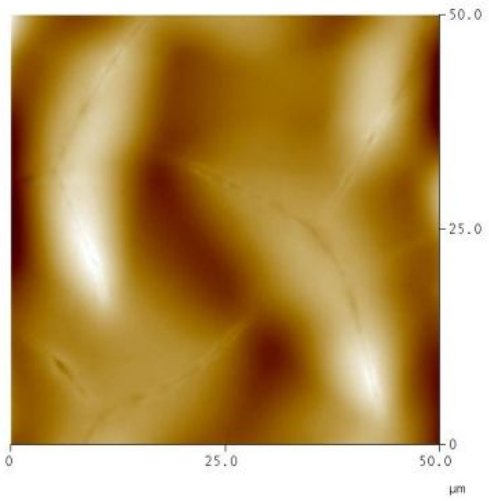

Figure 3.20: 50 µm AFM image of a 1200 nm thick film imaged in the middle.

Aside from the changes in width, amplitude, and wavelength, AFM images of the samples showed the presence of what resembles a crease (Fig. 3.21). This crease occurs in the middle of the wrinkles, regardless of film thickness or location of the instability. The creases were first observed after obtaining height images of the samples. By using sectional analysis, it is evident that these are present in the middle of the wrinkle. Section analysis of the samples at each thickness yielded similar results. The presence of these indentations has not been previously reported by any other group.

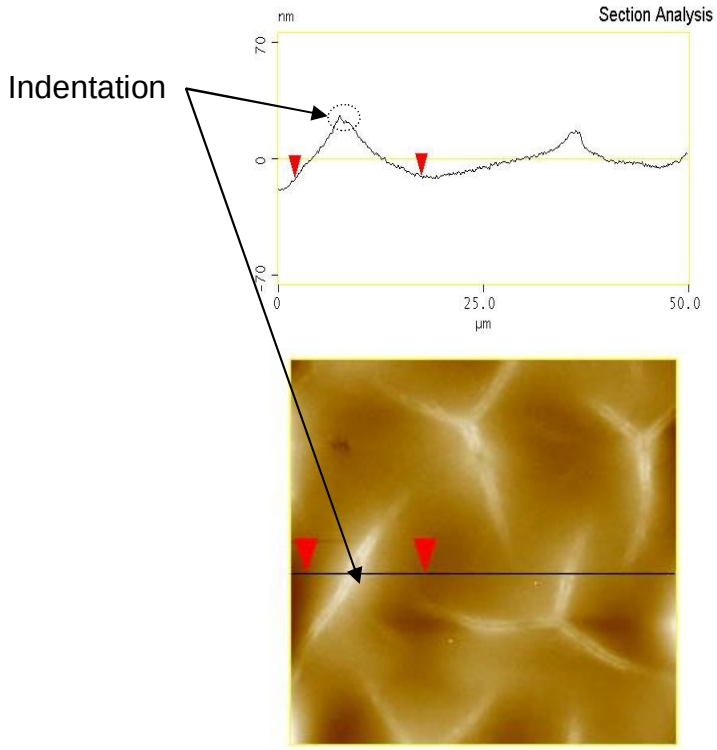

Figure 3.21: AFM image and section analysis showing the presence of an indentation along the length of the wrinkle.

As has been presented, wrinkle formation was evident using a variety of thicknesses. One interesting aspect of these instabilities is the wavelength. Throughout the investigations, this parameter was found to be fairly constant for each thickness. One question that arose from these was whether other wavelengths were present that had not been visible during the imaging step. To answer this, the images were rescaled to smaller values so that wrinkles with significantly lower values could be viewed if present. Figure 3.22 is an AFM image of a 400 nm thick film patterned with the 500 µm lines at a scale of 30 nm. When compared with Figure 3.23, which is an AFM image of the same sample but with a different scale, there were no additional wrinkles at the lower scale.

This rescaling was done on samples varying the range of thicknesses investigated. The rescaling showed that no other wavelengths or amplitudes were present.

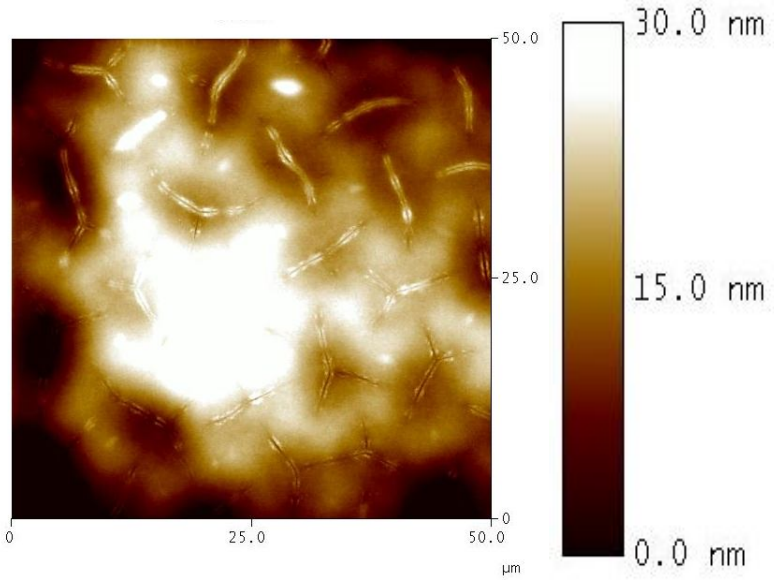

Figure 3.22: 50 µm AFM image of a 400 nm thick film; height image was obtained using a 30 nm scale.

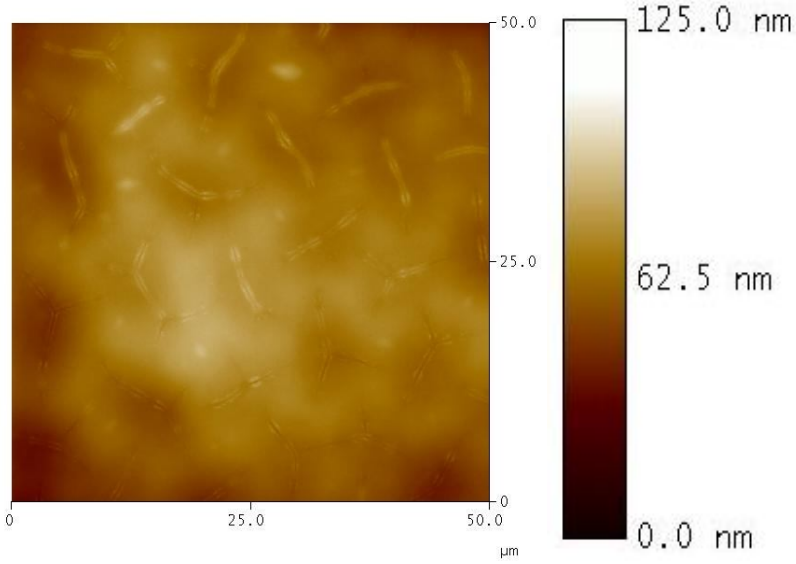

Figure 3.23: 50 µm AFM image of a 400 nm thick film (same image as Fig. 3.22); height image was obtained using a 125 nm scale.

3.5.3 Surface Roughness Analysis of Polymer Thin Films

The surface roughness of the films was also measured. This is of relevance to bioadhesion, where it is considered by some that this parameter affects whether cells or proteins will adhere, as well as the strength of adhesion of cells to the surface [71]. In the case of both patterns, there was an increase in RMS with an increase in film thickness. This relationship is approximately linear. Additionally, there was not any significant change in this parameter when comparing the middle to the edge of the pattern (Figs. 3.24 and 3.25).

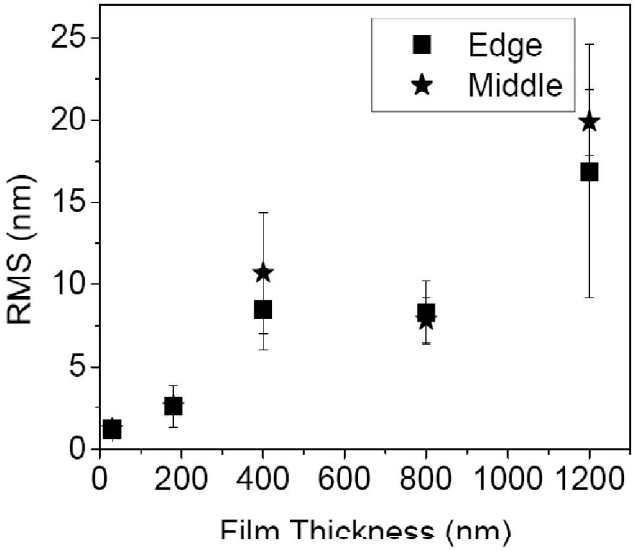

Figure 3.24: Surface roughness (RMS) versus film thickness for 500 um pattern, 1%MaBP.

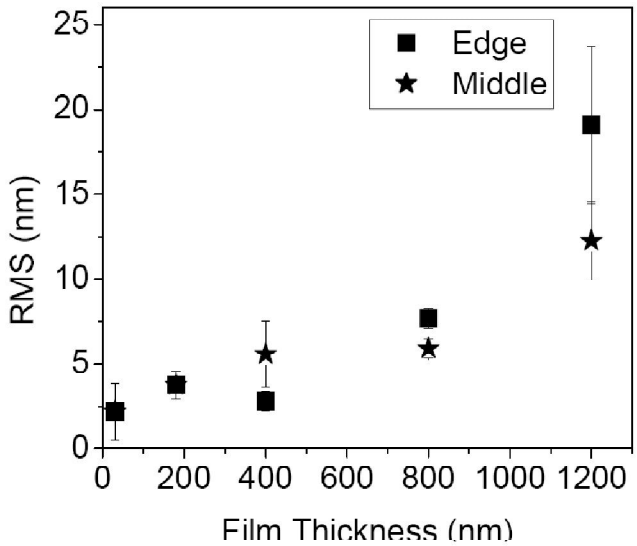

Figure 3.25: Surface roughness (RMS) versus film thickness for 170 um pattern, 1% MaBP.

3.5.4 Effects of Varying the Developing Step

In the previous section, each sample was fabricated with the following developing step- 10 s acetone rinse followed by 10 s water rinse. As aforementioned, these two solvents have different solubility parameters. This parameter is a thermodynamic property which assesses the miscibility of a polymer-solvent system. Miscibility is the ability of a substance to dissolve in a solvent. There need to be thermodynamically favorable interactions between the material and the solvent for this to occur. In work by Yagi *et al.*, the swelling of N-isopropylacrylamide was examined using various solvents [64]. The theory of Gee was employed for the experiments by Yagi; this theory predicts the extent to which a polymer will swell [64]. The maximum amount of swelling occurs with a

solvent that has a very close solubility parameter (or the same) to that of the polymer [64]. Table 3.1 has the solubility parameters of the solvents used in the work presented within this dissertation. Since this polymer is able to swell and contract depending on the solvent used, this may be affecting the morphology of the cusps and was therefore investigated.

Table 3.1: List of solvents and their solubility parameters.

Solvent	Solubility parameter at 25°C, $(cal/cm^3)^{1/2}$
Acetone	9.9
Dimethylformamide (DMF)	12.1
Ethanol (EtOH)	12.7
Methanol (MeOH)	15.5

A second solvent property which may be affecting the morphologies of the surface instabilities is the evaporation rate. This property is the decrease in volume with respect to time, or dV/dt [66]. It is conventionally reported as the rate relative to the evaporation rate of n-butyl-acetate, in which case the rate of this solvent is considered as 100 [72]. Acetone is considered as having a “fast” evaporation rate, followed by methanol, isopropanol, ethanol, and water. This parameter was deemed as having significance to this work as a result of previous reports which state that microstructures were observed after allowing various

solvents to evaporate on polymer surfaces and osmosis- related interactions between acetone and a polymer [56, 66].

To further investigate the effects of these solvents, samples were fabricated as previously mentioned. The general procedure was APTES adsorption, followed by spin-casting and patterning. The solvents were utilized directly after patterning for the development process. To understand the role of each solvent, they were individually examined during the developing step. It was observed that using water alone produced wrinkles, while acetone alone produced bubbles (Figs. 3.26 and 3.27).

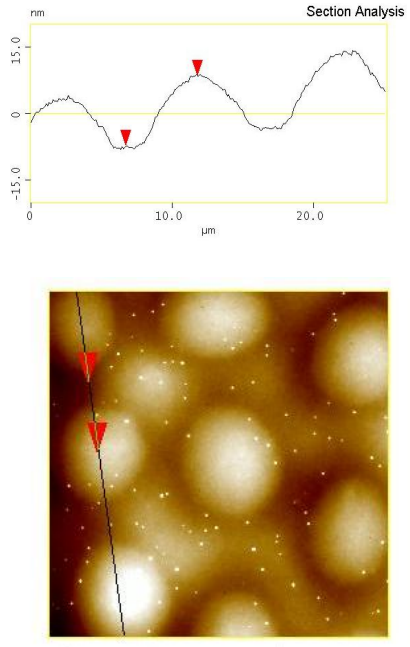

Figure 3.26: Section analysis of a 400 nm thick film, 25 um scan after a 10 s acetone rinse (no water rinse).

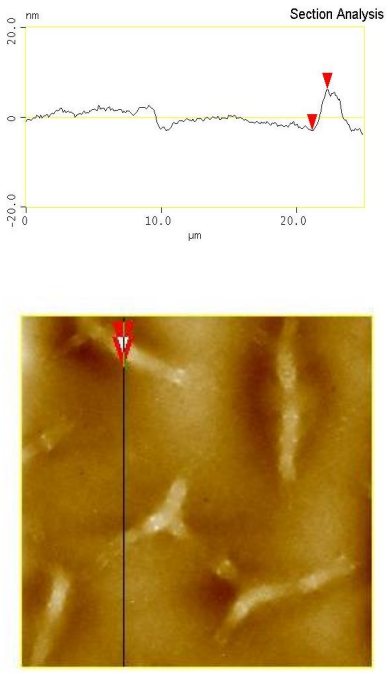

Figure 3.27: Section analysis of a 400 nm thick film, 25 um scan after a 10 s water rinse (no acetone).

The difference in topography is self evident. As aforementioned, the appearance of bubbles is in itself not novel, as it has been described before by Sharp *et al*. [65] . As mentioned in the introduction of this chapter, an aliphatic polyester, specifically poly(d-lactyde) (PLA), was utilized for their work. This polymer was spin-cast and subsequently submerged in water. The temperature of the water was varied, and from the AFM images bubbles and wells were observed. Bubbles were only observed when the sample was in the water, and wells were produced after taking the samples out of the water. This differs from the results presented within this work; the bubbles in Figure 3.26 were imaged after rinsing with acetone and drying. None of the samples produced bubbles when only water was used as the poor solvent, the effect from water as the sole

solvent was wrinkle formation. Additionally, all of the images were obtained with a dry sample. In Sharp's work, blisters were observed only when the sample was submerged in water [65].

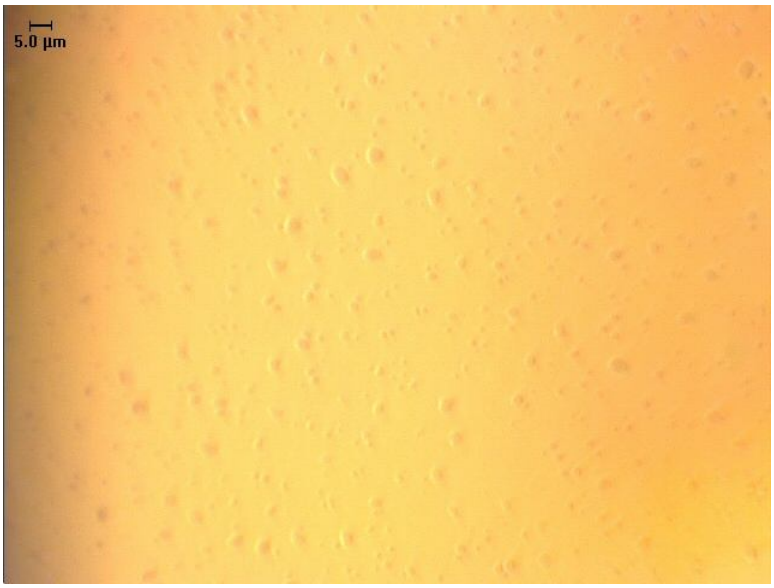

Figure 3.28: Optical image of bubble formation in a 500 um sample.

In the above experiment, samples were imaged after a 10 s acetone developing rinse while omitting water. For the next set of samples, the developing time was increased to 90 s. The bubbles were present throughout the surface, with varying widths. Not only were bubbles still produced as had occurred in the first case, but very small wrinkles formed as well (Fig. 3.29). The wrinkles formed in these samples, although also due to mechanical instability, have different characteristics than those formed during the 10 s acetone with 10 s water rinse, and also from the water alone as the developer samples. These

wrinkles do not have multiple branches, and are considerably shorter in length, width, and wavelength relative to other wrinkles produced using the aforementioned process conditions.

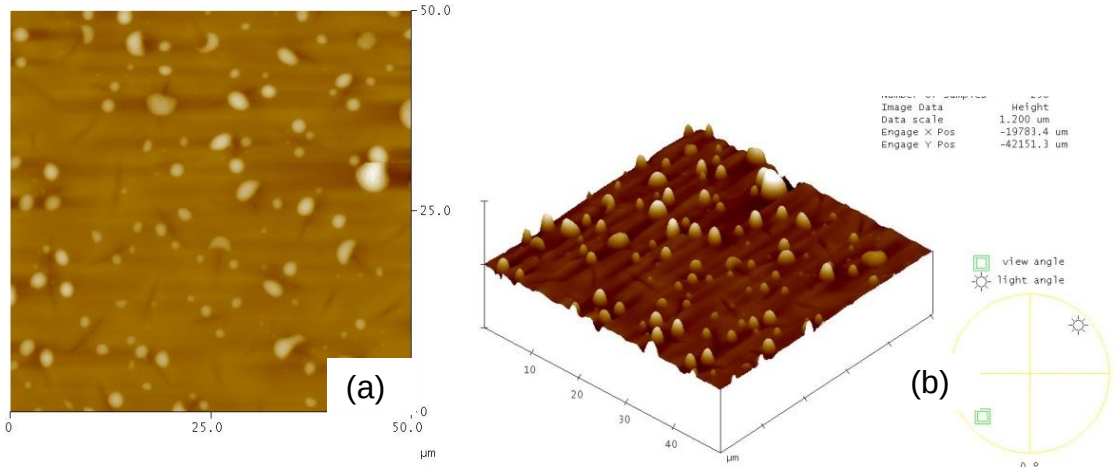

Figure 3.29: (a) 50 µm AFM height image and (b) surface view of a 400 nm thick polymer sample following a 90 s acetone dip and a 10 s water rinse.

The effects of increasing the final water time were also investigated. The processing conditions were again kept constant, except for the developing step. The water time following exposure to acetone for 10 s was increased for the last two sets. The data (Fig. 3.30) indicates that while the amplitude decreases with an increase in water exposure time, the wavelength stays between ~6 um to 11 um, regardless of this water time. The largest change in wavelength occurs after the time of water exposure is increased from 10 s to 10 s rinse plus a 60 s water dip. The last increase does not cause a significant change in either amplitude or wavelength (Figs. 3.31 and 3.32).

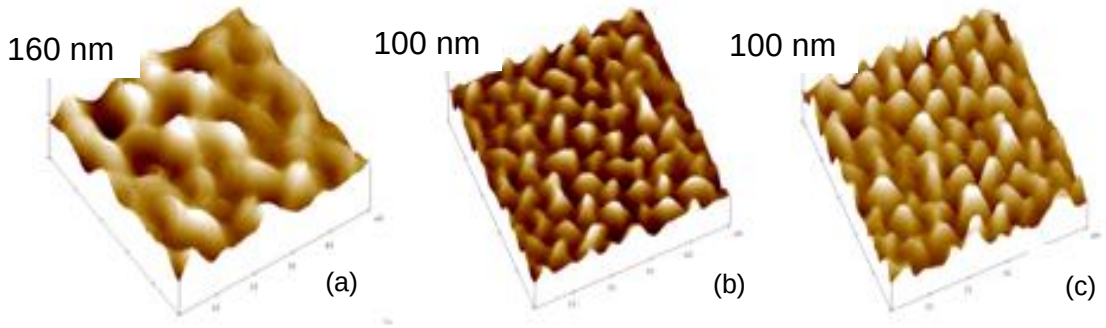

Figure 3.30: (a) AFM image of a 400 nm sample with a developing time of 10s acetone plus 10s water; (b) same conditions with an additional 60s water dip; (c) with an additional 180s water dip.

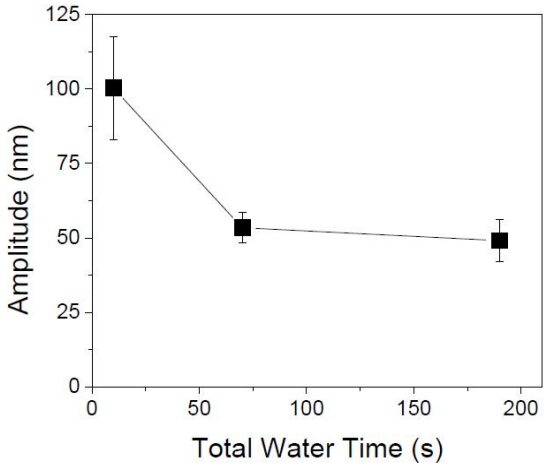

Figure 3.31: Amplitude versus water time for 400 nm thick films.

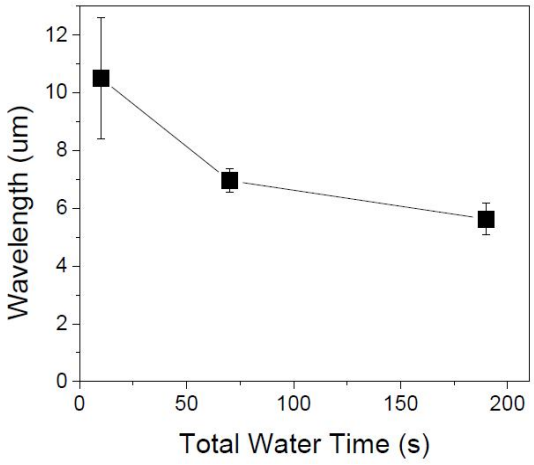

Figure 3.32 : Wavelength versus water time for 400 nm thick films.

As aforementioned, the difference in evaporation rate was taken into consideration. Different solvents with varying evaporation rates were indivudually used following the lithography step to investigate whether this would affect the surface instabilities. Dimethylformamide, or DMF, was one of the solvents investigated. This solvent was used instead of either acetone or water. As listed in Table 3.1, DMF has a higher swelling capability than acetone and water. Figure 3.34 and 3.36 are AFM images of a surface rinsed with DMF for 90s imaged in the middle and at the edge. The amplitude is considerably higher on this sample than in the sample in which only water was used (~750 nm vs. 70nm) (Figs. 3.33 and 3.35). From this, it seems there is a relationship between the solvent parameter and the instability produced.

Figure 3.37 shows AFM images of surfaces with the same processing conditions, except for the solvent used in the developing step was varied. The most significant morphology change occurs when comparing the acetone-rinsed

sample with the other samples. This sample has craters, while the other surfaces have only wrinkles. Another observation is the wavelength does not vary by any significant amount. On the other hand, the amplitude does change considerably. The highest wrinkle amplitude was obtained with the water rinsed sample, followed by ethanol. Regarding the evaporation rates of these solvents, ethanol evaporates the fastest but did not produce the highest amplitudes.

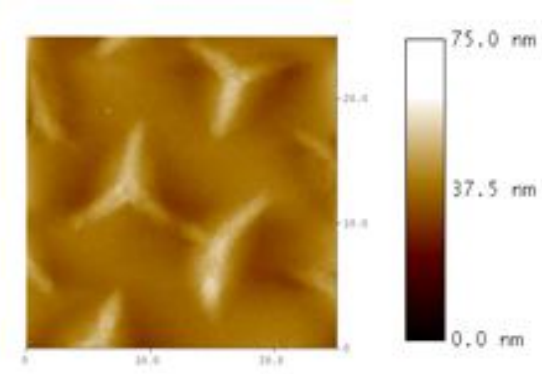

Figure 3.33: 25µm AFM image of a 400 nm thick film sample after a 90s water rinse.

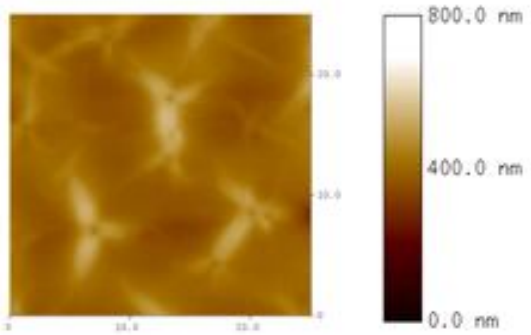

Figure 3.34: 25µm AFM image of a 400 nm thick film sample after a 90s DMF rinse.

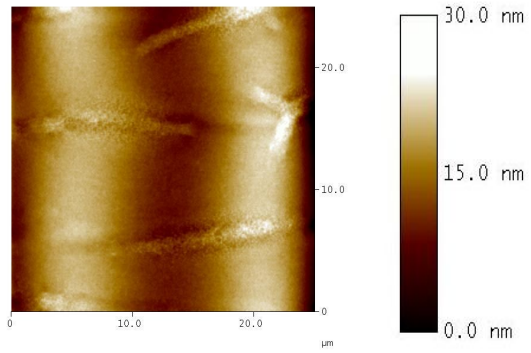

.

Figure 3.35: 25µm AFM image of the edge of a 400 nm thick film sample after a 90s water rinse.

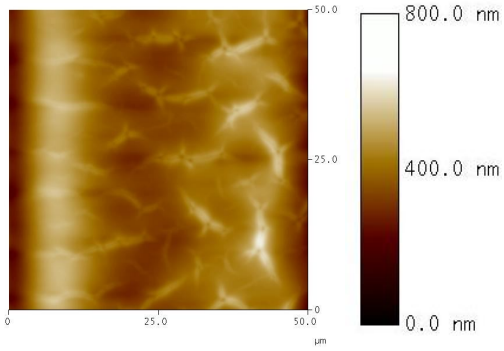

Figure 3.36: 50µm AFM image of the middle of a 400 nm thick film sample after a 90s water rinse.

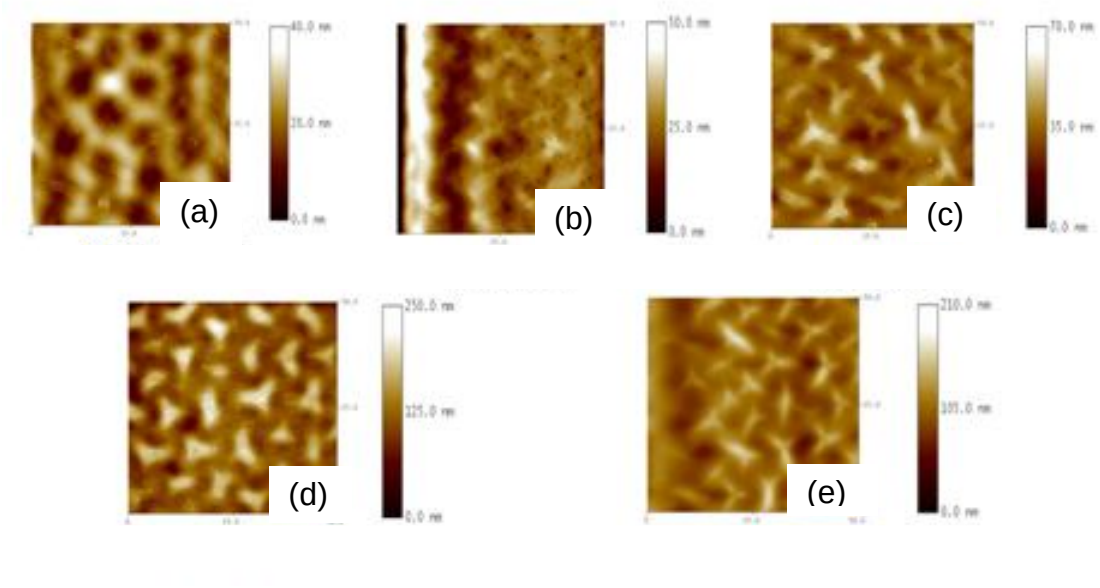

Figure 3.37: AFM images of 400nm thick samples, each with a 10s rinse of (a) acetone, (b) methanol, (c) isopropanol, (d) ethanol, (e) water.

3.5.5 Buckling Instabilities

Besides wrinkles, buckling was also observed in some of the samples. This type of instability occurs when the residual stress is high enough to delaminate the polymer from the surface [63]. Buckling, although sometimes used interchangeably with wrinkling, is in some reports distinguished by the difference in anchoring of the polymer film following the formation of the instabilities. In the case of wrinkling, the polymer is still attached. This difference in instability can be observed in Figure 3.38, where the polymer film seems to have detached from the APTES coated surface. Buckling was observed on the outer edges of the samples. This is due to the effects of spin casting, as the outer

edges of the sample end up with an increased amount of polymer. This region with increased thickness is able to swell more than the regions in the middle of the sample. From these experiments, it became evident that the choice of solvent is a factor in the morphology of the instability produced.

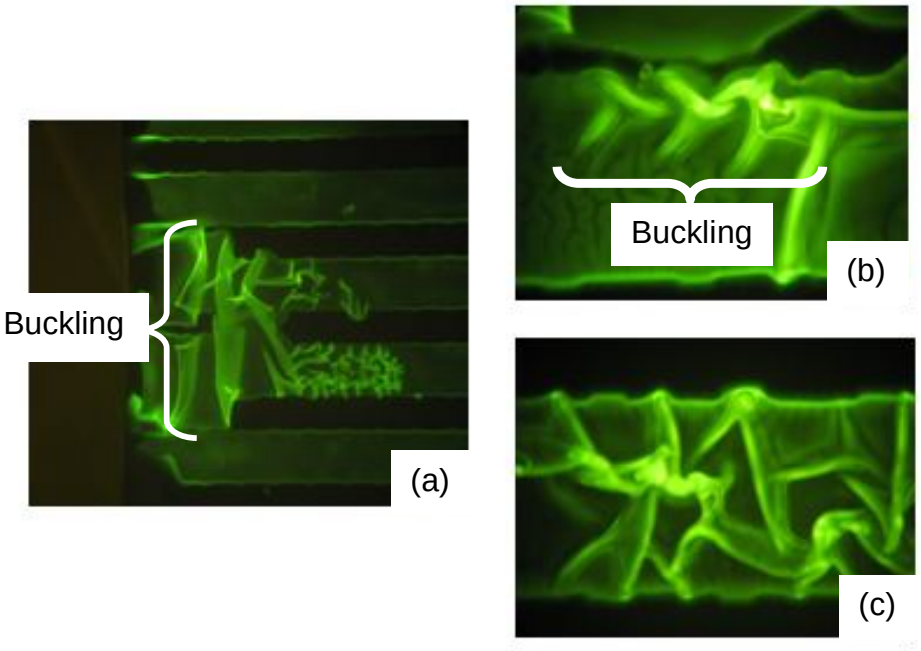

Figure 3.38: Examples of film buckling (a-c) on 400nm thick polymer films patterned using the 500µm lines. The samples had adsorbed FITC labeled poly-l-lysine for imaging purposes.

A short set of experiments was also done in an attempt to control the slippage of the polymer film over the silicon substrate. As aforementioned, all of the samples thus far have had a layer of APTES. In the next set of experiments, fluorosilane was patterned on the sample, and the rest was exposed to APTES. This was then followed by spin casting and lithography. After developing, it was observed through optical microscopy that three types of instabilities were

present: buckling, telephone cord, and wrinkles. Figure 3.39 is an optical image of such a sample. The region where the buckling occurred is where fluorosilane was used. Because the polymer was able to swell but was still anchored on opposite sides, it buckled only on the fluorosilane region.

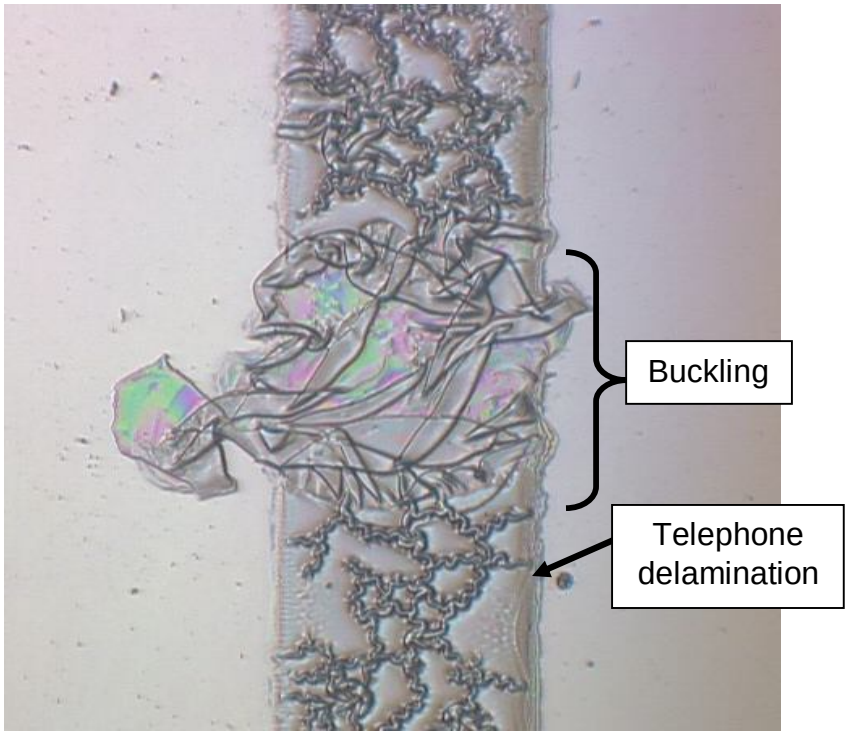

Figure 3.39: Optical image of a sample in which fluorosilane was patterned. Polymer was patterned perpendicular to those regions, which caused film buckling to form over the area with the fluorosilane.

3.6 Conclusions

In this work, a process was developed whereby spin-cast dynamic thin films were tuned to produce surface instabilities with characteristics (wavelength, width, amplitude) which increase linearly as a function of film thickness. AFM

images showed that wrinkle orientation is also dependent upon the direction of compressive force of the polymer pattern. Wrinkles close to the edges of the patterned polymer were perpendicular to the edge, while wrinkles in the middle of the polymer lines had no such orientation. The morphology was also different, as wrinkles at the edges were single branches, while those at the middle were shorter and had an increased number of branches. It was also concluded that the geometry of the patterned polymer affects the characteristics of the wrinkles. If there are four free edges, as in the case of the patterned rectangles, the wrinkles close to the edge have a decrease in amplitude relative to those in the middle. It was also evident that buckling using thick films is also possible, as this type of instability occurred in areas of the polymer where the thickness was considerably larger than the polymer thickness in the middle of the sample. There is a critical thickness which causes enough residual stress for the delamination, or buckling, of the polymer to occur. Buckling was also observed in samples where fluorosilane was patterned perpendicular to the polymer pattern. After exposing the sample to water, buckling in the fluorosilane area occurred.

Chapter 4

Characterization of Bioadhesion on Polymers

Cell adhesion to various types of surfaces has been investigated for some time. Factors affecting the adhesion of biological species onto surfaces include wettability, charge, topography, and functional groups. Cells are especially sensitive to these surface characteristics, which makes obtaining information of these factors essential. Common methods for characterizing surfaces for biomedical applications include: contact angle/ wettability measurements, optical microscopy, atomic force microscopy, among others.

4.1 Contact Angle and Cell Adhesion

Thermoresponsive substrates, specifically PNIPAAm, have been investigated since 1990 for cell tissue harvesting applications [73]. A wide range of methods have been reported to fabricate these substrates, which include e-beam grafting, solvent casting, plasma deposition, UV irradiation of a copolymer of NIPAAm and 4-(N-cinnamoylcarbamide) methylstyrene (CCMS) onto TCPS, UV irradiation of a NIPAAm copolymer with 4-azidoaniline groups, and spincasting [73-77]. Additionally a number of cell lines have been used to investigate their respective adhesive and/ or detachment behavior upon a

temperature change above or below the LCST. These include endothelial, fibroblast, hepatocyte, hepatoma, and ovary cells [78-81].

Within these investigations, there are instances where cell sheets are successfully attached and detached, while in others this behavior is not observed (Figure 4.1). Therefore, the primary goal of this work is to gain insight to explain these inconsistencies.

The wettability of a substrate is an important aspect of cell behavior on polymers (or any biomaterial). It has been reported that cells attach poorly to untreated polystyrene surfaces, but with plasma treatment the wettability changes from hydrophobic to hydrophilic, which then allows most cell types to attach [82]. This is contrary to the conditions upon which cells attach on PNIPAAm surfaces. When the film is hydrophobic, cells adhere. When the temperature of the polymer/media is decreased below the LCST, the film becomes hydrophilic and the cells are released [83].

Akiyama, Kikuchi, Yamato, and Okano have reported that cell sheet attachment and subsequent detachment is dependent on the thickness of the grafted polymer film [84] (Table 4.1). In their study, three polymer thicknesses were examined: 15.5 ± 7.2 nm, 29.5 ± 8.4 nm, and 5 µm. It was found that only the 15.5 nm thick film allowed for bovine endothelial cell attachment and detachment with a temperature change, while the other two thicknesses did not. It was explained that this result is due to the graft chain mobility, and its influence on wettability. Specifically, it was stated that in the case of the 15.5nm film, the TCPS (hydrophobic substrate) actually restricts the molecular motion of the

PNIPAAm grafted chains. This restriction was correlated to the increased hydrophobicity of this sample, and thus the wettability was stated to be the key factor in the difference in cell attachment/detachment between the films. The difference in contact angle (in the hydrophobic state) between the 15.5 and 29.5nm thick films is only 8°, which makes this explanation questionable.

It was also stated that solvent-cast substrates, which are usually microns thick, are non-fouling (non-adhesive). But interestingly enough, Moran *et al.* (among others) was able to grow confluent cell sheets on solvent cast films microns thick [3]. It should be noted that Moran used a copolymer, but nevertheless, the effects of thickness seem illusive when an attempt to correlate this to cell behavior on thermoresponsive polymers is reported.

Surface charge is interrelated to wettability. For example, plasma treated polystyrene dishes have increased negative charge with an increase in hydrophilicity relative to untreated dishes. This has been attributed to an increase in negatively charged oxygen groups, as observed by x-ray photoelectron spectroscopy [85]. This increase in negative charge has been correlated to an increase in cell adhesion time in Chinese Hamster Ovarian cells [10]. Haraguchi *et al.* have reported adhesion of cells onto anionic polymer/clay hydrogels. They state that even though the increased anionic surface charge increases cell adhesion on these composite hydrogels, this is not the case for other reported cell adhesion studies [86]. Other groups have documented the opposite effect (improved cell adhesion) using positively charged surfaces. It is proposed that the base polymer and cell type, coupled with the charge, must be considered.

One example of this within their study was the non-fouling behavior of a permanently hydrophilic, anionic polymer (PMMA) surface. Again, a polymer/ clay composite was utilized, but this time even though the surface was negative, the cells did not attach. This shows the dependence of cell behavior on the wettability, and that surface charge alone is unable to dictate the behavior of cells on polymers.

The wettability of a surface can be analyzed with contact angle measurements. This type of quantitative measurement utilizes the Young equation to obtain an angle formed by a liquid at the three phase (air, liquid, solid) boundary between a water droplet (or other liquid) and the surface under test. Akiyama *et al.* obtained sessile drop contact angle data for PNIPAAm surfaces. At 37°C, the contact angles were measured (θ= 69.5nm for the 29.5°, and 77.9° for the 15.5nm film). The temperature was decreased below the LCST to 20°C, and again contact angles were obtained (θ=60.0° for the 29.5nm, and 65.2° for the 15.5nm film). Although they also reported the fabrication of a thicker grafted film (5μm), they did not obtain the contact angle for this [84].

Other researchers have obtained larger differences in contact angle with a change in temperature; for example, Hendrick *et al.* measured a ~20° difference [11]. The surfaces measured in this report were made by adsorbing PNIPAAm from an aqueous solution onto oxidized polystyrene. In another instance, two [87] copolymers were synthesized- poly(IPAAm-co-AAc) (or IA-3) and semitelechelic PIPAAm with carboxyl end group (or Ic-120). When temperature-dependent dynamic contact angle measurements (Wilhelmy plate) were obtained, Takei *et*

al. measured a 40° difference in the advanced angle of the former, and a 25° difference in the latter [52]. This difference indicates the effects of PNIPAAm graft chain conformation on the polymer dehydration and hydrogen bonding with water molecules, as the response of the Ic-120 multipoint grafted surface had a more significant change in contact angle relative to the IA-3 terminally grafted surface with a change in temperature above and below the LCST.

Curti *et al.* observed static contact angle changes of over 20° in copolymers of PNIPAAm. The grafting was done in the presence DMAAm, AAm and NIPAAm. Two substrates, poly(ethylene terephthalate) (or PET) and polystyrene were premodified prior to grafting. From the contact angle data, the underlying substrate played a role in the wettability of the grafted polymer. The PET sample oxidized by Hg lamp had a lower hydrophilic contact angle relative to the PS sample. The PET samples with oxidation had a larger change in contact angle between the starting (25°) and final (45°) temperature. It was concluded that the oxidation process is effective in tuning the wettability of the surface to be more hydrophilic, when compared to unoxidized surfaces.

Table 4.1: Contact angle data.

Author	Polymer synthesis	Contact angle type	Contact angle
Akiyama *et al.*	Grafting of PNIPAAm	Sessile drop, static	9 º -13º
Hendrick *et al.*	Adsorption of PNIPAAm on polystyrene	Sessile drop, static	20º
Takei *et al.*	Grafting of PNIPAAm copolymers	Wilhelmy plate, dynamic	25 º -40º
Curti *et al.*	Grafting of PNIPAAm	Sessile drop, static	10 º -25 º
Liang *et al.*	Grafting of PNIPAAm	Wilhelmy plate, dynamic	92 º

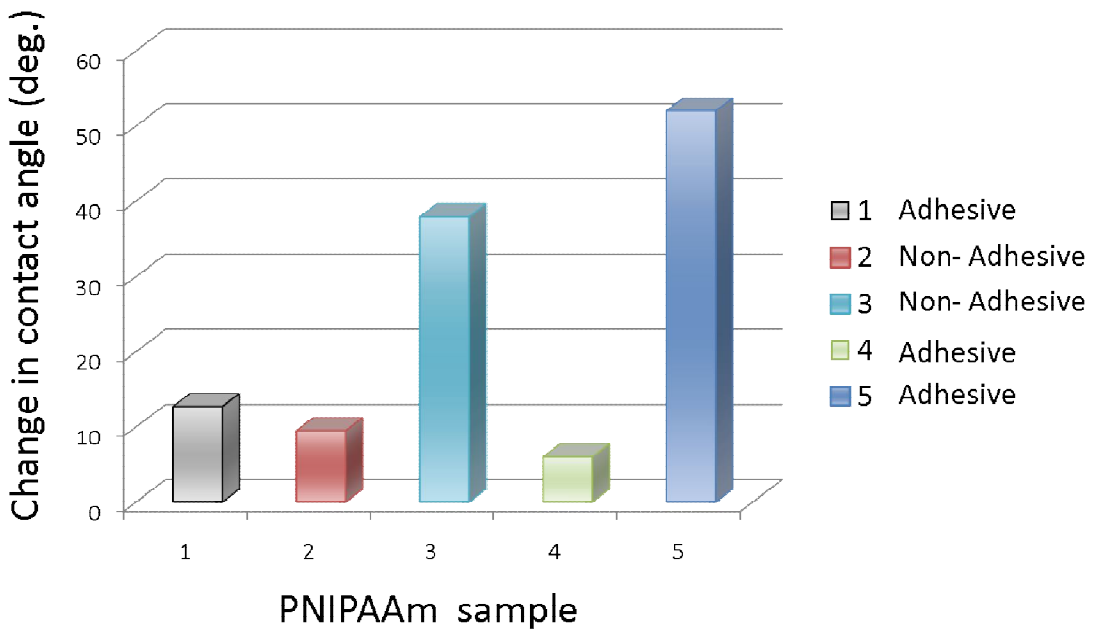

Figure 4.1: Change in contact angle versus cellular response.

One interesting result of this oxidation process is the change in surface roughness, which is known to affect advancing contact angle measurements. Liang *et al.* state that higher values of surface roughness result in increased advancing contact angles. It was further explained that in the case of hydrophilic (contact angle < 90°) surfaces, the drop of liquid is adsorbed the surface. When the surface is hydrophobic (contact angle > 90°), the liquid is no longer adsorbed by the cracks/crevices in the heterogeneous surface [88]. Both cases should lead to an increase in contact angle with an increase in surface roughness, as measured by AFM. But in the case of RMS data reported by Curti *et al*., it was the samples with the lower surface roughness (polystyrene) that had the higher advancing contact angles.

The morphology of the cells on thermoresponsive polymers is another issue that has been discussed in the literature. Although some groups have had success with using PNIPAAm for attaching cells, other groups have reported changes in morphology of the cells (such as rounding and clumping). Haraguchi *et al*. state that it was “almost impossible” to culture three types of cells (human hepatoma, normal human dermal fibroblast, and normal human umbilical vein endothelial) on conventional PNIPAAm surfaces. On the other hand, they found that a hydrogel composed of a copolymer of PNIPAAm with a type of inorganic clay (synthetic hectorite) did allow for confluent cell sheet growth and detachment, regardless of film thickness [86].

Moran *et al*. were also unable to grow confluent cell sheets on a PNIPAAm copolymer. They incorporated a hydrophobic comonomer, N-tert-butyl-acrylamide (NtBAm) to the polymer [75]. On the bare copolymer, 3T3 fibroblast-like cells barely attached, and the few that did had a rounded, clumped morphology. With the addition of adhesion promoters (collagen, laminin, and poly-l-lysine), cells were able to adhere and their morphology was comparable to that obtained on TCPS. The cells on these surfaces exhibited the attachment/detachment behavior upon a temperature change above or below the LCST.

Selezneva *et al.* compared PNIPAAm to the same copolymer as Moran *et al.*, PNIPAAm/NtBAAm, but unlike in the case of the latter, the copolymer surfaces were able to grow confluent NCTC L929 fibroblast cell sheets without the need for adhesion promoters [89]. Besides PNIPAAm, three ratios of

PNIPAAm/NtBAAm were investigated: 85/15, 65/35, and 50/50. Bare PNIPAAm, as in the case of Haraguchi *et al*., did not allow for confluent cell sheet attachment. They had a similar morphology- rounded and clumped. Cells cultured on all three ratios of the copolymer resulted in the typical morphology of healthy cells.

Cell morphology has been correlated to substrate mechanical characteristics, and this may explain the differences in morphology of the aforementioned studies. In a study by Pelham and Wang, substrates with varying degrees of flexibility were fabricated [90]. The morphological changes of 3T3 fibroblast cells were then correlated to this parameter. The mechanical properties of the polymer, specifically polyacrylamide (non-thermoresponsive), were changed by varying the amount of crosslinker (bis-acrylamide) from .26 to .03%. The substrates that were made with .26% crosslinker had an elastic modulus of ~7.3 x 10-7 N/m, while those made with .03% crosslinker had a modulus of ~4.6 x 10-8 N/m. It was concluded that cells seeded on the more flexible substrates (those with .03% crosslinker) showed reduced spreading, while those on the rigid substrates had “normal” morphologies [90].

Numerous advances have been made in the area of thermoresponsive polymers; nonetheless, there still exists a gap in knowledge when attempting to correlate certain aspects of these surfaces to the fouling behavior of biological cells. It has been shown that contact angle alone does not explain why certain films allow for cell adhesion, such as in the case of Akiyama *et al*. where the difference between samples was quite small [84]. Surface charge, a component

of wettability, has also been considered. But studies have shown that in certain instances cells will adhere to either anionic or cationic surfaces. The thickness is another parameter that has been discussed, but again certain reports have shown that a wide array of thicknesses may be used, while others show that only a specific range of thicknesses will work. There also appear to be changes in morphology with some of the thermoresponsive polymers, but the effects of mechanical characteristics have not been taken into consideration. This literature review illustrates the need for further investigations into these issues.

Besides the wettability of a surface, the topography also has a critical role in whether cells will adhere and their resulting in morphology. The effects of topography were discussed previously in Chapters 1 and 2. Topography has a ubiquitious role both *in vivo* and *in vitro*. The topography can be controlled via MEMS/ IC processing-based fabrication methods such as photolithography.

In this chapter, amino acids and cells have been adsorbed to the polymer thin films and analyzed. FITC labeled poly-l-lysine, a positively charged adhesion promoter, was initially used in the studies for purposes of viewing the lateral dimensions of patterned polymer lines before and after a temperature change. The purpose of this was to quantify the amount of swelling by obtaining images of the polymer lines and measuring the change in dimensions (only in the y-direction). Although this proved to not be a useful method for this type of measurement, it did reveal beautiful cusp patterns that had formed in the middle of the polymer, and perpendicular folds close to the edges. With this new data, it became clear that the presence of these wrinkles may be affecting how cells

attach or detach from these surfaces. As a result, cell adhesion on these surfaces was investigated. This was accomplished by loading cells to the thin films, followed by fixing and labeling of actin filaments. Actin was labeled to understand the reorganization, if any, of the cytoskeleton as a result of the changes in the topography of the polymer film.

4.2 Experimental Section

4.2.1 Contact Angle Measurements

The wettability of surfaces may be assessed with contact angle measurements, specifically the sessile drop method [91-95]. The contact angle is a result of the interface/surface tensions (surface free energies) between liquid and solid surrounded by vapor; this is also known as the three phase boundary (Figure 4.2). The contact angle, θ, is obtained with Young's equation, where γsl is the surface free energy of the solid-liquid interface, γsv is the surface free energy of the solid-vapor (gas) interface, and γlv is the surface free energy of the liquid-vapor interface. A surface is considered hydrophobic if the contact angle is above 90°, and hydrophilic if below this angle. A contact angle of 0° represents total wetting.

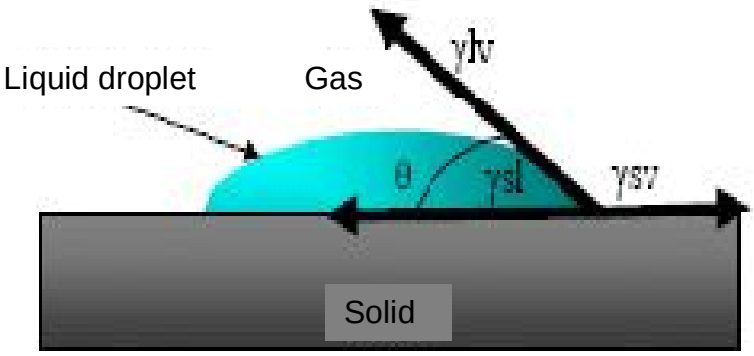

Figure 4.2: Schematic of the three-phase boundary.

Static measurements are obtained when a drop of liquid at the surface to be tested is not in motion. If the drop is in motion, as in the case of a tilted stage or increasing/ decreasing the volume of the drop on the surface, then the measurement is considered to be dynamic. Dynamic contact angle measurements can be used to characterize surface heterogeneity, roughness, and mobility [96].

The dynamic contact angle measurements were done at 23°C and 40°C. The heating was achieved with a temperature controlled chamber. For advancing contact angles, the needle was placed close to the substrate, a droplet was formed, and the volume of water was increased slightly while keeping the tip of the syringe inside the droplet. At each increase, an image was recorded and analyzed. To obtain receding contact angles, the volume of water was decreased with the tip of the syringe still embedded inside the droplet. Each type of measurement was done at least 5 times for statistical purposes.

4.2.2 Atomic Force Microscopy

A Digital Instruments Dimension 3100 Atomic Force Microscope with NanoScope Software was used to obtain non-contact atomic force microscopy images of cells.

4.2.3 Polymer Surface Preparation

Polymer samples were spin cast and processed as discussed in Chapter 3. Samples used for cell loading experiments were not patterned.

4.2.4 Surface Labeling of Polymer Thin Films

Fluorescein isothiocyanate (FITC) labeled poly-l-lysine, with a molecular weight of ~70 kDa, was used to view polymer thin films using a fluorescent microscope. Pol-l-lysine is a positively charged amino acid polymer used for imaging as well as an adhesion promoter. In this case it was initially used to image the patterned polymer adhesion/ detachment studies. The reason for using the higher molecular weight amino acid is due to the adhesion of the cells; a confluent layer of cells was not achieved with the 70 kDa molecular weight.

4.2.5 Cell Loading and Fixing

Mouse melanoma cells (B16 F10) were cultured in McCoy's media supplemented with 10% fetal bovine serum (Sigma) and 500 µL gentamicin. Cells were maintained in a humidified atmosphere of 95% air and 5% CO2 at 37°C and passaged every three or four days. The process for adhering, fixing, and labeling the cells was as follows:

1. Methanolic stock solution for staining cells- added 1.5 ml methanol to vial of phalloidin rhodamine (~1.3 micromoles).
2. Cell loading- confluent cells were detached from flasks using trypsin.
3. Cells, suspended in prewarmed media, were loaded onto the samples at a density of ~1 E 6/cm^2.
4. After the polystyrene control reached 100% confluence, the samples were exposed to cold treatment.
5. For cold treatment, the media was replaced with cold media (4ºC) and left at room temperature for 1.5 hours.
6. After the 1.5 hours, the samples were gently rinsed with PBS (pH=7.4) and fixed in 3.7% formaldehyde solution in PBS for 10 minutes at room temperature.
7. Washed two or more times with PBS.
8. To stain with fluorescent phallotoxin, 5 µL of methanolic stock solution were diluted into 200 µL PBS for each sample to be stained.

9. The staining solution was placed on the coverslip for 20 minutes at room temperature (generally, any temperature between 4°C and 37°C is suitable). To avoid evaporation, the coverslips were kept inside a covered container during the incubation.
10. Washed two or more times with PBS.
11. Dried at room temperature.

4.2.6 Optical Microscopy

A Zeiss Axiovert upright fluorescent microscope was used to obtain images of stained actin cytoskeleton.

4.2.7 Cell Area Measurements

Area and circumference measurements and shape factor were obtained by labeling the cells with phalloidin rhodamine, obtaining images, and then tracing cell boundaries manually using NIH ImageJ software. The motivation for performing these two measurements was that these indicate the lateral spreading of the cells and hence the state they are in. As a general rule, when cells are in a rounded state, their adhesion sites have retracted and the cells are in the process of detaching from the substrate. In the case of anchorage-dependent cells, this leads to a loss of cell function. Spreading occurs as a result of the cell probing the surface via surface integrins. Signal transduction occurs

from the cell to the substrate, and from the substrate back to the cell. This feedback mechanism is necessary for the cell to form focal adhesion complexes. When a cell anchors to a surface, contractile forces are generated. These forces are a result of actin and myosin filaments. Also known as traction forces, these have been previously observed in cases where cells cause wrinkling on PDMS surfaces. Actin is reassembled during the process of a cell spreading and rounding (Figure 4.3). Because actin assembly is modified depending on the lateral spreading of a cell, fluorescently labeling this cytoskeletal component provides information concerning the effects of a substrate on cell anchoring mechanisms.

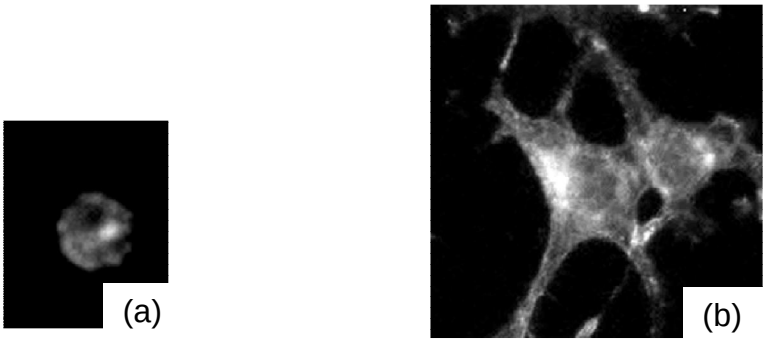

Figure 4.3: (a) Optical image of a rounded B16-F10 cell and (b) of a spread B16-F10 cell.

4.2.8 Image Processing

ImageJ was used for all image processing. This freeware is a public domain, Java-based image processing program developed at the National Institutes of Health.

4.3 Results

The first characterization study done on the polymer films was performed to obtain contact angle data above and below the LCST. Both static and dynamic measurements were employed (Figure 4.4). The contact angle meter had a temperature chamber. From the measurements, it was concluded that the wettability varied by less than 10ºC when comparing the values obtained above and below the LCST (Table 4.2).

Table 4.2: Polymer film thickness and contact angle data.

Thickness (nm)	Contact angle at 23ºC	Contact angle at 40ºC
5	73º ±2º	77º±2º
10	73º ±4º	84º±3º
15	70º ±4º	84º±3º
25	70º ±2º	88º±4º

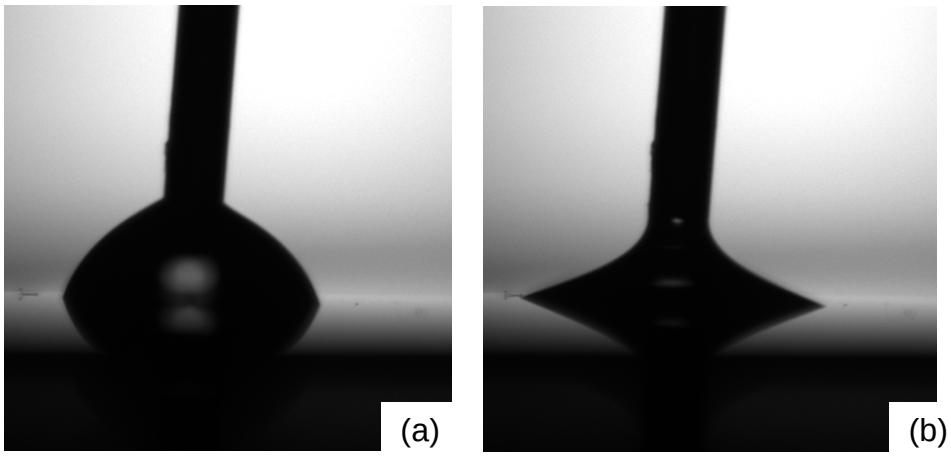

Figure 4.4: Example of (a) advancing and (b) receding contact angle measurement.

Following contact angle measurements, cells were loaded onto the samples. Although the cells were attaching to the surfaces (Figure 4.5), the detachment proved to be inconsistent. In these preliminary studies, HaCAT (non-malignant) and B16-F10 (malignant) cells were loaded. Following adhesion, samples were treated with cold media for one hour. Some of the cells detached, but the detachment was not uniform and did not occur on all of the samples.

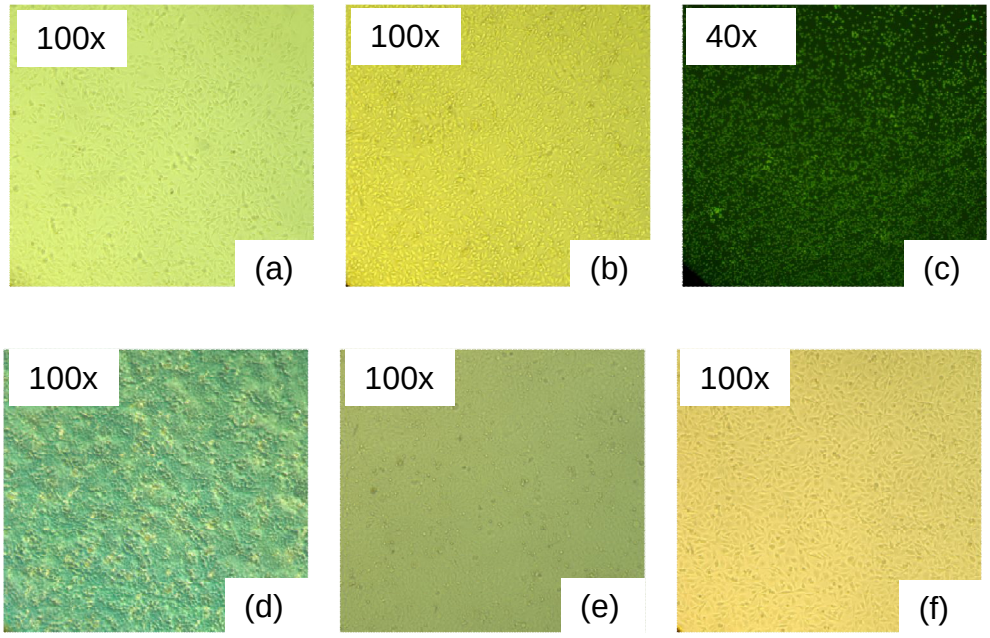

Figure 4.5: Images of B16-F10 (a-c) and HaCat (d-f) of cells without cold treatment.

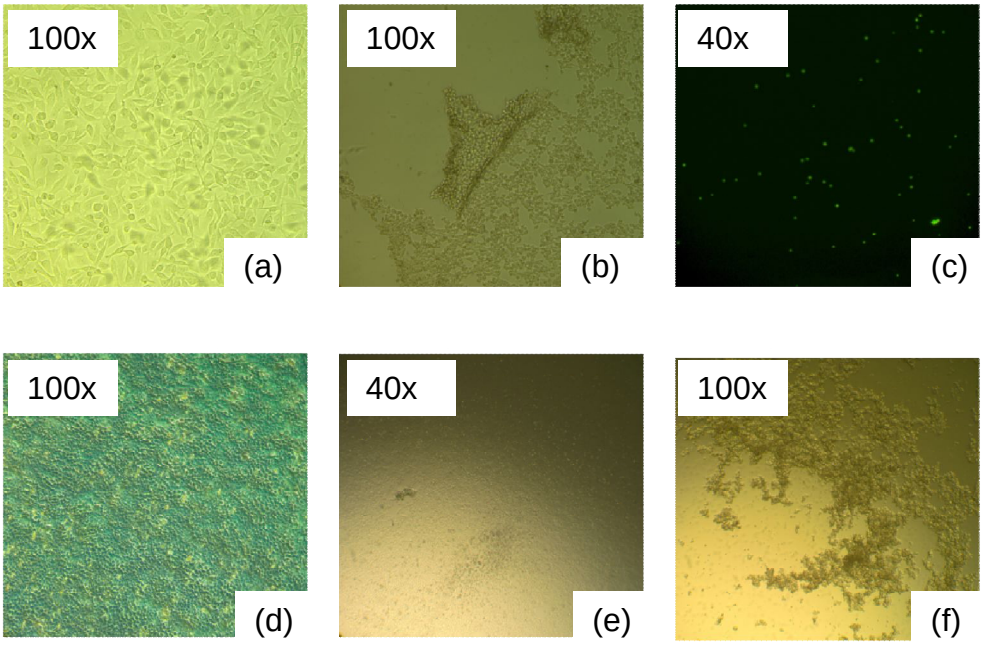

Figure 4.6: Images of B16-F10 (a-c) and HaCat (d-f) of cells after cold treatment.

FITC-labeled poly-l-lysine (PLL) was adsorbed to patterned polymer surfaces. The reasons for adsorbing this amino acid were twofold: the first was to view the polymer surface, and the second was to promote cell adhesion. Because this is polymer is thermoresponsive, the first experiment was to investigate whether the PLL would adsorb at room temperature (below the LCST), or if it would only adsorb above the LCST. Within literature, groups that have used adsorbed proteins on PNIPAAm surfaces have used different temperatures for the adsorption. For instance, Akiyama and colleagues adsorbed proteins at 37ºC, while Moran and colleagues adsorbed proteins at room temperature [75, 84].

In Figures 4.9 through 4.12, PLL was added to the polymer sample at room temperature. As can be observed from the images, the amino acid was adsorbed at RT. It was also added to polymer at 37ºC, where it was also found to adsorb. From the images, it was apparent that a pattern of surface instabilities had formed on the surfaces. Following the adsorption step, the samples were then exposed to DI water above and below the LCST. When the polymer is in the hydrophobic state, the folds are open (Figure 4.7). When the temperature was dropped below the LCST, the folds are closed (Figure 4.8).

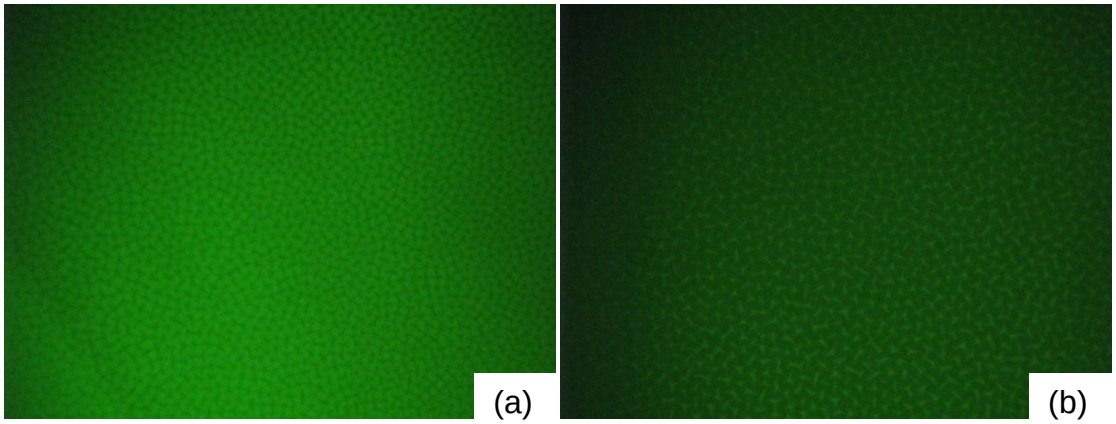

Figure 4.7: Fluorescent image of a 400nm thick polymer film with FITC-labeled poly-l-lysine adsorbed on the surface at a temperature (a) above and (b) below the LCST.

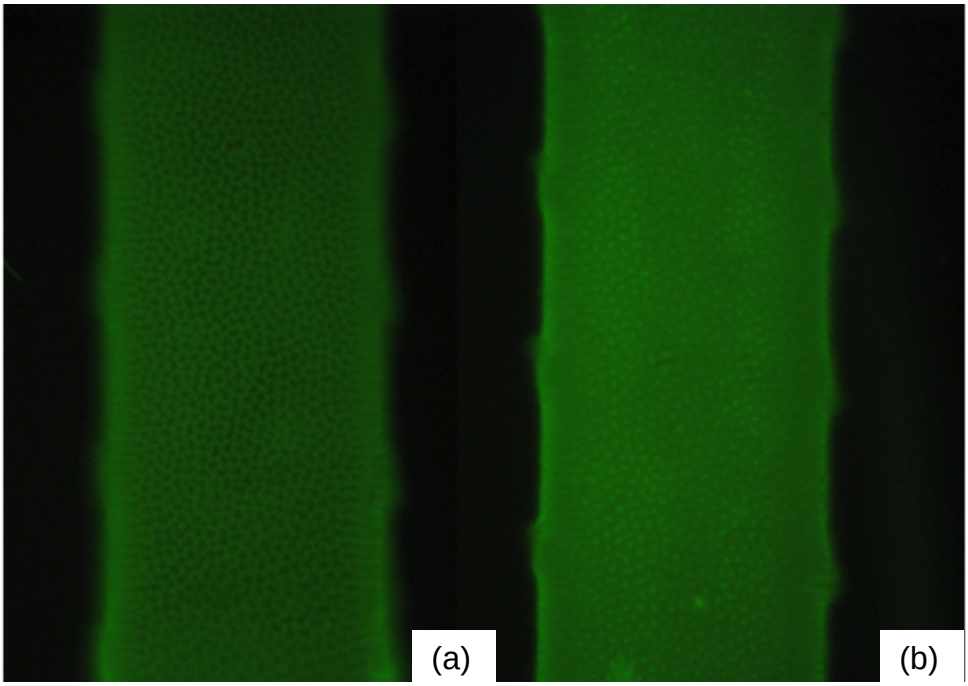

Figure 4.8: Fluorescent image of patterned polymer in water (a) above and (b) below the LCST.

After imaging the samples with FITC-labeled poly-l-lysine, the next set of experiments was to load samples with cells (B16-F10) and expose them to cold treatment to further study cell de-adhesion. The actin filaments were labeled to study the rearrangement, if any, of the cells on the surfaces. As was observed in the FITC-labeled images, the cusps open and close as a result of a change in temperature. Therefore, it was hypothesized that these patterns were affecting and perhaps even disrupting the anchoring of adhered cells. As a result of the cell detaching, the actin filaments in the cytoskeleton would rearrange themselves from lateral to circular due to the retracting of the anchoring sites.

The samples for these studies were prepared as follows. PNIPAAm-co-MaBP(1%) films were spin cast, producing thicknesses of 30, 100, and 300 nm.

Additionally, samples of 10% MaBP content were also produced for the purpose of understanding whether the swelling capability affected cell de-adhesion. The 10% films, because they have an increased amount of the hydrophobic monomer, have decreased swelling when in the hydrophilic state relative to the (1%). Silicon without polymer but with adsorbed poly-l-lysine was also used in the experiments.

Cells were loaded and incubated at 37ºC for 18 hours. Half of the samples were exposed to cold treatment, specifically cold media, for 1.5 hours. The other half of the samples were fixed after being taken out of the incubator. As was observed from the fluorescent images (Figures 4.9 - 4.12), the cells adhered to the polymer surfaces. Although the cells have lateral spreading, when compared to the silicon control samples (Figure 4.13), the growth rate was slower on the polymer surfaces. The silicon reached 100% confluence, while the cells on the polymer surfaces did not. The sample with almost 100% confluence had the 10% MaBP polymer on the surface. The surface topography is different from those with the 1% MaBP; specifically the 10% MaBP do not have wrinkles (Figure 4.12).

To further analyze the change in cytoskeletal rearrangement after cold treatment, the area was obtained from images of samples either without cold treatment or with cold treatment. According to theory, cells should decrease in area after cold treatment as a result of rounding of the cells. This change in morphology has been attributed to metabolic activity. The Okano group describes the cell adhesion and detachment to thermoresponsive polymers as a two-step

process. The first step is considered passive cell adhesion, since no metabolic activity is required. This includes electrostatic processes, such as those that occur between the negatively charged membrane and a charged surface. The second step does require metabolic activity and is regarded as the active step. In this step, a number of interrelated processes and signaling pathways allow cells to extend and anchor to a surface. Detachment is also described as a two-step process, again with a passive and active step. In their study, they also concluded that cells change their morphology as a result of both the wettability change of the PNIPAAm surface, and metabolic activity [30]. The change in morphology from spread to round was also observed on the PNIPAAm-co-MaBP surfaces. The actin filaments rearranged themselves from elongated to circular, as shown in the images. In the case of the silicon surface without polymer, some cells did change their morphology. This change is to be expected, as cells regardless of whether they are on a thermoresponsive surface or not, require a specific environment to remain anchored. The cold exposure was 1.5 hours, long enough for the cells on the silicon to be affected. But when comparing the cell area and confluence change, a difference between the control sample and those with polymer was observed.

Figure 4.14 is a graph of the cell areas with and without cold treatment. Without cold treatment, the average cell area is ~650 μm^2. With cold treatment, the cell area decreased to ~275 μm^2. This is roughly a decrease of 50%. This decrease was observed for the samples with the 1% MaBP content. The difference between the cell areas with and without cold treatment was plotted in

Figure 4.15. From this graph, it is evident that the difference in cell area is significantly larger for the cells grown on polymer films versus those that were grown on silicon without polymer.

The form factors of individual cells were calculated as $4\pi S/L2$, where S is the projected cell area and L is the cell perimeter [97] (Fig. 4.16). This index reflects the irregularity of cell shape: a perfectly round cell has a value of one, and a stellate cell has a value lower than one [97]. For all the thicknesses using 1% MaBP, the shape factor as a result of cold treatment changes from .35 with no treatment to almost 1. The control sample without polymer did show a change in shape factor, but this change was only by ~.15. The samples with polymer, on the other hand, had changes in shape factor of ~.6. It is clear that the change in shape is a result of interactions between the cell and polymer.

The change in confluence with and without cold treatment was also quantified. The silicon control sample had about a 30% decrease in confluence. This was after cold treatment of 1.5 hours with media at 4ºC. The length and temperature will obviously affect cells whether or not they are on thermoresponsive polymer surfaces. When compared to the samples with polymer, this change in confluence is considerably higher for the 30 and 100 nm samples. The change is ~80%. In the case of the 300 nm film with 1% MaBP, however, the cells did not reach the same confluence as the two other thicknesses. Although there was a decrease in confluence after cold treatment, the change was relatively lower than in the other cases. The 10% MaBP content showed a similar change in confluence to the sample without polymer. Again, the

fact that this polymer swells less due to its increased hydrophobic monomer, along with the difference in topography, seems to be the cause of this difference in response.

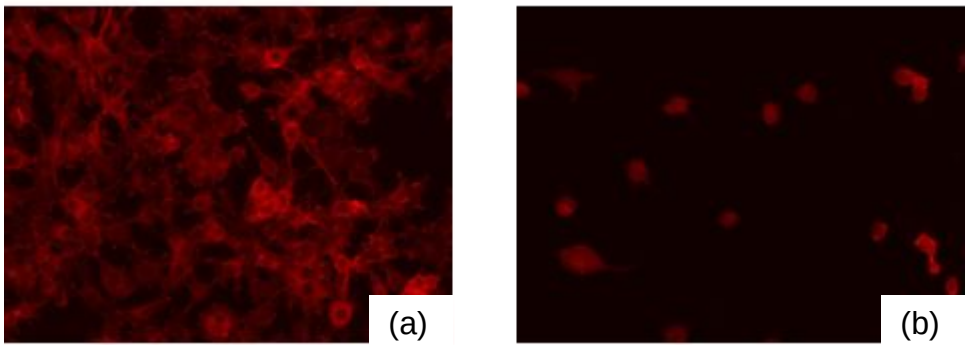

Figure 4.9: Fluorescent images of 30nm thick, 1% MaBP films (a) at 37ºC and (b) after 1.5 hours at 10ºC.

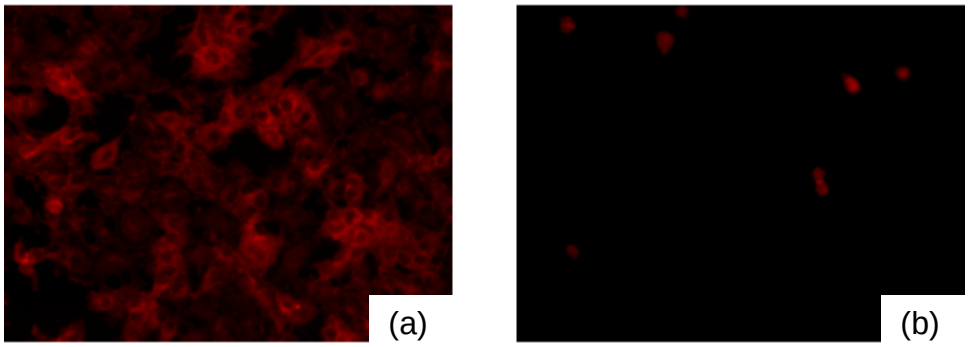

Figure 4.10: Fluorescent images of 100nm thick, 1% MaBP films (a) at 37ºC and (b) after 1.5 hours at 10ºC.

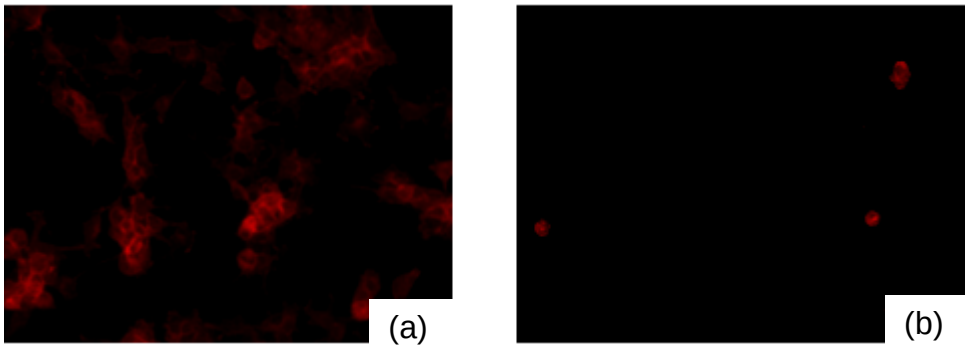

Figure 4.11: Fluorescent images of 300nm thick, 1% MaBP films (a) at 37ºC and (b) after 1.5 hours at 10ºC.

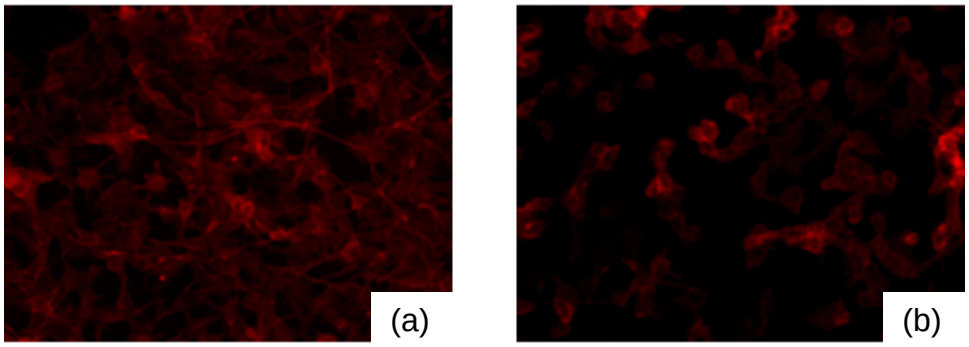

Figure 4.12: Fluorescent images of 300nm thick, 10% MaBP films (a) at 37ºC and (b) after 1.5 hours at 10ºC.

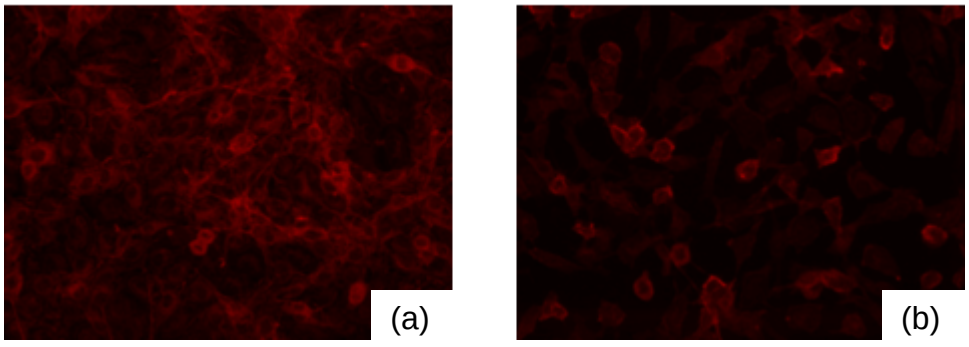

Figure 4.13: Fluorescent images of silicon substrate without polymer (a) at 37ºC and (b) after 1.5 hours at 10ºC.

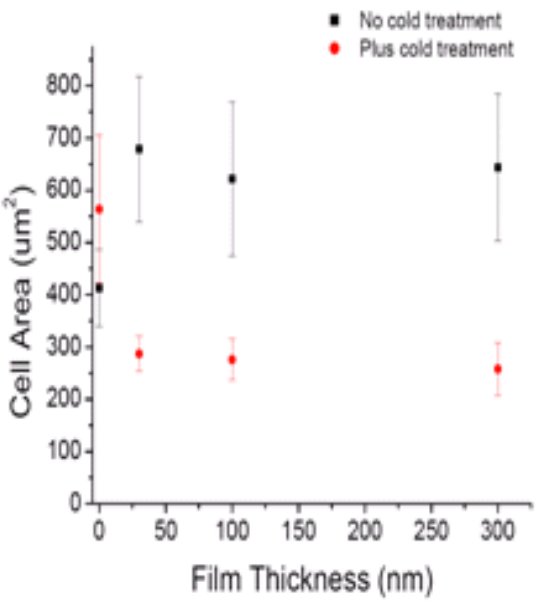

Figure 4.14: Cell area versus film thickness.

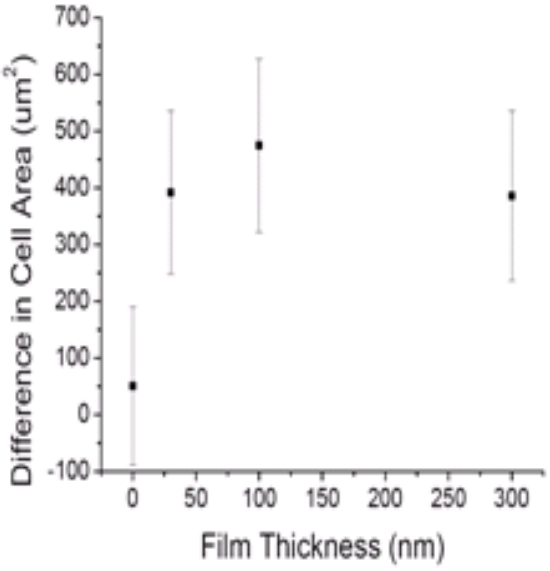

Figure 4.15: Difference in cell area versus film thickness.

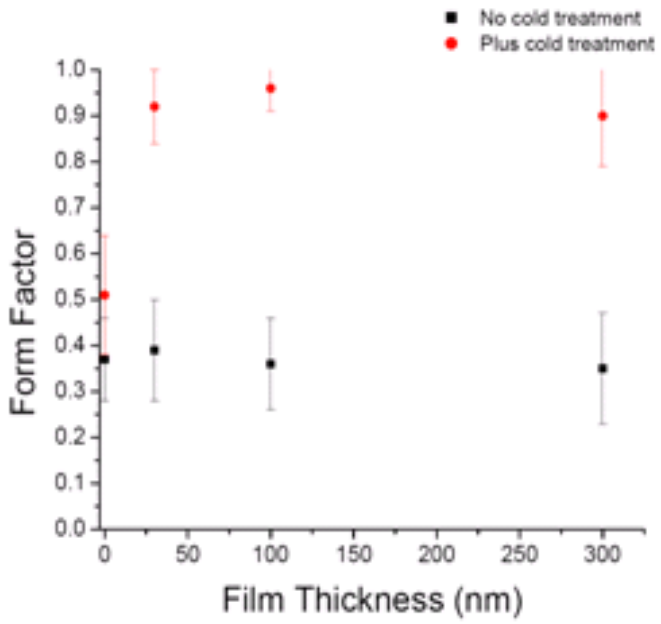

Figure 4.16: Form factor versus film thickness.

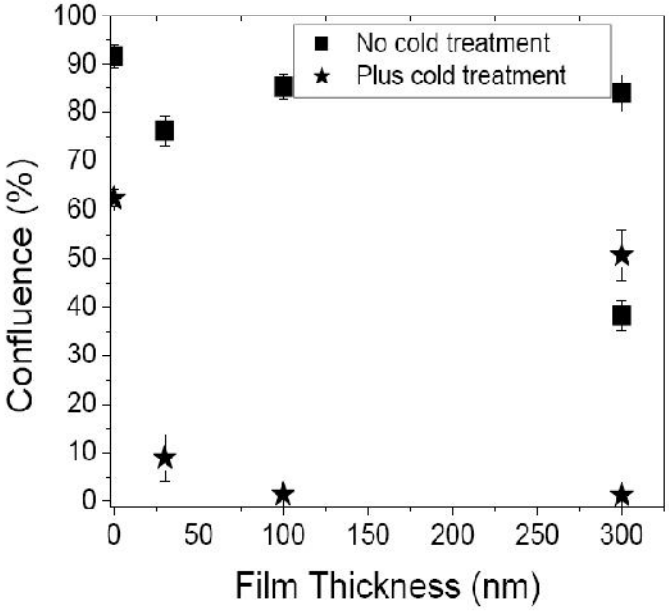

Figure 4.17: Confluence versus film thickness.

4.4 Detachment from Surfaces Without Wrinkles

The aforementioned data of cell adhesion and detachment of cells was obtained with samples developed using two solvents- a 10 s acetone rinse followed by a 10 s DI water rinse. As discussed in Chapter 3, this solvent combination produces surface instabilities in the form of wrinkles. A change in the developing step produces variations in the topography. A 10 s acetone rinse, with the rest of the processing conditions kept constant, produced surfaces without wrinkles (Figures 4.18 and 4.19). Although wrinkles were not evident, blister formation was. Cells were adhered to these surfaces and exposed to cold treatment, as done with the previous samples, for the purpose of studying topographical effects on cytoskeletal rearrangement.

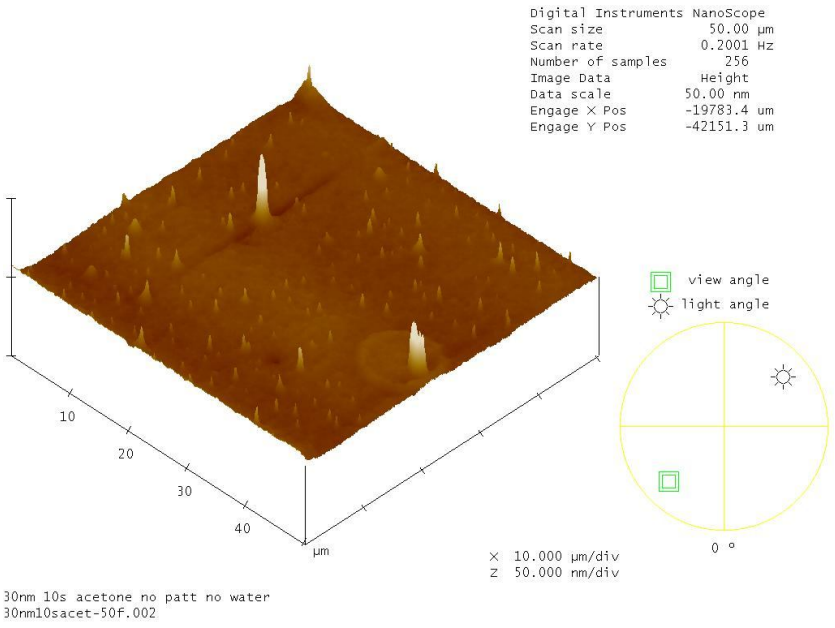

Figure 4.18: AFM image (surface view) of a PNIPAAm-co-MaBP (1%) 30 nm film with a 10 s acetone rinse.

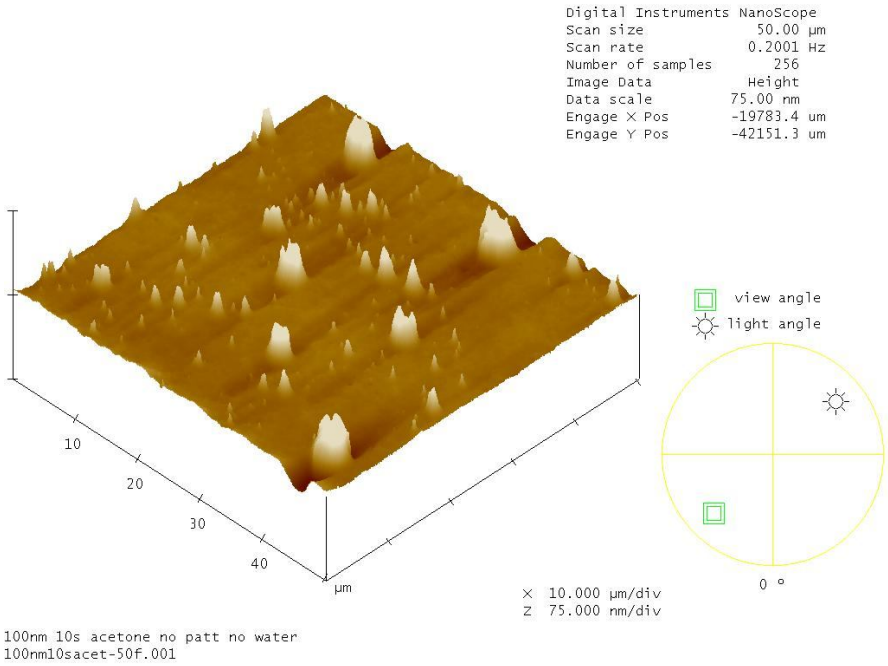

Figure 4.19: Atomic force microscope image (surface view) of a PNIPAAm-co-MaBP (1%) 100 nm film with a 10 s acetone rinse.

Cells were loaded on the samples and exposed to cold treatment, fixed and labeled. From fluorescent images obtained, it became evident that cells were not adhering with the same morphology as with the previous set of experiments in which samples with wrinkles were used (Figure 4.20). The cells were clumped and the surfaces did not reach confluence. This is not to say that they would not have reached confluence at some point, but rather, to point out the difference in growth rate between the samples with polymer versus the sample with no polymer (control). The control sample used was silicon without polymer, but with poly-l-lysine. The control sample had ~90% confluence (Figure 4.21).

The images were again analyzed and the shape factor was calculated. Although there was a change in the shape of the cells due to the cold treatment,

this difference was slightly less than the difference in shape factor quantified for the substrates with wrinkling. This difference in shape factor can be attributed to the differences in adhesion on these samples. Because the cells did not adhere laterally and spread as much, the shape factor was closer to 1. Therefore, after cold treatment, the difference between the samples with and without cold treatment was ~.4, whereas the previous set of experiments with wrinkles had a difference of ~.55.

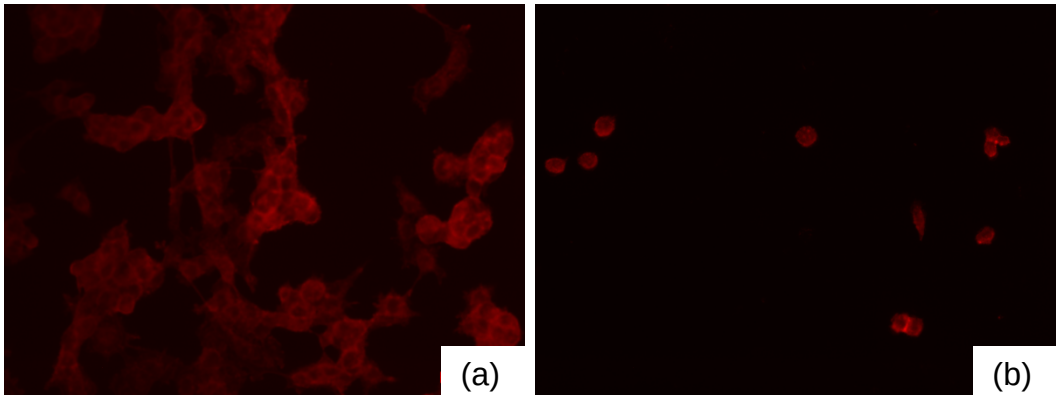

Figure 4.20: 30 nm, 1% MaBP film with a 10 s acetone rinse (a) without cold treatment and (b) with cold treatment.

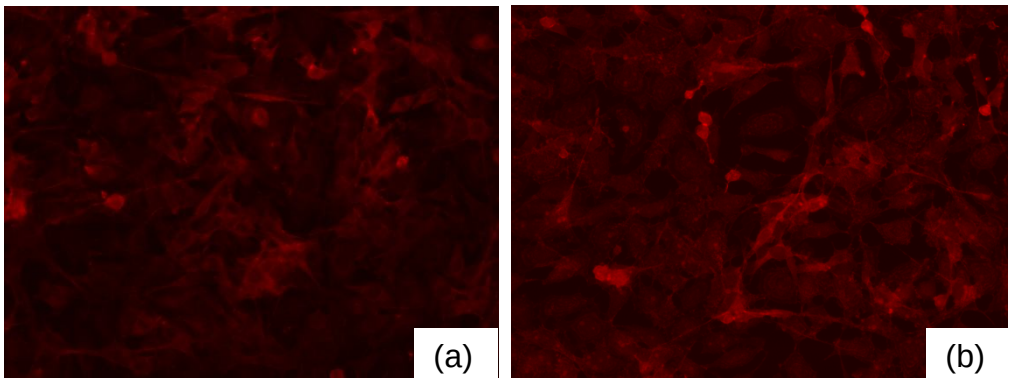

Figure 4.21: Silicon sample with adsorbed poly-l-lysine, no polymer (a) without cold treatment and (b) with cold treatment.

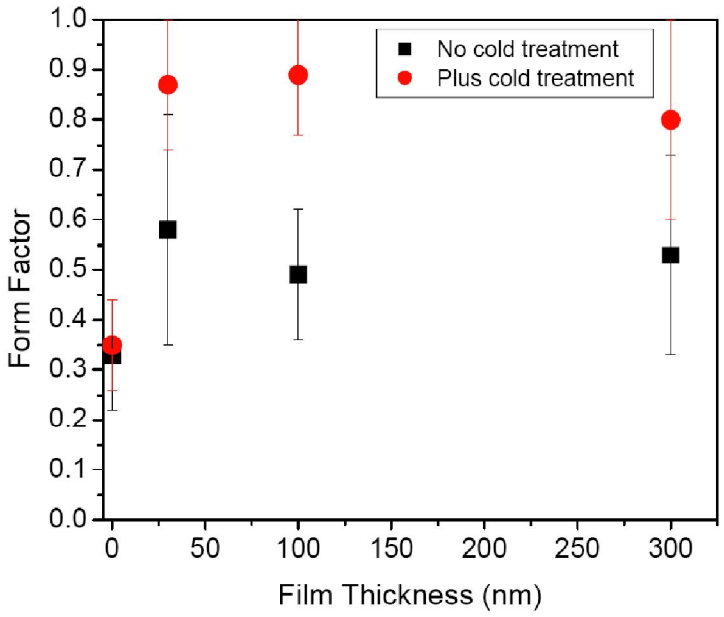

Figure 4.22: Form factor versus film thickness for 1% MaBP films with a 10 s acetone rinse.

4.5 Conclusions

Changes in form factor of cells have been reported in literature, and the significance is related to the effects of cell morphology on both cell function and cellular-surface anchoring. The cell morphology is a result of cytoskeletal arrangement, which in turn is mediated by contractile forces generated as a result of interactions between a substrate and focal adhesion sites. Anchorage dependent cells and their focal adhesion sites have been investigated by groups in an attempt to explain the various interactions and the effects of different variables on adhesion. Studies have shown that actin can be circular or in fibers, and additionally these can be correlated to cell adhesion strength [97]. This has

direct implications in cancer cell adhesion, since adhesion and de-adhesion are required in the mestastasis process. Although other cytoskeletal components may be labeled, in this work the actin cytoskeleton was chosen, as this is conventionally labeled to study cytoskeletal formation and rearrangement. The fluorescent images obtained are evidence of a change in the actin cytoskeleton rearrangement as a result of temperature change on the samples. The cells changed from having lateral fibers to round. Although each individual fiber was not observed, it is known that for cells to have lateral spreading, the actin must be distributed in a straight orientation.

After imaging (optical or AFM), the cell area and other measurements can easily be obtained (Figures 4.23-4.25). Other groups have studied the changes in cell area on thermoresponsive polymers and have found similar results, although there are differences in the sample surface and adhesion promoters. In the case of this work, wrinkled as well as non-wrinkled surfaces were studied. The cell adhesion promoter was poly-l-lysine. In the work of Chen and co-workers, only non-wrinkled surfaces were used. Collagen was adsorbed to these surfaces to promote cell adhesion, since it is well known that PNIPAAm surfaces are generally non-fouling. The change in adhesion energy was calculated using a contact mechanics model of adherent cells. The adhesion energy of cells was found to decrease with cold treatment. This correlates to the results presented within this work, as there was a change in confluence with cold treatment (Fig. 4.38 and 4.39). Additionally, the cells that were found to be adherent after this treatment had changed in morphology. It is quite possible then to conclude that a

change in adhesion energy of the cells caused the majority of cells that had adhered during the incubation process at 37ºC.

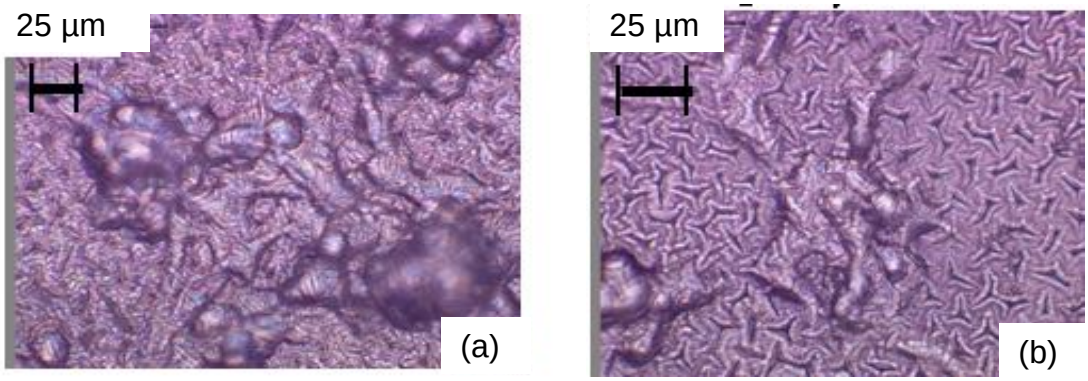

Figure 4.23: Optical images of cells attached to polymer surfaces.

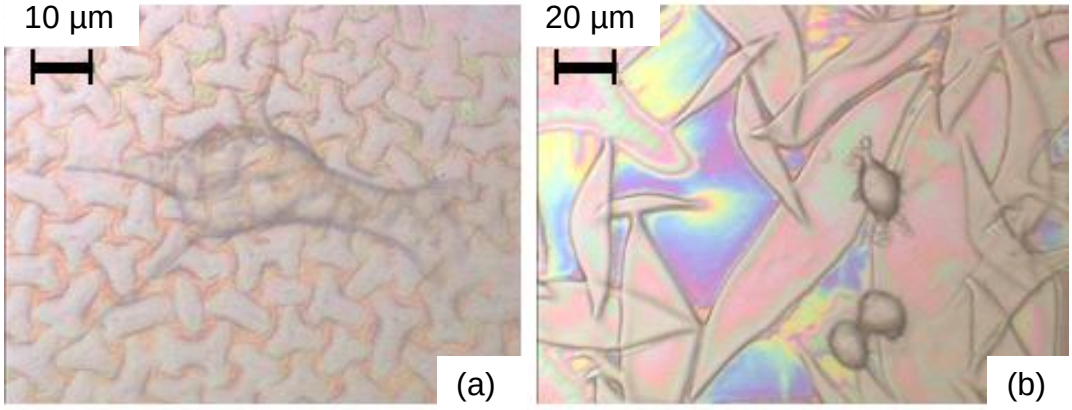

Figure 4.24: Optical images of cells attached to polymer wrinkles and buckles.

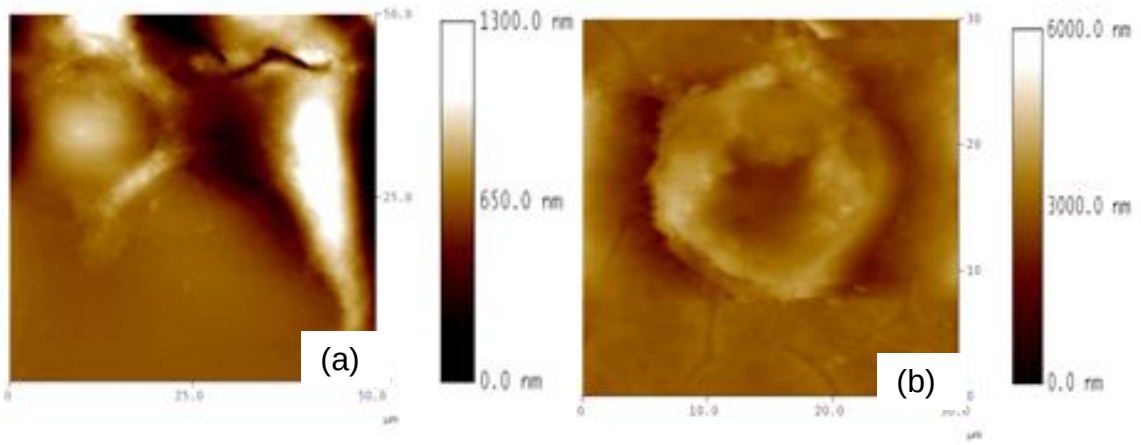

Figure 4.25: AFM images of cells attached to polymer surfaces.

References

[1] G. A. Abrams, *et al*., "Nanoscale topography of the basement membrane underlying the corneal epithelium of the rhesus macaque," *Cell and Tissue Research,* vol. 299, pp. 39-46, 2000.

[2] K. Anselme, "Osteoblast adhesion on biomaterials," *Biomaterials,* vol. 21, pp. 667-681, 2000.

[3] B. Thomas, 2008, Hematoxylin and eosin stained slide at 10x of normal epidermis and dermis.

[4] J. Genzer and J. Groenewold, "Soft matter with hard skin: from skin wrinkles to templating and material characterization," *Soft Matter,* vol. 2, pp. 310-323, 2006.

[5] R. M. Bremnes, R. Veve, F. R. Hirsch, and W. A. Franklin, "The E-cadherin cell–cell adhesion complex and lung cancer invasion, metastasis, and prognosis," *Journal of Lung Cancer,* pp. 115–124, 2002.

[6] S. E. Cross, Y.-S. Jin, J. Tondre, R. Wong, J. Rao, and J. K. Gimzewski, "AFM-based analysis of human metastatic cancer cells," *Nanotechnology,* vol. 19, p. 38400, 2008.

[7] H. M. Kowalczynska, *et al.*, "Interaction of L1210 cells with sulfonated polystyrene in the absence of serum: adhesion and three-dimensional cell shape," *Colloids and Surfaces B: Biointerfaces,* vol. 30, pp. 193-206, 2003.

[8] K. R. Porter, G. J. Todaro, and V. Fonte, "A scanning electron microscope study of surface features of viral and spontaneous transformants of mouse Balb/3T3 cells," *The Journal of Cell Biology,* vol. 59, pp. 633-642, 1973.

[9] A. F. Chambers, A. C. Groom, and I. C. MacDonald, "Dissemination and growth of cancer cells in metastatic sites," *Nature Reviews Cancer,* vol. 2, pp. 563-573, 2002.

[10] A. Folch and M. Toner, "Microengineering of cellular interactions," *Annu. Rev. Biomed. Eng.,* pp. 227-256, 2000.

[11] V. Hendrick, E. Muniz, G. Geuskens, and J. Werenne, "Adhesion, growth and detachment of cells on modified polystyrene surface," *Cytotechnology,* vol. 36, pp. 49-53, 2001.

[12] L. Lu, K. Nyalakonda, L. Kam, R. Bizios, A. Gopferich, and A. G. Mikos, "Retinal pigment epithelial cell adhesion on novel micropatterned surfaces fabricated from synthetic biodegradable polymers," *Biomaterials,* vol. 22, pp. 291-297, 2001.

[13] A. Jemal, R. Siegel, E. Ward, Y. Hao, and J. X. Taylor, "Cancer statistics, 2008," *CA: A Cancer Journal for Clinicians,* vol. 58, pp. 71-96, 2008.

[14] A. C. Society, "The history of cancer," 2009.

[15] H. Dell, *et al*., "Cancer milestones," *Nature,* pp. S7-S23, 2006.

[16] B. K. Edwards, E. Ward, B. A. Kohler, C. Eheman, A. G. Zauber, R. N. Anderson, A. Jemal, M. J. Schymura, I. Lansdorp-Vogelaar, L. C. Seeff, M. v. Ballegooijen, S. L. Goede, and L. A. G. Ries, "Annual report to the nation on the status of cancer, 1975-2006, featuring colorectal cancer trends and impact of interventions (risk factors, screening, and treatment) to reduce future rates," *Cancer,* pp. 1-32, 2010.

[17] E. L. Wynder and E. A. Graham, "Tobacco smoking as a possible etiologic factor in bronchiogenic carcinoma, a study of six hundred and eighty-four proved cases" *The Journal of the American Medical Association,* vol. 143, pp. 329-336, 1950.

[18] A. P. Hollander and P. V. Hatton, *Biopolymer methods in tissue engineering* vol. 238: Humana Press, 2004.

[19] A. Kikuchi and T. Okano, "Nanostructured designs of biomedical materials: applications of cell sheet engineering to functional regenerative tissues and organs," *Journal of Controlled Release,* vol. 101, pp. 69-84, 2005.

[20] J. Y. Wong, A.Velasco, P. Rajagopalan, and Q. Pham, "Directed movement of vascular smooth muscle cells on gradient-compliant hydrogels" *Langmuir,* vol. 19, pp. 1908-1913, 2003.

[21] A. Ravne, *Principles of polymer chemistry*, second ed.: Plenum Publishers, 2000.

[22] A. S. G. Curtis and *et al*., "Adhesion of Cells to Polystyrene Surfaces," *The Journal of Cell Biology,* vol. 97, pp. 1500-1506, 1983.

[23] W. Pfleging, M. Bruns, A. Welle, and S. Wilson, "Laser-assisted modification of polystyrene surfaces for cell culture applications," *Applied Surface Science,* vol. 253, pp. 9177-9184, 2007.

[24] Y. Sasai, N. Matsuzaki, S.-i. Kondo, and M. Kuzuya, "Introduction of carboxyl group onto polystyrene surface using plasma techniques," *Surface & Coatings Technology,* vol. 202, pp. 5724–5727, 2008.

[25] M. A. Hjortso and J. W. Roos, *Cell adhesion: fundamentals and biotechnological applications*: CRC Press, 1995.

[26] T. Yeung, P. C. Georges, L. A. Flanagan, B. Marg, M. Ortiz, M. Funaki, N. Zahir, W. Ming, V. Weaver, and P. A. Janmey, "Effects of substrate stiffness on cell morphology, cytoskeletal structure, and adhesion," *Cell Motility and the Cytoskeleton,* vol. 60, pp. 24-34, 2005.

[27] R. Freitag, *Synthetic polymers for biotechnology and medicine*: Eurekah.com/ LandesBioscience, 2003.

[28] B. Jeong and A. Gutowska, "Lessons from nature: stimuli-responsive polymers and their biomedical applications," *TRENDS in Biotechnology,* vol. 20, pp. 305-311, 2002.

[29] A. Vidyasagar, J. Majewski, and R. Toomey, "Temperature induced volume-phase transitions in surface-tethered Poly(N-isopropylacrylamide) networks," *Macromolecules,* vol. 41, pp. 919-924, 2008.

[30] T. Okano, N. Yamada, H. Sakai, and Y. Sakurai, "A novel recovery system for cultured cells using plasma-treated polystyrene dishes grafted with poly(N-isopropylacrylamide)," *Journal of Biomedical Materials Research,* vol. 27, pp. 1243-1251, 1993.

[31] J.-P. Chen and T.-H. Cheng, "Thermo-responsive chitosan-graft-poly(N-isopropylacrylamide) injectable hydrogel for cultivation of chondrocytes and meniscus cells," *Macromolecular Bioscience,* pp. 1026-1029, 2006.

[32] A. Curtis and C. Wilkinson, "Topographical control of cells," *Biomaterials,* pp. 1573-1583, 1997.

[33] E. N. Marieb, *Human Anatomy & Physiology*, 6 ed. San Francisco: Pearson Benjamin Cummings, 2004.

[34] J. Tan, H. Shen, and W. M. Saltzman, "Micron-scale positioning of features influences the rate of polymorphonuclear leukocyte migration," *Biophysical Journey,* vol. 81, pp. 2569–2579, 2001.

[35] A. J. Ridley, M. A. Schwartz, K. Burridge, R. A. Firtel, M. H. Ginsberg, G. Borisy, J. T. Parsons, and A. R. Horwitz, "Cell migration: integrating signals from front to back," *Science,* vol. 302, p. 1709, 2003.

[36] J. Lacovara, E. B. Cramer, and J. P. Quigley, "Fibronectin enhancement of directed migration of B16 melanoma cells," *Cancer Research,* vol. 44, pp. 1657-1663, 1984.

[37] N. W. Karuri, S. Liliensiek, A. I. Teixeira, G. Abrams, S. Campbell, P. F. Nealey, and C. J. Murphy, "Biological length scale topography enhances cell-substratum adhesion of human corneal epithelial cells," *J Cell Sci.,* vol. 117, pp. 3153-3164, 2004.

[38] M. Yamato, M. Okuhara, F. Karikusa, A. Kikuchi, Y. Sakurai, and T. Okano, "Signal transduction and cytoskeletal reorganization are required for cell detachment from cell culture surfaces grafted with a temperature-responsive polymer," *Journal of biomedical materials research,* vol. 44, pp. 44-52, 1999.

[39] D. Lehnert, B. Wehrle-Haller, C. David, U. Weiland, C. Ballestrem, B. A. Imhof, and M. Bastmeyer, "Cell behaviour on micropatterned substrata: limits of extracellular matrix geometry for spreading and adhesion," *Journal of Cell Science,* vol. 117, pp. 41-52, 2003.

[40] F. H. Wezeman, "Morphological foundations of precartilage development in mesenchyme," *Microscopy Research and Technique,* vol. 43, pp. 91-101, 1998.

[41] L. A. Liotta, "Tumor Invasion and Metastases: Role of the basement membrane," *American Journal of Physics,* vol. 117, pp. 339-348, 1984.

[42] D. E. Discher, P. Janmey, and Y.-l. Wang, "Tissue cells feel and respond to the stiffness of their substrate," *Science,* vol. 310, pp. 1139-1143, 2009.

[43] M. Lampin, R. Warocquier-Clerout, C. Legris, M. Degrange, and M. F. Sigot-Luizard, "Correlation between substratum roughness and wettability, cell adhesion, and cell migration," *Journal of Biomedical Materials Research Part A,* vol. 36, pp. 99-108, 1998.

[44] Y. Arima and H. Iwata, "Effect of wettability and surface functional groups on protein adsorption and cell adhesion using well-defined mixed self-assembled monolayers," *Biomaterials,* vol. 28, pp. 3074-3082, 2007.

[45] R. Tzoneva, N. Faucheux, and T. Groth, "Wettability of substrata controls cell–substrate and cell–cell adhesions," *Biochimica et Biophysica Acta,* vol. 1770, pp. 1538-1547, 2007.

[46] E. Moy, F. Y. H. Lin, J. W. Vogtle, Z. Policova, and A. W. Neumann, "Contact angle studies of the surface properties of covalently bonded poly-L-lysine to surfaces treated by glow-discharge," *Colloid and Polymer Science,* vol. 272, pp. 1245-1251, 1994.

[47] C. F. Deroanne, C. M. Lapiere, and B. V. Nusgens, "*In vitro* tubulogenesis of endothelial cells by relaxation of the coupling extracellular matrix-cytoskeleton," *Cardiovascular Research,* vol. 49, pp. 647-658, 2001.

[48] J. Rho, R. Ashman, and C. Turner, "Young's modulus of trabecular and cortical bone material: Ultrasonic and microtensile measurements," *Journal of Biomechanics,* vol. 26, pp. 111-119, 1993.

[49] T. A. Krouskop, T. M. Wheeler, F. Kallel, B. S. Garra, and T. Hall, "Elastic moduli of breast and prostate tissues under compression," *Ultrasonic Imaging,* vol. 20, pp. 260-274, 1998.

[50] D. J. Goetz, M. E. El-Sabban, D. A. Hammer, and B. U. Pauli, "Lu-ECAM-1 mediated adhesion of melanoma cells to endothelium under conditions of flow," *International Journal of Cancer,* vol. 65, 1996.

[51] B. Alberts, D. Bray, K. Hopkin, A. Johnson, J. Lewis, M. Raff, K. Roberts, and P. Walter, *Essential cell biology*, 2 ed. New York City: Garland Science, 2004.

[52] Y. G. Takei, T. Aoki, K. Sanui, N. Ogata, Y. Sakurai, and T. Okano, "Dynamic contact angle measurement of temperature-responsive surface properties for poly (N-isopropylacrylamide) grafted surfaces," *Macromolecules,* vol. 27, pp. 6163-6166, 1994.

[53] P. Filippini, G. Rainaldi, A. Ferrante, B. Mecheri, G. Gabrielli, M. Bombace, P. L. Indovina, and M. T. Santini, "Modulation of osteosarcoma cell growth and differentiation by silane-modified surfaces," *Journal of Biomedical Materials Research Part A,* vol. 55, pp. 338-349, 2001.

[54] E. Cerda and L. Mahadevan, "Geometry and physics of wrinkling," *Physical Review Letters,* vol. 90, pp. 743021-743024, 2003.

[55] M.-W. Moon, *et al*., "Wrinkles hard skins on polymers created by focused ion beam," *Proceedings of the National Academy of Sciences,* vol. 104, pp. 1130-1133, 2007.

[56] J. S. Sharp and R. A. L. Jones, "Micro-buckling as a route towards surface patterning," *Advanced Materials,* vol. 14, pp. 799-802, 2002.

[57] A. I. Texeira, *et al.*, "Epithelial contact guidance on well-defined micro- and nanostructured substrates," *Journal of Cell Science,* vol. 116, pp. 1881-1892, 2003.

[58] R. Murali, *BioNanoFluidic MEMS*: Springer-Verlag New York, LLC, 2008.

[59] M. R. Hynd, J. P. Frampton, N. Dowell-Mesfin, J. N. Turner, and W. Shain, "Directed cell growth on protein-functionalized hydrogel surfaces," *Journal of Neuroscience Methods,* vol. 162, pp. 255-263, 2007.

[60] H. Tanaka, "Morphological and kinetic evolution of surface patterns in gels during the swelling process: evidence of dynamic pattern ordering" *Physical Review Letters,* vol. 68, pp. 2794-2797, 1992.

[61] N. Bowden, S. Brittain, A. G. Evans, J. W. Hutchinson, and G. M. Whitesides, "Spontaneous formation of ordered structures in thin films of metals supported on an elastomeric polymer," *Nature,* vol. 393, pp. 146-149, 1998.

[62] W. T. S. Huck, *et al*., "Ordering of spontaneously formed buckles on planar surfaces" *Langmuir* vol. 16, pp. 3497-3501, 2000.

[63] R. C. Hayward, B. F. Chmelka, and E. J. Kramer, "Template cross-linking effects on morphologies of swellable block copolymer and mesostructured silica thin films," *Macromolecules,* vol. 38, pp. 7768-7783, 2005.

[64] Y. Yagi, H. Inomata, and S. Saito, "Solubility parameter of an N-isopropylacrylamide gel" *Macromolecules,* vol. 25, pp. 2997-2998, 1992.

[65] J. S. Sharp and R. A. L. Jones, "Swelling-induced morphology in ultrathin supported films of poly(d,l-lactide)," *Physical Review Letter E,* vol. 66, pp. 0118011-0118019, 2002.

[66] Y. Li, C. Li, and Z. Hu, "Pattern formation of constrained acrylamide/sodium acrylate copolymer gels in acetone/water mixture" *Journal of Chemical Physics,* vol. 100, pp. 4637-4644, 1994.

[67] R. Toomey, J. Mays, and M. Tirrell, "In situ thickness determination of adsorbed layers of poly(2-vinylpyridine)-polystyrene diblock copolymers by ellipsometry," *Macromolecules,* vol. 37, pp. 905-911, 2004.

[68] C. M. Stafford, C. Harrison, K. L. Beers, A. Karim, E. J. Amis, M. R. Vanlandingham, H.-C. Kim, W. Volksen, R. D. Miller, and E. E. Simonyi, "A buckling-based metrology for measuring the elastic moduli of polymeric thin films," *Nature Materials,* vol. 3, pp. 545-550, 2004.

[69] P. J. Yoo, *et al*., "Physical self-assembly of microstructures by anisotropic buckling," *Advanced Materials,* vol. 14, pp. 1383-1387, 2002.

[70] Z. Y. Huang, W. Hong, and Z. Suo, "Nonlinear analyses of wrinkles in a film bonded to a compliant substrate" *Journal of the Mechanics and Physics of Solids,* vol. 53, pp. 2101-2118, 2005.

[71] N. J. Hallab, K. J. Bundy, K. O'Connor, R. L. Moses, and J. J. Jacobs, "Evaluation of metallic and polymeric biomaterial surface energy and surface roughness characteristics for directed cell adhesion," *Tissue Engineering,* vol. 7, pp. 55-71, 2000.

[72] H. E. Hoffman, "Evaporation rates of organic liquids," *Industrial and Engineering Chemistry,* vol. 24, pp. 135-140, 1932.

[73] R. M. D. d. Silva, J. F. Mano, and R. L. Reis, "Smart thermoresponsive coatings and surfaces for tissue engineering: switching cell-material boundaries," *TRENDS in Biotechnology,* vol. 25, pp. 577-583, 2007.

[74] M. Yamato, *et al*., "Nanofabrication for micropatterned cell arrays by combining electron beam-irradiated polmer grafting and localized laser ablation," *Journal of Biomedical Materials Research A,* pp. 1065-1071, 2003.

[75] M. T. Moran, W. M. Carroll, I. Selezneva, A. Gorelov, and Y. Rochev, "Cell growth and detachment from protein-coated PNIPAAm-based copolymers," *Journal of Biomedical Materials Research Part A,* vol. 81, pp. 870-876, 2007.

[76] X. Cheng, Y. Wang, Y. Hanein, K. F. Bohringer, and B. D. Ratner, "Novel cell patterning using microheater-controlled thermoresponsive plasma films," *Journal of Biomedical Materials Research,* pp. 159-168, 2004.

[77] M. Nitschke, *et al*., "Thermo-responsive poly(NiPAAm-co-DEGMA) substrates for gentle harvest of human corneal endothelial cell sheets," *Journal of Biomedical Materials Research Part A,* vol. 80, pp. 103-1010, 2006.

[78] H. E. Canavan, D. J. Graham, X. Cheng, B. D. Ratner, and D. G. Castner, "Comparison of native extracellular matrix with adsorbed protein films using secondary ion mass spectrometry," *Langmuir,* vol. 23, pp. 50-56, 2007.

[79] I. I. Selezneva, A. V. Gorelov, and Y. A. Rochev, "Use of Thermosensitive Polymer Material on the Basis of N-Isopropylacrylamide and N-Tert-Butylacrylamide Copolymer in Cell Technologies," *Cell Technologies in Biology and Medicine,* vol. 2, pp. 538-541, 2006.

[80] K. M. Yamada and E. Cukierman, "Modeling tissue morphogenesis and cancer in 3D," *Cell,* vol. 130, pp. 601-610, Aug 2007.

[81] M. Harimoto, M. Yamato, A. Kikuchi, and T. Okano, "Cell sheet engineering: intelligent polymer patterned surfaces for tissue engineered liver," *Macromolecular Symposia,* vol. 195, pp. 231-235, 1993.

[82] D. O. H. Teare, N. Emmison, C. Ton-That, and R. H. Bradley, "Cellular attachment to ultraviolet ozone modified polystyrene surfaces," *Langmuir,* vol. 16, pp. 2818-2824, 2000.

[83] O. H. Kwon, A. Kikuchi, M. Yamato, Y. Sakurai, and T. Okano, "Rapid cell sheet detachment from poly(N-isopropylacrylamide)-grafted porous cell culture membranes," *Journal of Biomedical Materials Research Part A,* vol. 50, pp. 82-89, 1999.

[84] Y. Akiyama, A. Kikuchi, M. Yamato, and T. Okano, "Ultrathin Poly(N-isopropylacrylamide) grafted layer on polystyrene surfaces for cell adhesion/detachment control," *Langmuir,* vol. 20, pp. 5506-5511, 2004.

[85] T. G. v. Kooten, H. T. Spijker, and H. J. Busscher, "Plasma-treated polystyrene surfaces: model surfaces for studying cell-biomaterial interactions," *Biomaterials,* vol. 25, pp. 1735-1747, 2004.

[86] K. Haraguchi, T. Takehisa, and M. Ebato, "Control of cell cultivation and cell sheet detachment on the surface of polymer/clay nanocomposite hydrogels," *Biomacromolecules,* vol. 7, pp. 3267-3275, 2006.

[87] P. S. Curti, *et al*., "Characterization of PNIPAAm photografted on PET and PS surfaces," *Applied Surface Science,* vol. 245, pp. 223-233, 2005.

[88] L. Liang, *et al*., "Surfaces with reversible hydrophilic/ hydrophobic characteristics on cross-linked poly(N-isopropylacrylamide) hydrogels" *Langmuir,* vol. 16, pp. 8016-8023, 2000.

[89] I. I. Selezneva, A. V. Gorelov, and Y. A. Rochev, "Use of thermosensitive polymer material on the basis of N-Isopropylacrylamide and N-Tert-Butylacrylamide copolymer in cell technologies," *Cell Technologies in Biology and Medicine,* vol. 2, pp. 538-541, 2006.

[90] R. J. Pelham and Y.-L. Wang, "Cell locomotion and focal adhesions are regulated by substrate flexibility," *Proceedings of the National Academy of Sciences,* vol. 94, pp. 13661-13665, 1997.

[91] L. H. Lee, *Fundamentals of cell adhesion*. New York: Plenum Press, 1991.

[92] J. D. Andrade, *Surface and interfacial aspects of biomedical polymers*. New York: Plenum Press, 1985.

[93] D. Quere, M.-J. Azzopardi, and L. Delattre, "Drops at rest on a tilted plane," *Langmuir,* vol. 14, pp. 2213-2216, 1998.

[94] M. Sakai, J.-H. Song, Y. Akutsu, S. Suzuki, N. Yoshida, Y. Kameshima, M. Sugibuchi, and A. Nakajima, "Relationship between sliding acceleration of water droplets and advancing-receding contact angles," in *Proc. of the 4th International Symposium on Surface Science and Nanotechnology*, Omiya, Japan, 2005.

[95] S. Sikalo, C. Tropea, and E. N. Ganic, "Dynamic wetting angle of a spreading droplet," *Experimental Thermal and Fluid Science,* vol. 29, pp. 795-802, 2005.

[96] A. W. Adamson and A. P. Gast, *Physical Chemistry of Surfaces*, 6 ed. New York: Wiley Interscience, 1997.

[97] Y. Senju and H. Miyata, "The role of actomyosin contractility in the formation and dynamics of actin bundles during fibroblast spreading," *Journal of Biochemistry,* vol. 145, pp. 137-150, 2008.

About the Author

Ophir Ortiz obtained both the B.S. and M.S. degrees in Electrical Engineering from USF. She is currently working towards the Ph.D. degree in Electrical Engineering at USF. She is a McKnight Doctoral Fellow, NSF/GK-12 Fellow, SLOAN Fellow, and Latino Fellow.